A photograph of a petri dish with a coiled orange ribbon inside, set against a solid orange background. The ribbon is coiled in a complex, non-linear pattern, resembling a fractal or a complex liquid structure. The petri dish is positioned in the upper half of the frame, and the ribbon extends from the top left, loops through the center, and continues towards the bottom right.

On Hidden Order  
in Luttinger Liquids

Harm Vincent Kruis

Universiteit Leiden



1 481 365 8

BIBLIOTHEEK  
GORLAEUS LABORATORIA  
Postbus 9502  
2300 RA LEIDEN  
Tel.: 071 - 527 43 66 / 67

8 JUL 2003

# On Hidden Order in Luttinger Liquids

Harm Vincent Kruis

THE UNIVERSITY OF CHICAGO  
LIBRARY

B. JUL 200

On Hidden Order  
in Lattinger Lipids

Helm V. Kohn

On Hidden Order  
in Luttinger Liquids

PROEFSCHRIFT

TER VERKRIJGING VAN  
DE GRAAD VAN DOCTOR AAN DE UNIVERSITEIT LEIDEN,  
OP GEZAG VAN DE RECTOR MAGNIFICUS DR. D. D. BREIMER,  
HOGLERAAR IN DE FACULTEIT DER WISKUNDE EN  
NATUURWETENSCHAPPEN EN DIE DER GENEESKUNDE,  
VOLGENS BESLUIT VAN HET COLLEGE VOOR PROMOTIES  
TE VERDEDIGEN OP DONDERDAG 19 JUNI 2003  
TE KLOKKE 16.15 UUR

DOOR

Harm Vincent Kruis

GEBOREN TE APELDOORN IN 1973

**Promotiecommissie:**

Promotor: Prof. dr. J. Zaanen  
Referent: dr. J. van den Brink  
Overige leden: dr. J. Aarts  
Prof. dr. A. Achúcarro  
Prof. dr. C. W. J. Beenakker  
Prof. dr. P. H. Kes  
Prof. dr. ir. H. T. C. Stoof (Universiteit Utrecht)

# Contents

<b>1</b>	<b>Introduction</b>	<b>1</b>
1.1	Fermi and Luttinger Liquids . . . . .	1
1.2	Order and Disorder . . . . .	3
1.3	The stripe dislocation transition . . . . .	4
1.4	The hidden order in Haldane spin-1 chains . . . . .	8
1.5	Hidden order in Luttinger Liquids . . . . .	10
1.6	Outline of the thesis . . . . .	13
<b>2</b>	<b>Pseudogap</b>	<b>15</b>
2.1	Introduction . . . . .	15
2.2	$T$ - matrix approximation . . . . .	16
<b>3</b>	<b>The Bosonization procedure</b>	<b>23</b>
3.1	The free spinless fermion gas . . . . .	23
3.1.1	Bosonization of spinless fermions . . . . .	25
3.1.2	The density density operator . . . . .	28
3.2	The spinful fermion gas . . . . .	29
3.3	Bosonizing the interactions terms . . . . .	31
3.3.1	Bosonizing the Tomonaga-Luttinger model . . . . .	32
3.3.2	The correlation functions . . . . .	34
3.3.3	Spin and Charge gap . . . . .	36
3.4	The Hubbard Model . . . . .	37
3.5	Summary . . . . .	37
<b>4</b>	<b>The Bethe Ansatz</b>	<b>39</b>
4.1	The Bethe Ansatz for the Heisenberg Model . . . . .	39
4.1.1	The case $N = 2$ : two reversed spins . . . . .	40
4.1.2	General $N$ case . . . . .	44
4.2	The Bethe Ansatz for the Hubbard Model . . . . .	47
4.2.1	The case $N = 2$ : two electrons . . . . .	48
4.2.2	General $N$ case . . . . .	50
4.2.3	Large $U$ limit . . . . .	52
4.3	Hubbard model spin-spin correlations for large $U$ . . . . .	53

4.3.1	Lemma . . . . .	54
4.3.2	Final result . . . . .	56
4.3.3	Interpretation . . . . .	57
<b>5</b>	<b>Sublattice Parity Order</b>	<b>61</b>
5.1	Sublattice parity order for $U \rightarrow \infty$ . . . . .	61
5.2	Probing the internal spin-spin correlations . . . . .	64
<b>6</b>	<b>Sublattice parity order for <math>U = 0</math></b>	<b>69</b>
6.1	Introduction . . . . .	69
6.2	Spinless fermion numerics . . . . .	70
6.3	Final result spinful case . . . . .	75
<b>7</b>	<b>The failures of Bosonization</b>	<b>79</b>
7.1	Examples of where things go wrong . . . . .	79
7.2	Why does bosonization fail? . . . . .	80
7.3	Bosonizing using the proper continuum limit . . . . .	84
7.4	Bosonizing the hidden order string correlator . . . . .	90
<b>8</b>	<b>DMRG calculations</b>	<b>93</b>
8.1	Introduction . . . . .	93
8.2	$SO(4)$ Symmetry . . . . .	96
8.3	Specifications of the DMRG calculations . . . . .	98
8.4	Outline of the DMRG calculations . . . . .	99
8.5	Calculating $D_s(x)$ . . . . .	99
8.6	Calculating $\rho_s = \langle n_s(x) \rangle$ . . . . .	100
8.7	Calculating $\langle n_s(x)(-1)^{\sum_{j=1}^{x-1} n_s(j)} n_s(0) \rangle$ . . . . .	103
8.8	Calculating the correlator $O_{top}(x)$ . . . . .	106
<b>9</b>	<b>Conclusions</b>	<b>109</b>
9.1	Removing the effect of the holons . . . . .	109
9.2	Removing the effects of the spinons . . . . .	112
9.3	Removing the effects of spinons and holons . . . . .	114
9.4	Summary Hidden order . . . . .	115
9.5	Local Gauge Symmetry . . . . .	116
	<b>Bibliography</b>	<b>119</b>
	<b>List of publications</b>	<b>125</b>
	<b>Samenvatting</b>	<b>127</b>
	<b>Curriculum Vitæ</b>	<b>131</b>
	<b>Nawoord</b>	<b>133</b>

# Chapter 1

## Introduction

This thesis analyses the so-called sublattice parity order which we prove to occur in a special class of low dimensional systems, the so called Luttinger Liquids [1]. Although Luttinger Liquids have been investigated in great detail [2], this kind of order has been overlooked. Before we indicate what is meant by this type of ordering, we give a brief overview of Luttinger Liquids and order in general. After this we will describe the sublattice parity as it occurs in two dimensions in high  $T_c$  superconductors and in Haldane spin-1 chains. We end this chapter by summarizing the work presented in this thesis.

### 1.1 Fermi and Luttinger Liquids

Condensed matter physics describes the behavior of huge amounts of particles. A gram of material such as a simple metal houses the unimaginable number of  $10^{23}$  particles which all interact, for instance through Coulomb interactions. Faced with these enormous quantities it seems impossible to do any theoretical calculations on physical systems. Fortunately, this is not true for three dimensional metals.

Most of the characteristics of these materials can qualitatively be described by a gas of non-interacting electrons. The reason for this was given in 1956 by Landau in his so called Fermi Liquid theory [3]. Among other things, due to the discontinuity of the particle density around the Fermi level, the elementary excitations of the strongly interacting system can be described by effectively non-interacting quasi particles. These quasi particles obey Fermi Dirac statistics and have the same quantum numbers as free electrons. The electron-electron interactions lead to a renormalization of the kinetic parameters compared to free electrons, like the effective mass. The Fermi Liquid theory provides a systematic way to calculate these kinetic parameters and quantify the changes produced by the interactions.

However, for a one dimensional system, the Fermi Liquid theory breaks down. This is because for  $d = 1$  the momentum distribution function  $n(k)$  is expected to be smooth at the Fermi wave vector and quasiparticles with a finite lifetime cannot be defined. Instead of the quasiparticles with charge  $e$  and spin  $\frac{1}{2}$ , the elementary excitations are collective

charge and spin density fluctuations with bosonic character, the so-called spinons and holons. These spin and charge excitations propagate with different velocities which lead to the separation of spin and charge. This is known as the Luttinger Liquid [1]. Such a model has been solved by means of a bosonization technique [2].

The one dimensional Hubbard model is an example of such a Luttinger Liquid and describes spinful electrons which interact through a Coulomb interaction  $U$  [4]. In this model there is a straightforward interpretation of spin charge separation. For consider the large  $U$  limit for  $\rho_{tot} = 1$ , with  $\rho_{tot}$  the total electron density. In that case, there are no doubly occupied sites and because of the strong short range antiferromagnetic order, a typical local configuration will be as depicted in figure 1.1a. Consider what happens when we remove one up electron and move the spin vacancy to the left. The neighboring spins move in the opposite direction. Due to this spin movement, the original hole has split into a so called holon and a spinon. The holon is a pure charge excitation and is characterized by a hole surrounded by antiferromagnetically ordered aligned spins. The spinon is a pure spin excitation characterized by two adjacent up or down spins, which has an excess spin  $\pm \frac{1}{2}$  with respect to the initial antiferromagnet. The spinon and holon can move separately.

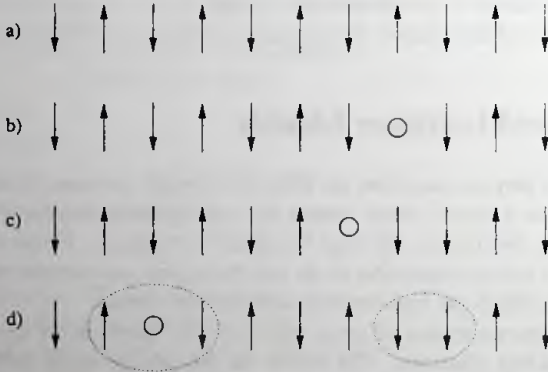


Figure 1.1: Cartoon picture of the mechanism of spin charge separation in one dimension. a) The typical local configuration for large  $U$  in the Hubbard model. By removing one up electron we introduce a hole (figure b), which can move due to the hopping of the electrons and is split into a holon and a spinon (figure d). The left dashed oval indicates the holon, and the oval on the right marks the spinon.

In this thesis we analyse an order that occurs in these Luttinger Liquids. To do so, we review the concept of order in a physical systems in the next section.

## 1.2 Order and Disorder

Almost all phase transitions encountered in condensed matter physics are transitions from an ordered to a disordered phase [5]. The first phase displays certain correlations which are absent in the second phase. Since the disordered phase has less order than the ordered phase, the system has a higher symmetry. In other words, in the disordered phase the system is invariant under a symmetry which is spontaneously broken in the ordered phase. The two phases can be distinguished by a so called order parameter which is an average  $\langle \phi \rangle$  of an operator which is not invariant under the symmetry. This quantity is zero in the disordered phase and non-zero in the ordered phase.

A simple model to explain order and correlations occurring in physical systems is the Ising model [6, 7] on a square lattice defined by the Hamiltonian

$$H = -J \sum_{\langle \vec{i}\vec{j} \rangle} \sigma(\vec{i}) \sigma(\vec{j}). \quad (1.1)$$

Here  $\sigma(\vec{j}) = \pm 1$  are defined on a lattice and  $\langle \vec{i}\vec{j} \rangle$  denotes a pair of neighboring sites  $\vec{i}$  and  $\vec{j}$ . We consider ferromagnetic interactions with  $J > 0$ , so neighboring sites want to align. The Ising model has been solved exactly and has a phase transition from an ordered to a disordered state at the critical temperature  $T_c$  [8].

At low temperatures  $T < T_c$  the spins tend to align and the system is ordered. This is expressed by the non-zero spontaneous magnetization  $\langle \sigma(\vec{r}) \rangle = M(T) \neq 0$  which breaks the global  $Z_2$  symmetry of the Hamiltonian (1.1). For these temperatures, the kinetic energy destroys the order of the aligned spins only over a maximum distance of the finite correlation length  $\xi(T)$ . And thus for large distances the spins stay correlated with

$$\langle \sigma(\vec{r}) \sigma(0) \rangle = \langle \sigma(\vec{r}) \rangle^2 + A e^{-|\vec{r}|/\xi(T)} \rightarrow [M(T)]^2 \neq 0, \quad (1.2)$$

for large  $|\vec{r}|$  and with  $A$  a constant. So the model displays long range order. When the temperature increases the correlation length  $\xi(T)$  becomes longer until it becomes infinite at the critical temperature  $T_c$ . At this point the kinetic energy is powerful enough to break up the aligned spin order throughout the system and the staggered magnetization has decreased to zero. For these critical temperature the model is on the point of becoming disordered.

For high temperatures  $T > T_c$  the system is in the disordered phase which can be characterized by a zero magnetization  $\langle \sigma(\vec{r}) \rangle = M(T) = 0$ . In this region neighboring spins still want to align but due to their kinetic energy, they can only do so up to a maximal distance of the correlation length  $\xi(T)$ . Now, the model is short ranged ordered and for large distances the spins are uncorrelated which is expressed by

$$\langle \sigma(\vec{r}) \sigma(0) \rangle = \langle \sigma(\vec{r}) \rangle^2 + A e^{-|\vec{r}|/\xi(T)} \rightarrow [M(T)]^2 = 0. \quad (1.3)$$

So the high and low temperature regions are qualitatively different and can be distinguished by the spontaneous magnetization  $M(T)$  which serves as the order parameter.

In this Ising model the order parameter can easily be identified. In other more complicated cases, the identification of an order parameter is not that simple. For instance,

after the discovery of superconductivity in 1911 in Leiden by Kamerlingh Onnes [9] it took till 1956 for the order parameter for the superconducting state to be found [10]. For these systems the density of the so-called Cooper pairs [11] can be used to distinguish the superconducting from the normal state. But as we will discuss now, not every system can display long range order.

In this thesis we analyse the so-called sublattice parity order in an example of a Luttinger model, namely the one dimensional Hubbard model. In this system the spins have a continuous symmetry, instead of the discrete  $Z_2$  symmetry of the Ising model. Therefore, according to the Mermin-Wagner theory [12], this model cannot have long range order. Instead a correlation function like the spin correlator decays algebraically to zero  $\langle S^z(x)S^z(0) \rangle \rightarrow 0$ . This is referred to as quasi long range order. Furthermore, there is another difference between the order in the Ising model and the order analysed in this thesis.

The order in the Ising model can be detected using a local two-point correlator  $\langle \sigma(\vec{r})\sigma(0) \rangle$  which depends only on the value of  $\sigma(j)$  on the lattice sites 0 and  $\vec{r}$ . In our study we investigate a topological order which can be detected with the correlator  $O_{top}(x) = -\langle S^z(x)(-1)^{\sum_{j=1}^{x-1} n_{tot}(j)} S^z(0) \rangle$ . This correlator cannot be expressed as the product of two operators and is highly non-local. Because of this, this order is difficult to measure in an experiment and the order is referred to as an hidden order.

So the sublattice parity order analysed in this thesis is a form of hidden topological order. This kind of order is also studied in two dimensions by Zaanen and Nussinov [13]. In this article they describe a phase transition in which the sublattice parity disorders. As an introduction to the sublattice parity order, we will review this transition in the next section.

### 1.3 The stripe dislocation transition

A topological phase transition closely connected to the order described in this thesis is the quantum phase transition addressed in a geometrical language by Zaanen and Nussinov [13]. The transition is in more algebraic terms studied by Sachdev *et al* [14] and describes the destruction of the sublattice parity order in two dimensions. As we will discuss now, this kind of order is associated with the so-called striped phase.

The stripe phase occurs in high  $T_c$  superconductors which were first discovered in 1986 [15]. These compounds consist of parallel copper oxide planes which are sandwiched between layers containing oxygen, rare earth materials like  $La$ , and sometimes copper atoms. By chemical substitution of the rare earth materials, one can add or remove electrons from the  $CuO_2$  planes in which the conduction takes place. Examples of such compounds are  $La_{2-x}Sr_xCuO_4$  and  $YBa_2Cu_3O_{6+\delta}$ . At zero doping, the compounds are Mott insulators. When the materials are doped, the holes do not spread homogeneously over the two dimensional  $CuO_2$  plane, but can instead form lines in the antiferromagnetic, Mott insulating background, as is schematically indicated in figure 1.2. These lines of holes form domain walls in the spin system and are referred to as stripes.

Stripes have to do with a kind of topological order. They form domain walls in a

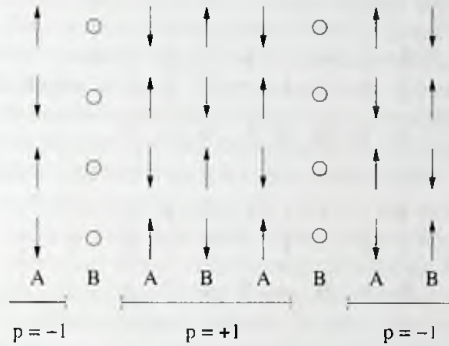


Figure 1.2: Schematic illustration of the stripe ordering. The stripe is an antiphase boundary for the antiferromagnetic order. For the lowest line we have indicated the  $A$  and  $B$  sublattices as well as the sublattice parity defined in figure 1.3. This shows that the stripes are domain walls of equal sublattice parity and the parity changes sign across the stripe.

geometrical quantity, the so called sublattice parity which has to do with the notion of bipartiteness. A lattice is called bipartite when it can be subdivided into two sublattices  $A$  and  $B$ , such that all sites on the  $A$  sublattice are neighbored by  $B$  sublattice sites and vice versa. This division can be done in two ways ( $\dots - A - B - A - B \dots$  and  $\dots - B - A - B - A \dots$ , see figure 1.3) defining a  $Z_2$  valued quantity  $p = \pm 1$ , which we will refer to as the sublattice parity. Stripe order means that every time one passes a charge stripe, the sublattice parity  $p$  changes sign. This is indicated in figure 1.2. One can refer to this as the ordering of the sublattice parity. This 'topological' aspect of the stripe order can be seen as a form of long range order, which is of geometrical nature. So when only fully connected stripes occur, the stripes are domain walls of regions of equal sublattice parity as is shown in figure 1.4a. In this figure the value for the sublattice parity is indicated and the lines represent the stripes.

In their article [13], Zaanen and Nussinov showed that the destruction of the sublattice parity order is governed by an Ising gauge theory. This transition is due to the fact that topological excitations associated with the destruction of charge and the excitations responsible for the disordering of the sublattice parity are different, as is shown in figure 1.4. The charge dislocations, represented by connected stripes, cause the charge to disorder but leave the sublattice parity intact. On the other hand, the stripe dislocations which are represented by stripes coming to an end destroy both charge and sublattice parity order. When the charge dislocations quantum proliferate, the sublattice parity turns into an Ising gauge field, and the confinement transition of the gauge theory describes the unbinding of charge dislocations into stripe dislocations. For small doping

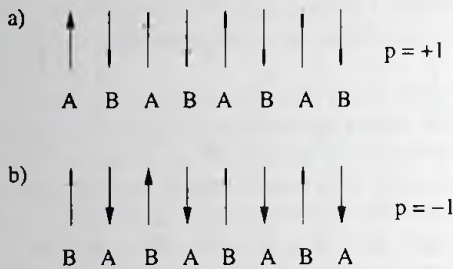


Figure 1.3: The subdivision of an antiferromagnetic chain into  $A$  and  $B$  sublattices according to a sublattice parity  $p = +1$  and  $p = -1$ .

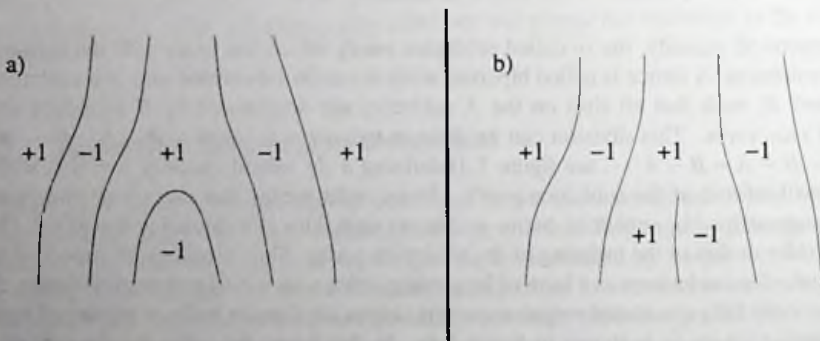


Figure 1.4: One can distinguish two types of topological defects in the stripe phase, namely charge dislocations (a) and stripes dislocations (b). The charge dislocations, represented by connected stripes, cause the charge to disorder but leave the sublattice parity intact, whereas the stripe dislocations, represented by stripes coming to an end, destroy both charge and sublattice parity order. In these figures, the  $+1$  or  $-1$  indicates the value of the sublattice parity and the lines represent the stripes.

the dislocations are suppressed and we are in the deconfined phase of the  $Z_2$  gauge theory. For higher doping the dislocations have a finite density and proliferate destroying the sublattice parity. This is the confining phase of the  $Z_2$  gauge theory. It is suggested that this quantum phase transition might be the one responsible for the quantum criticality near optimal doping in the high  $T_c$  superconductors. However, since the order in this confinement-deconfinement transition is topological, one needs to consider non-local correlation functions to observe this. But experimentally, it is very difficult to measure such correlation functions and therefore it is called hidden order.

Up to now, we implicitly assumed that not only the charge order but also the antiferromagnetic spin order is fully destroyed. This leads to two phases, a deconfining and confining phase. However, there is also another possibility. In principle a state can occur where the charge is disordered while next to the ordering of the sublattice parity also the spin system is antiferromagnetic ordered. However due to the stripe fluctuations this is a spin nematic instead of a normal antiferromagnet. Also this phase can easily be calculated with a gauge theory which is the quantum interpretation of the classical  $O(3)/Z_2$  model. Such models were studied in great detail by Lammert, Rokhsar and Toner [16] and Senthil and Fischer [17].

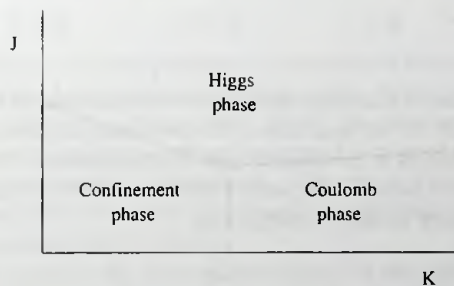


Figure 1.5: The quantum interpretation of the  $O(3)/Z_2$  model has three phases [16]. One phase in which the spins are ordered the Higgs phase or quantum spin nematic phase and two phases where the spins are disordered, namely the confinement phase where stripe dislocations proliferate and the Coulomb phase where they are suppressed.

The phase diagram of this model has the previously outlined three phases as function of the interaction  $J$  of the spins and the  $Z_2$  confining-deconfining parameter  $K$ . For small  $J$ , the spin system is disordered and we find the two phases which were discussed first, the confinement phase in which stripe dislocations occur, and the so called Coulomb phase in which the dislocations are suppressed. For large  $J$  the spin is ordered and we obtain the quantum spin nematic phase, which is also referred to as the Higgs phase. The phase diagram is depicted in figure 1.5.

In summary, the sublattice parity order is important to distinguish different phases in

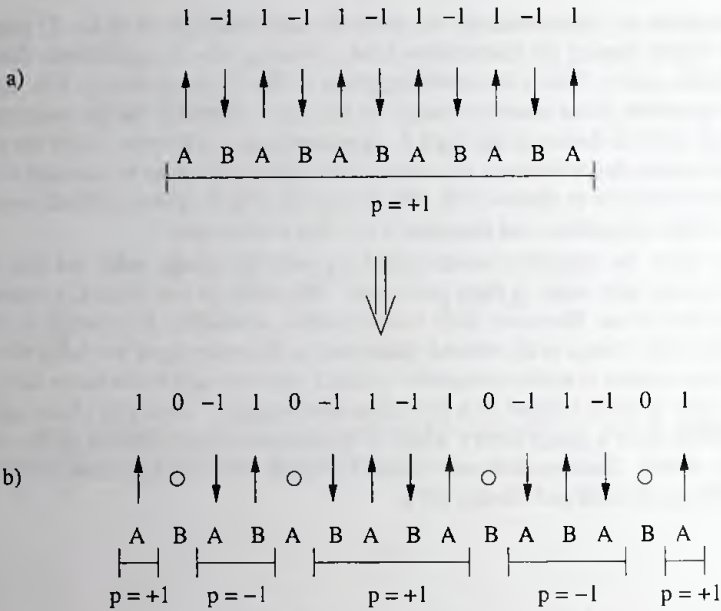


Figure 1.6: Construction of a configuration in the AF spin ordered fluid phase by insertion of holes to a perfect AF without holes. The two configurations are denoted both in the spin-1 representation as in the diluted spin- $\frac{1}{2}$  reformulation. This process changes on the constant sublattice parity in the perfect holefree AF. Due to this process, the holes cause the sublattice parity locally to change sign.

these two dimensional system. In this thesis we investigate to what extend the sublattice parity order occurs in one dimensional Luttinger Liquids represented by the Hubbard model. A similar study was done on Haldane spin-1 chains by den Nijs and Rommelse [18], which we address first in the next section.

## 1.4 The hidden order in Haldane spin-1 chains

As was shown by den Nijs and Rommelse [18], sublattice parity order also occurs in Haldane spin-1 chains. This is most easily seen when the spin-1 chain is described as a diluted spin- $\frac{1}{2}$  chain. In this language the state  $S^z(x) = 0$  in the spin-1 model represents an empty site and  $S^z(x) = \pm 1$  denotes a site occupied by spin- $\frac{1}{2}$  particles with respectively spin up or spin down. Using this reformulation, the phase diagram consists of different regions where the spin- $\frac{1}{2}$  particles behave like a solid, fluid or dilute gas with or without long-range AF spin order.

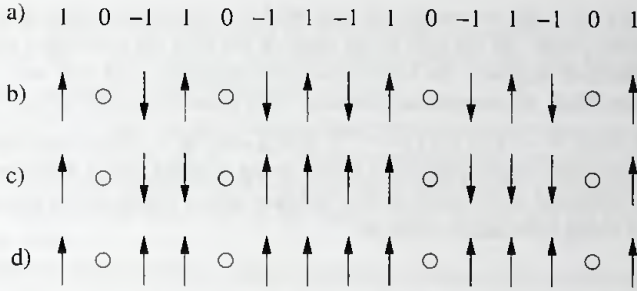


Figure 1.7: A typical configuration in the AF spin ordered fluid phase depicted (a) in the spin-1 Haldane chain representation and (b) in the diluted spin- $\frac{1}{2}$  reformulation. Figure c displays the staggered spin  $M^z(x) = (-1)^x S^z(x)$  and figure d shows the altered staggered spin  $(M')^z(x) = (-1)^{\sum_{j=-\infty}^x (1-n(j))} M^z(x)$ . The positions of the spin  $\frac{1}{2}$  particles are ordered and the spins have AF long-range order. Using  $(M')^z(x)$  the chain in figure b turns into a FM like spin fluid.

Consider the phase where the positions of the particles behave like a fluid while the spins are AF ordered. A typical configuration of this phase in both spin-1 and dilute spin- $\frac{1}{2}$  language is depicted in figure 1.6b. Since the spins are AF ordered, one can construct this configuration from a perfect holefree AF ordered state by inserting holes, which are  $S^z(x) = 0$  states in the diluted spin  $\frac{1}{2}$ . This process is indicated in figure 1.6a. We will refer to this perfect holefree AF ordered state as 'squeezed space' because it can be obtained by 'squeezing' out the holes.

The process of inserting the holes has an impact on the sublattice parity defined in figure 1.3. Since the spins in the squeezed space are AF ordered, the sublattice parity is uniformly constant. Let us fix the gauge in squeezed space, by choosing a particular sublattice parity, let say  $p = +1$ , and consider what happens when we insert the holes. In this process of unsqueezing, together with the holes, also the lattice sites are inserted. These lattice sites cause the sublattice parity to flip sign every time a hole is passed. So the insertion operation can be parametrized by attaching a sublattice parity flip to every hole.

In figure 1.7 we have displayed the configuration of figure 1.6 again together with its staggered magnetization  $M^z(x) = (-1)^x S^z(x)$ . Here one can see that the sublattice parity flip induced by the hole causes a kink in the staggered magnetization. Since the particles behave like a fluid, these holes and thus the kinks fluctuate which cause the spin-spin correlation function to be zero with  $\langle S^z(x) S^z(0) \rangle \rightarrow 0$  for large  $x$ .

So although the configuration in figure 1.7 clearly displays an order, the spin-spin correlation function is not the proper correlator to measure it. Instead of the normal spin  $S^z(x)$  or the staggered spin  $M^z(x)$ , one can consider the altered staggered spin  $(M')^z(x) = (-1)^{\sum_{j=-\infty}^x (1-n(j))} M^z(x) = (-1)^{\sum_{j=-\infty}^x n(j)} S^z(x)$  which is pictured in figure

1.7d. Here  $n(x) = 0$  for an empty site and  $n(x) = 1$  for an occupied site. So every time one crosses a hole, all the spin to the right of the hole are multiplied with a minus sign. This function removes the kinks from the staggered spin and turn the system into a FM spin fluid. Its correlation function does show the order in the system with  $\langle (M')^z(x)(M')^z(0) \rangle = -\langle S^z(x)(-1)^{\sum_{j=1}^{x-1} n(j)} S^z(0) \rangle = C \neq 0$ . This correlation function measures not just one single spin, but a whole string of spins and is therefore very non-local. So the sublattice parity order in this Haldane spin-1 chain can be measured using this non-local string correlation function.

## 1.5 Hidden order in Luttinger Liquids

Now let us focus on the order described in this thesis. We will show that Luttinger Liquids represented by the positive  $U$  Hubbard model, display the (quasi) hidden sublattice parity order. This is a new kind of order that has been overlooked in previous studies of the Luttinger Liquid.

The sublattice parity order becomes most transparent in the Bethe Ansatz solution of the one dimensional Hubbard model in the limit  $U \rightarrow \infty$  as described by Woynarovich, Ogata and Shiba [19, 20]. Generally speaking, the Bethe Ansatz provides for every Coulomb interaction  $U$  the complicated way in which the spin and charge degrees of freedom are entangled [21]. The spin degrees of freedom depend on the charge degree of freedom and vice versa. Only in the limit of large  $U$  these equations are disentangled and show a relative simple structure. In that limit the wave function is built from first placing the electrons with unspecified spin over the lattice like spinless fermions and subsequently distributing the spins over these electrons like the spins on an undoped Heisenberg chain. This construction is very similar to the construction of the wave function for the Haldane spin-1 chain and suggests that behind the complicated wave functions a simple internal spin system is present in which the spins live, where the spins have antiferromagnetic interactions. This spin system is obtained by squeezing out all the holes and is therefore also referred to as the squeezed chain. Note that this internal spin system is only accessible to the spins and not to external observers like a person who is doing an experiment. For an external observer this simple spin system is obscured by the movement of the holes, resulting in the complicated wave function calculated by the Bethe Ansatz. It can easily be shown that this construction of the wave function gives rise to sublattice parity order, indicating that the spins are anti-parallel over a hole. Or more precise, the holes can be thought of as providing an antiferromagnetic exchange interaction between its neighboring spin. One can view this as the holes binding to flips in the sublattice parity.

Is this construction also valid for intermediate  $U$ ? We show that the algebraical order in these one dimensional systems displays a lot of information and reveals the presence of quasi sublattice parity topological order. This can be demonstrated by considering the non-local order string correlator  $\langle S^z(x)(-1)^{\sum_{j=1}^{x-1} n_{\text{ol}}(j)} S^z(0) \rangle$ . If the sublattice parity is ordered, we expect the operator  $(-1)^{\sum_{j=1}^{x-1} n_{\text{ol}}(j)}$  to untangle the obscuring effect of the holes on the wave function and reach the internal spin space. This space con-

sists only of singly occupied sites and all of the holes and doubly occupied sites have been squeezed out. Using various calculations we demonstrate that for all  $U \geq 0$ , the squeezed spin correlator  $\langle S^z(x)(-1)^{\sum_{j=1}^{x-1} n_{tot}(j)} S^z(0) \rangle \sim -1/x^{K_s}$  and thus has an algebraic order which is longer ranged than the usual unsqueezed spin-spin correlation function  $\langle S^z(x)S^z(0) \rangle \sim \cos(2k_F x)/x^{K_s+K_c}$ . So by considering the squeezed spin correlator, we do indeed measure asymptotically the spin-spin correlations as they are seen by the spins in the internal spin space free of any holes, which proves that the system has sublattice parity order.

The sublattice parity order can also be denoted in terms of the elementary collective excitations of the Luttinger Liquid, the spinon and the holon which are depicted in figure 1.1. Spinons and holons cause kinks in the staggered magnetization  $M^z(x)$ , which are responsible for the decay of the staggered spin-spin correlation function. This can be seen from the Parola and Sorella approximation for the staggered spin correlator in the  $U \rightarrow \infty$  limit [22] valid for large distances  $x$

$$\begin{aligned} \langle M^z(x)M^z(0) \rangle &\sim \langle n_{tot}(x)(-1)^{\sum_{j=1}^{x-1}(1-n_{tot}(j))} n_{tot}(0) \rangle \langle S^z(\rho_{tot}x)S^z(0) \rangle_{par.Heis.} \\ &\sim \frac{\cos[(2k_F - \pi)x]}{\sqrt{x}} \frac{1}{x}. \end{aligned} \quad (1.4)$$

The first decaying term in this product is caused by the kinks attached to the holons. The second one is produced by the fluctuations of the kinks due to the spinons in the internal spin system. Note that, because we are using the staggered magnetization, we lost the staggering terms and the spin correlations have turned into those of an effectively parallel spin system with  $\langle S^z(\rho_{tot}x)S^z(0) \rangle_{par.Heis.} = |\langle S^z(\rho_{tot}x)S^z(0) \rangle_{Heis.}| \sim 1/x$ .

In this thesis we demonstrate that a similar approximation is valid away from the limit  $U \rightarrow \infty$ . We show that the staggered magnetization correlator can be written as

$$\begin{aligned} \langle M^z(x)M^z(0) \rangle &\sim \langle n_s(x)(-1)^{\sum_{j=1}^{x-1}(1-n_s(j))} n_s(0) \rangle \langle S^z(\rho_s x)S^z(0) \rangle_{par.internal} \\ &\sim \frac{\cos[(2k_F - \pi)x]}{x^{K_c}} \frac{1}{x^{K_s}}. \end{aligned} \quad (1.5)$$

Here  $n_s(x)$  is the density operator for single occupied sites, defined by  $n_s(x) = 1$  for single occupied sites and  $n_s(x) = 0$  for double or non occupied sites. The correlator  $\langle S^z(\rho_s x)S^z(0) \rangle_{par.internal} = |\langle S^z(\rho_s x)S^z(0) \rangle_{internal}|$  describes the spin correlations in the internal spin space which are rescaled Heisenberg correlations. This term is proportional to  $1/x^{K_s}$  and describes the decay caused by spinons in the internal space. Note again that in this procedure the spin correlations are similar to those of an effectively parallel spin system. The first term in (1.5) is due to the fluctuations of holon kinks. This formula is valid for all  $U \geq 0$ . In the limit  $U \rightarrow \infty$ , we find  $n_s(x) \rightarrow n_{tot}(x)$  and formula (1.5) equals equation (1.4).

Formula (1.5) indicates that in calculating the spin correlator  $\langle M^z(x)M^z(0) \rangle$  for  $U \geq 0$ , the wave function can be thought of to first order as constructed in a similar way as in the limit  $U \rightarrow \infty$  used by Parola and Sorella. The difference is that now we only consider the single occupied sites. So for general  $U$  we first place the single occupied electrons with unspecified spins over the lattice such that  $\langle n_s(x)n_s(0) \rangle \sim \rho_s^2$  and

subsequently we distribute the spins over these electrons like the spins on a chain with a spin correlator  $\langle S^z(x)S^z(0) \rangle_{\text{internal}} \sim (-1)^x/x$ . Note that in this construction doubly occupied sites are treated as empty sites. This is correct since  $S^z(x) = 0$  in both cases and therefore they can not be seen by the spin correlator. In the limit  $U \rightarrow \infty$ , the distribution of the spin sites becomes that of spinless fermions and the correlations of the spins on these sites turn into those of spins on a Heisenberg chain.

Using this interpretation using holons and spinons we also can investigate the effect of the sublattice parity operator  $(-1)^{\sum_{j=1}^{x-1}(1-n_{\text{tot}}(j))}$ . In adding the operator to the staggered spin operator  $M^z(x)$ , we remove the kinks due to the holons. This can be seen in the correlator function

$$\begin{aligned} \langle M^z(x)(-1)^{\sum_{j=1}^{x-1}(1-n_{\text{tot}}(j))} M^z(0) \rangle &\sim \langle n_s(x)n_s(0) \rangle \langle S^z(\rho_s x)S^z(0) \rangle_{\text{par.internal}} \\ &= \rho_s^2 \langle S^z(\rho_s x)S^z(0) \rangle_{\text{par.internal}} \\ &\sim \frac{1}{x} = \frac{1}{x^{K_s}}, \end{aligned} \quad (1.6)$$

with  $\rho_s = \langle n_s(x) \rangle$ . So by multiplying the operator  $(-1)^{\sum_{j=1}^{x-1}(1-n_{\text{tot}}(j))}$  to the spin operator, we remove the decay of the holons and we measure the rescaled internal spin-spin correlations. This indicates that the system has quasi sublattice parity order.

Using a similar method we can remove the influence of the spinons on the spin correlation function. This is done by multiplying the staggered magnetization  $M^z(x)$  with the operator  $M^z(x)(-1)^{\sum_{j=1}^{x-1}(1-n_{\text{tot}}(j))}$  instead of the term  $(-1)^{\sum_{j=1}^{x-1}(1-n_{\text{tot}}(j))}$ . We will show that the correlation function of this product operator equals

$$\begin{aligned} \langle (M^z(x))^2 (-1)^{\sum_{j=1}^{x-1}(1-n_{\text{tot}}(j))} (M^z(0))^2 \rangle &= \frac{1}{16} \langle n_s(x)(-1)^{\sum_{j=1}^{x-1}(1-n_s(j))} n_s(0) \rangle \\ &\sim \frac{\cos[(2k_F - \pi)x]}{x^{K_c}}, \end{aligned} \quad (1.7)$$

and yields only the decaying term caused by the holes.

Finally we can wonder what happens if we first remove the holon kink and subsequently we take out the kink attached to the spinon or vice versa. This process yields the operator  $(M^z(x))^2$  and the correlator function gives

$$\langle (M^z(x))^2 (M^z(0))^2 \rangle = \frac{1}{16} \langle n_s(x)n_s(0) \rangle. \quad (1.8)$$

To zeroth order this correlator is proportional to  $\rho_s^2 = \langle n_s(x) \rangle^2 = \rho_s^2$  and describes the lattice of single occupied sites on which the spins contributing to the correlator  $\langle S^z(x)S^z(0) \rangle_{\text{internal}}$  are defined.

In summary, the construction of the wave function using equation (1.5) which is described above gives rise to sublattice parity order and indicates that the spins have anti-parallel spin interactions over holes or a doubly occupied sites. This form of hidden order in these systems can be unveiled by considering the squeezed string operator  $O_{\text{top}}(x) = -\langle S^z(x)(-1)^{\sum_{j=1}^{x-1} n_{\text{tot}}(j)} S^z(0) \rangle$ .

## 1.6 Outline of the thesis

The thesis is organized in the following manner.

Before turning to the subject of the hidden order in Luttinger Liquids we start by taking a closer look at the pseudogap regime in chapter 2 and study the effect of a single magnetic and nonmagnetic impurity in high  $T_c$  superconductors. We will predict that as long as the band density of states is depleted at the Fermi energy the existence of impurity resonant states is robust regardless of the microscopic origin of the pseudogap state.

In chapter 3 we summarize the main properties of Luttinger Liquids. Using the technique of bosonization, the results for the usual density-density and spin-spin correlation function are described. Furthermore, we bosonize the one dimensional Hubbard model giving the relation between the Hubbard model and a generic Luttinger Liquid.

The Bethe Ansatz for the Hubbard model for general Coulomb repulsion  $U$  is introduced in chapter 4. This is used as an introduction for the technique used by Parola and Sorella to calculate the spin-spin correlation function  $\langle S^z(x)S^z(0) \rangle$  in the  $U \rightarrow \infty$  limit.

In chapter 5 we study the sublattice parity order in the Hubbard model as it can be seen from the Bethe Ansatz wave function in the  $U$  large limit. We introduce the topological correlator  $O_{top}(x) = -\langle S^z(x)(-1)^{\sum_{j=1}^{x-1} n_{tot}(j)} S^z(0) \rangle$ , which can be used to demonstrate the sublattice parity order and show that in the large  $U$  limit  $O_{top}(x) \sim 1/x^{K_s}$ , indicating that the sublattice parity is ordered.

In chapter 6 we consider a different limit of the Hubbard model, namely the case of no Coulomb interactions ( $U = 0$ ), which reduced to a gas of spinless fermions. We will calculate the topological correlator  $O_{top}(x)$  and show that the sublattice parity is also ordered in this limit.

After the discovery of sublattice parity order for  $U = 0$  and  $U \rightarrow \infty$  we turn in chapter 7 to the technique of bosonization in order to demonstrate sublattice parity order for intermediate Coulomb repulsion  $U$ . But as it turns out, bosonization is not equipped to calculate non-local string correlators like  $O_{top}(x)$ .

To resolve the ambiguity in the bosonization results McCulloch performed DMRG calculations which are analysed in chapter 8. This study indicates that the sublattice parity is also ordered for intermediate Coulomb repulsion  $U \geq 0$ .

In the final chapter 9 we will interpret the results found in the previous chapters and describe what the sublattice parity order means in terms of spinons and holons. Furthermore, we investigate whether the sublattice parity order is induced by a local gauge symmetry.



## Chapter 2

# Pseudogap

Before addressing the issue of the hidden order correlations in one dimension, we will first take a closer look at the pseudogap regime in this chapter and investigate impurities in high  $T_c$  superconductors. This work was done together with Balatsky and Martin at the Los Alamos National Laboratory and published in [23]. We predict a resonance impurity state generated by the substitution of one  $Cu$  atom with a nonmagnetic atom, such as  $Zn$ , in the pseudogap state of a high- $T_c$  superconductor.

### 2.1 Introduction

The copper oxide high temperature superconductors are constructed from  $CuO_2$  planes and the superconductivity is believed to originate from strongly interacting electrons in these planes. The effects of a single magnetic and a nonmagnetic impurity in such a plane have been studied intensively both theoretically [24–28] and more recently experimentally by scanning tunneling microscopy (STM) [29–31]. Understanding of the impurity states in these high- $T_c$  materials is important because the impurity atoms qualitatively modify the superconducting properties, and these impurity-induced changes can be used to identify the nature of the pairing state in superconductors.

In this chapter we investigate the impurity induced resonance, or quasibound state, which is generated by a strong nonmagnetic impurity scattering in a  $CuO$  plane in the normal state of high- $T_c$  materials. Specifically we calculate the resonant state generated by the substitution of one  $Cu$  atom with a  $Zn$  atom using the self consistent  $T$  matrix approach. We rely on the fact that the density of states (DOS) is depleted at the Fermi energy in the pseudogap regime. We argue that the mere fact that the DOS is depleted at the Fermi energy is sufficient to produce a resonance near the nonmagnetic impurity, such as  $Zn$ . However no particular use of the superconducting correlations above  $T_c$  is needed in our analysis. For example, the results we present will be valid in the pseudogap state with no superconducting phase or amplitude fluctuations above  $T_c$ , as long as there are interactions that lead to the pseudogap state, as indicated by a depleted DOS. This is an important feature that broadens the validity of the model regardless of the

microscopic origin of the pseudogap in the high- $T_c$  superconductor. The approach we take is similar to a previous analysis of the nonmagnetic impurity in the superconducting state [24]. See also Figure 2.1.

Up to now, the theoretical analysis of the impurity states has been focused on the low temperature regime  $T \ll T_c$ , well below the superconducting transition temperature  $T_c$ . On the other hand it is well known that in the normal state ( $T \geq T_c$ ) of the underdoped cuprates, the electronic states at the Fermi energy are depleted due to the pseudogap (PG)  $\Delta_{PG}$ , as was seen by STM [32] and by angular resolved photoemission [33]. One can consider the temperature evolution of the impurity state as the temperature increases and eventually becomes larger than  $T_c$ . Then there are two possibilities for the evolution of the impurity resonance at  $T > T_c$ : a) the impurity resonance gradually broadens until the superconducting gap vanishes, at which point the impurity resonance totally disappears and b) the resonance broadens, but still survives above  $T_c$ . Which of these two possibilities is realized depends on the normal state phase that the superconductor evolves into. It has been argued [34,35] that in the underdoped regime the superconducting gap opens up in addition to the pseudogap present well above  $T_c$ . In this chapter we claim that the depletion of states due to the pseudogap regime gives rise to a resonance impurity state. Hence, we find that the impurity resonance survives above  $T_c$  in the pseudogap state of high- $T_c$  materials. The position and the width of the resonance are determined by the impurity scattering strength and the pseudogap scale. In the absence of a pseudogap above  $T_c$  the impurity state disappears.

## 2.2 $T$ -matrix approximation

The Hamiltonian for the problem of a single potential impurity of local strength  $U$  is given by

$$\begin{aligned} H &= H_0 + H_{imp}, \\ H_{imp} &= U \hat{n}_0 = U \sum_{\mathbf{k}\mathbf{k}'\sigma} c_{\mathbf{k}\sigma}^\dagger c_{\mathbf{k}'\sigma}, \end{aligned} \quad (2.1)$$

where  $H_0$  is the Hamiltonian for the clean system, with the corresponding Green function  $G_{\mathbf{k}}$ . The scattering  $T$ -matrix [24] can be written as

$$T = \frac{U}{1 - U \sum_{\mathbf{k}} G_{\mathbf{k}}(\omega)} = \frac{U}{1 - U G_0(\omega)}, \quad (2.2)$$

with  $G_0(\omega)$  the on site Green's function. The states generated by the impurity are given by the poles of the  $T$  matrix:

$$G_0(\Omega) = \frac{1}{U}. \quad (2.3)$$

This is an implicit equation for  $\Omega$  as a function of  $U$ , the strength of the scattering. This solution can be complex, indicating the resonant nature of the virtual state. To solve this equation, we split  $G_0$  into its real and imaginary part  $G_0 = G'_0 + iG''_0$ . Note that  $G''_0(\omega) = -\pi N_0(\omega)$ , with  $N_0(\omega)$  the density of states.

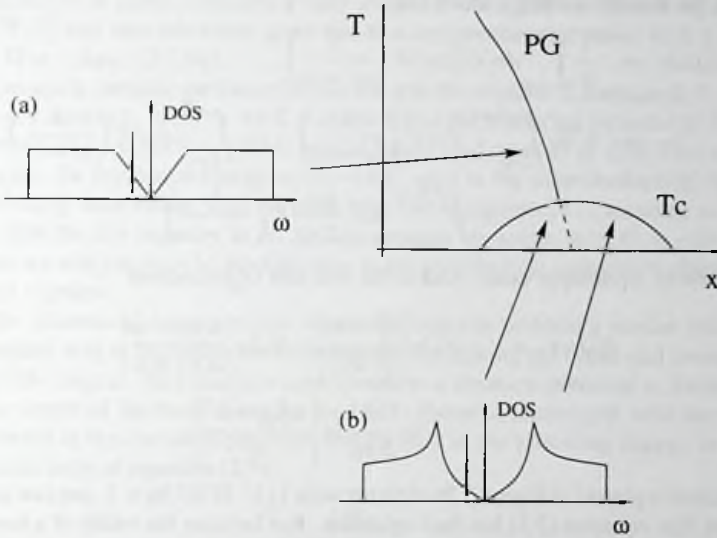


Figure 2.1: An impurity state in a high  $T_c$  superconductor: (a) The DOS in the pseudogap regime used in this article (see also [11]), and (b) the DOS in the superconducting state as was used in [24]. In both phases there is a resonant state.

To be specific, we need a model DOS that captures the main features of the pseudogap in high- $T_c$  materials. For this purpose we use the DOS that was measured by Loram *et al.* [34]. These measurements on the electronic specific heat show that the normal state pseudogap opens abruptly in the underdoped region below a hole doping equal to  $p_{crit} \sim 0.19$  holes/ $CuO_2$ . Inspired by these data, we will assume that around the pseudogap region, states are partly depleted and the density of states is linear, that is  $N(\omega) = N_0|\omega|/\Delta_{PG}$  for  $|\omega| \leq \Delta_{PG}$  and  $N(\omega) = N_0$  for  $\Delta_{PG} < |\omega| < W/2$  with  $W$  the bandwidth. This density of states is depicted in figure 2.2a. As it is obvious from the solution of equation (2.3), the precise position and the width of the resonance will depend on the specific form of the pseudogap. For starters, we will use this linearly vanishing pseudogap DOS. Later, we will briefly consider the results for other forms of  $N(\omega)$  like a fully gapped DOS or a DOS with a quadratic dependent gap, which can be obtained in the same way and lead essentially to similar expressions.

From the Kramer-Kronig relation [42]

$$\begin{aligned}
 G'_0(\omega) &= \frac{1}{\pi} \int_{-\infty}^{\infty} d\omega' G''_0(\omega') P\left(\frac{1}{\omega' - \omega}\right) \\
 &= -N_0 \int_{-\frac{W}{2}}^{-\Delta_{PG}} d\omega' P\left(\frac{1}{\omega' - \omega}\right) - N_0 \int_{\Delta_{PG}}^{+\frac{W}{2}} d\omega' P\left(\frac{1}{\omega' - \omega}\right) \\
 &\quad - N_0 \int_{-\Delta_{PG}}^{+\Delta_{PG}} d\omega' \frac{|\omega|}{\Delta_{PG}} P\left(\frac{1}{\omega' - \omega}\right), \tag{2.4}
 \end{aligned}$$

with  $P$  Cauchy's principle value. And so the real part  $G'_0(\omega)$  equals

$$\begin{aligned}
 G'_0(\omega) &= -N_0 \ln \left| \frac{\frac{W}{2} - \omega}{\frac{W}{2} + \omega} \right| + N_0 \ln \left| \frac{\Delta_{PG} - \omega}{\Delta_{PG} + \omega} \right| \\
 &\quad - N_0 \frac{\omega}{\Delta_{PG}} \ln \left| \frac{\Delta_{PG}^2 - \omega^2}{\omega^2} \right|. \tag{2.5}
 \end{aligned}$$

This function is plotted in Figure 2.2b together with  $1/U$ . If  $2UN_0 > 1$ , one can see from this figure that equation (2.3) has four solutions. But because the width of a resonance state is proportional to  $|\Omega|$ , the only state with sharp width is the solution with  $|\Omega|$  close to zero and we will only consider this solution. After the expansion in  $\omega$  of equation (2.5) we arrive at an expression for this solution  $\Omega$  of equation (2.3):

$$G_0(\Omega) = -\frac{2\Omega N_0}{\Delta_{PG}} \left[ \ln \left| \frac{\Delta_{PG}}{\Omega} \right| + 1 - \frac{i\pi \operatorname{sign}(U)}{2} \right] = \frac{1}{U}. \tag{2.6}$$

This equation can be solved exactly in terms of LambertW functions  $Lw(-1, x)$ . The exact solution equals  $\Omega = -\Delta_{PG} \operatorname{sign}[U] \exp[Lw(-1, B(U, N_0))] + 1 - i\pi/2$  where the term  $B(U, N_0)$  equals  $B(U, N_0) = -\operatorname{sign}[U] \exp[i\pi/2 - 1]/(2N_0U)$  and  $Lw(x)$  is defined by  $Lw(x) \exp Lw(x) = x$ . To logarithmic accuracy this solution equals

$$\begin{aligned}
 \Omega &= \Omega' + i\Omega'' \\
 &= -\frac{\Delta_{PG}}{2UN_0} \frac{1}{\ln|2UN_0|} \left[ 1 - \frac{1}{\ln|2UN_0|} + \frac{i\pi \operatorname{sign}(U)}{2 \ln|2UN_0|} \right]. \tag{2.7}
 \end{aligned}$$

Here  $\Omega'$  is the energy and  $\Omega''$  denotes the decay rate of the impurity state. Furthermore we have assumed the impurity scattering to be strong enough so that the result can be calculated to logarithmic accuracy with  $\ln|2UN_0| > 1$ .

These results strongly depend on the specific shape of the DOS. However, we argue that the appearance of the intragap impurity state is a robust feature of any depleted DOS around the Fermi energy. We also considered the model DOS with a quadratic dependent gap where  $N(\omega) = N_0 [a + (1-a)\omega^2/\Delta_{PG}^2]$  which leads essentially to similar results as a function of the impurity strength with a resonant state at

$$\begin{aligned}
 \Omega &= -\frac{\Delta_{PG}}{4N_0U(1-a-\Delta_{PG}/W)} [1 + i\pi a N_0U] \\
 &\approx -\frac{\Delta_{PG}}{(4N_0U(1-a))} [1 + i\pi a N_0U] \tag{2.8}
 \end{aligned}$$

when  $\Delta_{PG}/W$  is small. But also a fully gapped DOS equal to  $N(\omega) = N_0$  for  $|\omega| \in [\Delta_{PG}, W/2]$  and zero otherwise gives rise to a comparable expression with a resonant state at  $\Omega = -\Delta_{PG}/(2UN_0)$ .

Let us again consider the linear DOS leading to the solution of formula (2.7), and taking  $N_0 = 1$  state/eV,  $\Delta_{PG} \sim 300K \sim 30meV$  and the scattering potential  $U \approx \pm 2eV$ , we estimate  $\Omega \sim \pm 2meV \sim \pm 20K$  as was found by Loram *et al.* [34] This energy is close to the Zn resonance energy  $\omega_0 = -16K$ , seen in the superconducting state [29]. By combining these results with the band-structure arguments [41], we come to the conclusion that the Zn impurity in Bi2212 is strongly attractive, with  $U \sim -2eV$ . This result, as we will see, may be modified due to the particle-hole asymmetry characteristic of doped cuprates.

In the absence of a particle-hole symmetry, one can perform a similar calculation. The simplest way to introduce the asymmetry is by making the upper and lower cutoffs in the DOS unequal. This situation corresponds to a chemical potential  $\mu$ , located away from the center of the band. Keeping the DOS otherwise unchanged, with the pseudogap centered at the chemical potential, results only in the following change in the first logarithmic term of equation (2.5):

$$-N_0 \ln \left| \frac{\frac{W}{2} - \mu - \omega}{\frac{W}{2} + \mu + \omega} \right|. \quad (2.9)$$

Neglecting the frequency  $\omega$  relative to the chemical potential  $\mu$  and assuming that  $\mu$  is small relative to the bandwidth, we obtain that the results for the asymmetric case can be obtained from the symmetric ones by the substitution

$$\frac{1}{U} \rightarrow \frac{1}{U} - \frac{4N_0\mu}{W}. \quad (2.10)$$

The effect of the asymmetry term can be estimated for superconducting cuprates. For 20% hole doping,  $\mu \sim -(1/5)W/2 = -W/10$ . Hence, the modified value for the Zn impurity strength in Bi2212 can be obtained from the symmetric result,  $1/U^* = 1/U + 4N_0\mu/W$ . The new value is  $U^* \sim -1 eV$ , which is a strongly attractive potential, as is expected from the band structure arguments.

The solution of the impurity state deep in the superconducting regime involves two aspects: the energy position and the width of the resonance and secondly, the real space shape of the impurity state. We have discussed the energy of the impurity state above. A great advantage of the on-site impurity solution for the localized potential  $U$  is that only the on-site propagator  $G_0(\omega)$  enters into the calculation. Hence, the knowledge of the DOS is sufficient to calculate the impurity state. On the other hand, to calculate the real space image of the impurity induced resonance, one would require more detailed knowledge of the Green's functions in the pseudogap regime. Quite generally, one would expect for a d-wave like pseudogap with nearly nodal points along the  $(\pm\pi/2, \pm\pi/2)$  directions, that the impurity resonance in the pseudogap regime would be four-fold symmetric, similar to superconducting solutions [24–31]. This calculation would require a specific model for the pseudogap state and goes beyond the scope of this investigation.

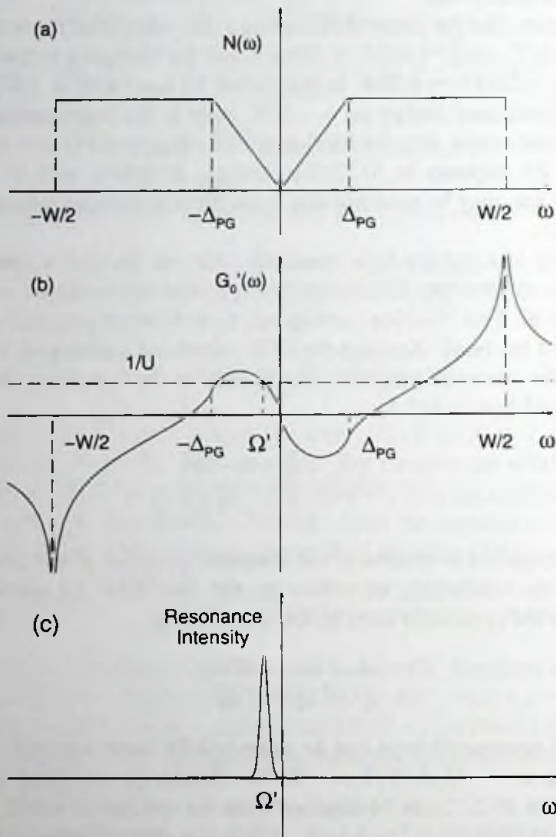


Figure 2.2: (a) The density of states  $N(\omega) = -G''_0(\omega)/\pi$ . Around the pseudogap states are only partly depleted e.g.  $N(\omega) = N_0|\omega|/\Delta_{PG}$ , where  $N(\omega) = N_0$  for  $\Delta_{PG} < |\omega| < W/2$  with  $W$  the bandwidth. (b) The real part  $G'_0(\omega)$  of Green's function together with  $1/U$  and  $U$  positive.  $\Omega'$  is the real part of the solution of the equation  $G_0(\Omega) = 1/U$  close to zero and therefore with sharp bandwidth. (c) The impurity induced resonance at  $\Omega' = -\Delta_{PG}/2UN_0 \ln(2UN_0)$ . Because the other three solutions of equation (2.3) have much broader bandwidth, they are not depicted here. All the figures are taken on the impurity site.

In conclusion, we present a theory for the resonance state that is induced by a non-magnetic impurity in the normal state of a high- $T_c$  superconductor in the pseudogap regime. The precise microscopic origin of the pseudogap is not important for this state to be formed, in particular this resonance will be present even in the absence of superconducting fluctuations in the normal state. The nature of this impurity resonance is similar to the previously studied resonance in the d-wave superconducting state. For the particular model of linearly vanishing DOS we find the impurity state energy, equation (2.7). We also analyze the effects of the particle-hole asymmetry. Impurity states survive at high temperature  $T > T_c$  since the pseudogap produces the DOS depletion. This depletion is all that is necessary to produce the intragap state.

## The linearization procedure

The linearization procedure is a standard technique used to solve the T-matrix equation in the normal state of a superconductor. It involves expanding the Green's function in powers of the impurity potential and keeping only the lowest order terms. This procedure is valid when the impurity potential is weak compared to the energy scale of the system. In the case of a pseudogap, the linearization procedure is still applicable, but the resulting equations are more complex due to the presence of the gap. The linearization procedure is used to derive the impurity state energy equation (2.7).

### 3.1. Linearizing system Green's function

The linearization procedure is a standard technique used to solve the T-matrix equation in the normal state of a superconductor. It involves expanding the Green's function in powers of the impurity potential and keeping only the lowest order terms. This procedure is valid when the impurity potential is weak compared to the energy scale of the system. In the case of a pseudogap, the linearization procedure is still applicable, but the resulting equations are more complex due to the presence of the gap. The linearization procedure is used to derive the impurity state energy equation (2.7).

$$G(\mathbf{k}, \omega) = \frac{1}{\omega - \epsilon_{\mathbf{k}} - \Sigma(\mathbf{k}, \omega)}$$

The linearization procedure is a standard technique used to solve the T-matrix equation in the normal state of a superconductor. It involves expanding the Green's function in powers of the impurity potential and keeping only the lowest order terms. This procedure is valid when the impurity potential is weak compared to the energy scale of the system. In the case of a pseudogap, the linearization procedure is still applicable, but the resulting equations are more complex due to the presence of the gap. The linearization procedure is used to derive the impurity state energy equation (2.7).

The linearization procedure is a standard technique used to solve the T-matrix equation in the normal state of a superconductor. It involves expanding the Green's function in powers of the impurity potential and keeping only the lowest order terms. This procedure is valid when the impurity potential is weak compared to the energy scale of the system. In the case of a pseudogap, the linearization procedure is still applicable, but the resulting equations are more complex due to the presence of the gap. The linearization procedure is used to derive the impurity state energy equation (2.7).



## Chapter 3

# The Bosonization procedure

In this chapter we summarize the main properties of a Luttinger Liquid. The dynamics of the electrons living in these one dimensional models is described using the technique of bosonization. Bosonization is based on the equivalence between interacting fermions and non interacting bosons [45]. Using this formalism, the fermion operators can be expressed in bosonic ones. In this chapter we review how to get expressions for correlation functions like  $\langle n_{tot}(x)n_{tot}(0) \rangle$  and  $\langle S^z(x)S^z(0) \rangle$  using these bosonization operators. But apart from showing these characteristics of a Luttinger liquid we will also need this introduction in chapter 7 where we will show that bosonization is not always suited in the calculation of string operators. We start our summary with the most simple example, the non-interacting spinless fermion gas. After this we consider interactions that finally lead to the bosonization of the Hubbard model.

### 3.1 The free spinless fermion gas

To explain the principles of bosonization [46] we will start by describing the method for the simple case of non-interacting spinless fermions in a one dimensional metal. The Hamiltonian describing this trivial problem consists only of a kinetic term

$$H = \sum_k \varepsilon_k c^\dagger(k)c(k), \quad (3.1)$$

with  $c(k)$  the electron annihilation operator at wave vector  $k$ . In a simple tight binding model the energy equals  $\varepsilon_k = -2t \cos k$ . Our main goal is to transform this fermionic expression into one consisting of bosonic terms. An important first step in doing this is linearization.

At low temperatures the energy band is filled to the Fermi energy  $\varepsilon_F$  and the particle-hole excitations are restricted to the regions near the Fermi points  $\pm k_F$ . In this case, it makes sense to linearize the electron dispersion around these Fermi points as depicted

in figure 3.1, and write the Hamiltonian (3.1) as

$$H = \sum_{q=\pm k_F} \sum_{k=-\Lambda}^{\Lambda} \left( \frac{\partial \varepsilon}{\partial k} \Big|_q \right) c^\dagger(q+k) c(q+k). \quad (3.2)$$

The energy derivative is related to the Fermi velocity  $v_F = \frac{\partial \varepsilon_k}{\partial k} |_{k_F} = -\frac{\partial \varepsilon_k}{\partial k} |_{-k_F}$ . We only consider states with distances  $\Lambda$  to the Fermi points as shown in figure 3.1 and imply a momentum cutoff  $\Lambda$ . In the Luttinger liquid model, this cutoff  $\Lambda$  is taken to infinity. This means that we add to the model an infinity of states far from the Fermi energy that were not present in the original model. We assert that adding these extra states far from the Fermi energy will not change the physics.

Using the linearization in (3.2) it is possible to identify (3.1) with a relativistic field theory of free Dirac fermions, as we now demonstrate. Namely, the expansion of the annihilation operator  $c(x)$  in position space around the Fermi points yields

$$c(x) = \sum_{q=\pm k_F} \int_{-\Lambda}^{\Lambda} \frac{dk}{2\pi} e^{i(q+k)x} c(q+k). \quad (3.3)$$

The operator  $c(x)$  can be expressed in terms of the so-called left and right mover operators

$$c(x) = e^{ik_F x} \psi(x) + e^{-ik_F x} \bar{\psi}(x), \quad (3.4)$$

where the right and left movers  $\psi(x)$  and  $\bar{\psi}(x)$  are defined as

$$\begin{aligned} \psi(x) &= \int_{-\Lambda}^{\Lambda} \frac{dk}{2\pi} e^{ikx} c(q+k_F) \\ \bar{\psi}(x) &= \int_{-\Lambda}^{\Lambda} \frac{dk}{2\pi} e^{-ikx} c(q+k_F). \end{aligned} \quad (3.5)$$

Using (3.2) and (3.5) it is easy to show that the Hamiltonian in (3.1) is exactly the Dirac Hamiltonian given by

$$H = -iv_F \int dx \left[ \psi^\dagger(x) \partial_x \psi(x) - \bar{\psi}^\dagger(x) \partial_x \bar{\psi}(x) \right], \quad (3.6)$$

and  $\psi$  and  $\bar{\psi}$  are completely decoupled. If we also consider the time dependence of  $\psi$ , the Hamiltonian equals

$$\begin{aligned} H &= -iv_F \int dx \left[ \psi^\dagger(x,t) \left( \partial_x - \frac{1}{v_F} \partial_t \right) \psi(x,t) - \bar{\psi}^\dagger(x,t) \left( \partial_x + \frac{1}{v_F} \partial_t \right) \bar{\psi}(x,t) \right] \\ &= -2v_F \int dx \left[ \psi^\dagger(z) \partial_z \psi(z) + \bar{\psi}^\dagger(\bar{z}) \partial_{\bar{z}} \bar{\psi}(\bar{z}) \right], \end{aligned} \quad (3.7)$$

where we make use of complex coordinates defined by

$$\begin{aligned} z &= -i(x - v_F t) \\ \bar{z} &= +i(x + v_F t). \end{aligned} \quad (3.8)$$

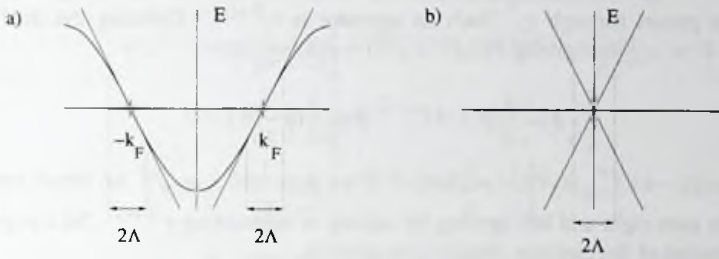


Figure 3.1: The energy dispersion for the non-interacting spinless fermions and the fermions in the Dirac Hamiltonian. Linearizing the dispersion and moving the branches to respectively the right and left maps both dispersions onto each other.

This shows that the spinless fermions can be mapped on massless ‘relativistic’ fermions, moving at the speed of light with  $c = v_F$ . How do we bosonize these fermions?

### 3.1.1 Bosonization of spinless fermions

Without going into details, we will sketch the basic ideas behind bosonization.<sup>1</sup>

The technique is based on the observation that particle hole excitations and thus the electron density  $n_{SF}(x)$  is bilinear in the electron fields and is therefore bosonic in character. Let us suppose that it is the derivative of a boson field  $\varphi(x)$

$$\begin{aligned} n_{SF}(x) &= -\frac{1}{\lambda} \partial_x \varphi(x) \\ \varphi(x) &= \lambda \int_x^\infty dy n_{SF}(y), \end{aligned} \quad (3.9)$$

where  $\lambda$  is a constant to be determined. This means that if we want to create a particle on site  $x$ , we have to create a kink of height  $\lambda$  in  $\varphi$  and  $\varphi$  has to be increased by  $\lambda$  at points to the left of  $x$ . We split the field  $\varphi$  into a left and a right moving part  $\varphi(x, t) = \phi(x - v_F t) + \tilde{\phi}(x + v_F t)$  or in complex variables  $\varphi(z, \bar{z}) = \phi(z) + \tilde{\phi}(\bar{z})$ . What is the expression for the creation operator for right movers?

Since the momentum operator generates displacement, our first guess would be

$$\psi^\dagger(x) \sim e^{-i\lambda \int_{-\infty}^x dy \Pi(y)}. \quad (3.10)$$

Here  $\Pi$  is the momentum density conjugate to  $\phi$  with  $[\phi(x), \Pi(y)] = i\delta(x - y)$ . However, this operator commutes with itself instead of satisfying anticommuting relations.

<sup>1</sup> Here the notation presented in [47] was used. Other reviews can be found in [46].

This can be repaired by multiplying it with an operator that changes sign each time a particle passes through  $x$ . Such an operator is  $e^{\frac{i\pi}{\lambda}\varphi(x)}$ . Defining the dual boson  $\partial_x \vartheta = -\Pi = -\frac{1}{v_F} \partial_t \varphi$  giving  $\vartheta(z, \bar{z}) = \phi(z) - \bar{\phi}(\bar{z})$  so that

$$\phi = \frac{1}{2}(\varphi + \vartheta) \quad \bar{\phi} = \frac{1}{2}(\varphi - \vartheta), \quad (3.11)$$

we can write  $-i\lambda \int_{-\infty}^x dy \Pi(y) = i\lambda \vartheta(x)$ . If we now take  $\lambda = \sqrt{\pi}$  we obtain operators which are pure right and left moving by adding or subtracting  $e^{\frac{i\pi}{\lambda}\varphi(x)}$ . So a reasonable representation of the electron creation operators is

$$\begin{aligned} \psi^\dagger(x) &= A e^{2i\sqrt{\pi}\phi(x)} \\ \bar{\psi}^\dagger(x) &= A e^{-2i\sqrt{\pi}\bar{\phi}(x)}. \end{aligned} \quad (3.12)$$

After the proper scaling of the field  $\psi$  one finds  $A = 1/\sqrt{2\pi}$ .

Using this heuristic and incomplete derivation of the bosonization principle we obtain the following bosonization formulas [47] for the right moving fermions

$$\begin{aligned} \psi(x) &= \frac{e^{-i\sqrt{4\pi}\phi(x)}}{\sqrt{2\pi}} \\ \psi^\dagger(x) &= \frac{e^{i\sqrt{4\pi}\phi(x)}}{\sqrt{2\pi}}, \end{aligned} \quad (3.13)$$

and similarly for the left movers

$$\begin{aligned} \bar{\psi}(x) &= \frac{e^{i\sqrt{4\pi}\bar{\phi}(x)}}{\sqrt{2\pi}} \\ \bar{\psi}^\dagger(x) &= \frac{e^{-i\sqrt{4\pi}\bar{\phi}(x)}}{\sqrt{2\pi}}. \end{aligned} \quad (3.14)$$

The bosonization formulas (3.13) and (3.14) are the basis for the translation of fermion operators to bosonic operators. Using these formulas we can for instance calculate the boson form of the fermion current operators  $J = \psi^\dagger \psi$  and  $\bar{J} = \bar{\psi}^\dagger \bar{\psi}$ . These operators contain the product of an exponent of the fluctuating field  $\phi$  and  $\varphi$  and we have to define this exponent carefully in order to gain finite averages of this operator. We can regularize this divergent product of two fields at the same point by adopting the point splitting prescription. For  $J(z)$  it is defined as

$$: J(z) : = \lim_{\epsilon \rightarrow 0} \left[ \psi^\dagger(z + \epsilon) \psi(z) - \langle \psi^\dagger(z + \epsilon) \psi(z) \rangle \right]. \quad (3.15)$$

From the mode expansion (3.5) one can show that the Green function  $\langle \psi^\dagger(z + \epsilon) \psi(z) \rangle$  equals

$$\langle \psi^\dagger(z + \epsilon) \psi(z) \rangle = \frac{1}{2\pi} \frac{1}{\epsilon}. \quad (3.16)$$

And so, using the bosonization formulation this can be expressed as

$$\begin{aligned}
 : J(z) : &= \frac{1}{2\pi} \lim_{\epsilon \rightarrow 0} \left[ e^{i\sqrt{4\pi}\phi(z+\epsilon)} e^{-i\sqrt{4\pi}\phi(z)} - \frac{1}{\epsilon} \right] \\
 &= \frac{1}{2\pi} \lim_{\epsilon \rightarrow 0} \left[ e^{i\sqrt{4\pi}[\phi(z+\epsilon) - \phi(z)]} \frac{1}{\epsilon} - \frac{1}{\epsilon} \right] \\
 &= \frac{1}{2\pi} \lim_{\epsilon \rightarrow 0} \left[ e^{i\epsilon\sqrt{4\pi}\partial_z\phi(z)} \frac{1}{\epsilon} - \frac{1}{\epsilon} \right] \\
 &= \frac{1}{2\pi} i\sqrt{4\pi}\partial_z\phi = \frac{i}{\sqrt{\pi}}\partial_z\phi.
 \end{aligned} \tag{3.17}$$

Note that  $\partial_z\phi = \partial_z\varphi$ . In the second line we used  $e^A e^B = e^{A+B} e^{\frac{1}{2}[A,B]}$  and  $e^{2\pi(\phi(z+\epsilon) - \phi(z))} = \frac{1}{\epsilon}$ . Similar we find for the left moving density

$$: \bar{J}(\bar{z}) : = -\frac{i}{\sqrt{\pi}}\partial_{\bar{z}}\varphi. \tag{3.18}$$

So for the sum of both densities we find

$$J(x) + \bar{J}(x) = -\frac{1}{\sqrt{\pi}}\partial_x\varphi. \tag{3.19}$$

Using the method of point splitting, we can also bosonize the Dirac Hamiltonian (3.7). For instance, the first term can be expressed as

$$: \psi^\dagger(z)\partial_z\psi(z) : = \lim_{\epsilon \rightarrow 0} \left[ \psi^\dagger(z+\epsilon)\partial_z\psi(z) - \langle \psi^\dagger(z+\epsilon)\partial_z\psi(z) \rangle \right]. \tag{3.20}$$

Making use of the expansions

$$\begin{aligned}
 \psi^\dagger(z+\epsilon)\psi(z) &= \frac{1}{2\pi\epsilon} + i\frac{1}{\sqrt{\pi}}\partial_z\varphi + i\frac{\epsilon}{\sqrt{4\pi}}\partial_z^2\varphi - \epsilon(\partial\varphi)^2 + \mathcal{O}(\epsilon^2) \\
 \psi^\dagger(z+\epsilon)\partial_z\psi(z) &= \frac{1}{2\pi\epsilon^2} + i\frac{1}{2\sqrt{\pi}}\partial_z^2\varphi + (\partial_z\varphi)^2 + \mathcal{O}(\epsilon),
 \end{aligned} \tag{3.21}$$

we find

$$: \psi^\dagger(z)\partial_z\psi(z) : = \frac{1}{2\sqrt{\pi}}\partial_z^2\varphi + (\partial_z\varphi)^2. \tag{3.22}$$

Since  $\varphi$  is periodic, the term proportional to  $\partial_z^2\varphi$  does not contribute to (3.7). So after point splitting the Dirac equation transforms into

$$\begin{aligned}
 H_0 &= -2v_F \int dx \left[ (\partial_z\varphi)^2 + (\partial_{\bar{z}}\varphi)^2 \right] \\
 &= \frac{v_F}{2} \int dx \left[ \Pi^2 + (\partial_x\varphi)^2 \right],
 \end{aligned} \tag{3.23}$$

which is the Hamiltonian for a free boson fields. So we have transformed the fermionic free Hamiltonian (3.1) into the Hamiltonian of free bosons.

In the next section we will calculate the charge-charge and spin-spin correlation functions for this boson model.

### 3.1.2 The density density operator

After linearization using equation (3.4), it follows that the density operator acquires the bosonized form

$$\begin{aligned}
 n_{SF}(x) &= :c^\dagger(x)c(x): = : \psi^\dagger(x)\psi(x) : + : \bar{\psi}^\dagger(x)\bar{\psi}(x) : \\
 &\quad + e^{-2ik_F x} : \psi^\dagger(x)\bar{\psi}(x) : + e^{2ik_F x} : \bar{\psi}^\dagger(x)\psi(x) : \\
 &= -\frac{1}{\sqrt{\pi}} \partial_x \varphi + \frac{e^{-2ik_F x}}{2\pi} e^{i\sqrt{4\pi}\varphi(x)} + \frac{e^{2ik_F x}}{2\pi} e^{-i\sqrt{4\pi}\varphi(x)} \\
 &= -\frac{1}{\sqrt{\pi}} \partial_x \varphi + \mathcal{O}_{2k_F}(x) + \mathcal{O}_{2k_F}^\dagger(x), \tag{3.24}
 \end{aligned}$$

where  $\mathcal{O}_{2k_F}(x)$  and  $\mathcal{O}_{2k_F}^\dagger(x)$  express respectively the  $e^{-2ik_F x}$  and  $e^{2ik_F x}$  component of  $n_{SF}(x)$ . This equation shows that expansion of the fermion operator  $c(x)$  around the Fermi points relates it to fluctuating to periodic density waves. The operator  $\mathcal{O}_{2k_F}^\dagger$  can be taken as the order parameter for this wave and can be expressed as

$$\mathcal{O}_{2k_F}(x) = e^{-2ik_F x} \psi^\dagger(x) \bar{\psi}(x) = \frac{e^{-2ik_F x}}{2\pi} e^{i\sqrt{4\pi}\varphi(x)}, \tag{3.25}$$

or in Fourier language

$$\mathcal{O}_{2k_F}(q = 2k_F) = \sum_k \psi^\dagger(k) \bar{\psi}(k + 2k_F). \tag{3.26}$$

The fact that the fluctuation has period  $2k_F$  is a consequence of exchange of the particles between the Fermi points. We find for the density-density correlation function

$$\langle n_{SF}(x) n_{SF}(0) \rangle = \frac{1}{\pi} \langle \partial_x \varphi(x) \partial_x \varphi(0) \rangle + \left[ \langle \mathcal{O}_{2k_F}(x) \mathcal{O}_{2k_F}^\dagger(0) \rangle + h.c. \right]. \tag{3.27}$$

Since the bose fields are free we can use standard gaussian identities and it follows that

$$\begin{aligned}
 \frac{1}{\pi} \langle \partial_x \varphi(x) \partial_x \varphi(0) \rangle &= -\frac{1}{2\pi^2 x^2} \\
 \langle \mathcal{O}_{2k_F}(x) \mathcal{O}_{2k_F}^\dagger(0) \rangle &= \frac{1}{4\pi^2} e^{-2ik_F x} \langle e^{i\sqrt{4\pi}[\varphi(x) - \varphi(0)]} \rangle \\
 &= \frac{1}{4\pi^2} \frac{e^{-2ik_F x}}{x^2}, \tag{3.28}
 \end{aligned}$$

which yields the total expression for the charge-charge correlation function

$$\langle n_{SF}(x) n_{SF}(0) \rangle_{BOS} = -\frac{1}{2\pi^2} \frac{1}{x^2} + \frac{1}{2\pi^2} \frac{\cos(2k_F x)}{x^2}. \tag{3.29}$$

The exact analytic expression for  $\langle n_{SF}(x)n_{SF}(0) \rangle$ , starting from the free fermion Hamiltonian (3.1), can be calculated using Wick's theorem

$$\begin{aligned}
 \langle n_{SF}(x)n_{SF}(0) \rangle &= \frac{1}{V^2} \sum_{k_1 \dots k_4} e^{i(k_1 - k_2)x} \langle a_{k_1}^\dagger a_{k_2} a_{k_3}^\dagger a_{k_4} \rangle \\
 &= \frac{1}{V^2} \sum_{k_1 \dots k_4} e^{i(k_1 - k_2)x} \left( \langle a_{k_1}^\dagger a_{k_2} \rangle \langle a_{k_3}^\dagger a_{k_4} \rangle - \langle a_{k_1}^\dagger a_{k_4} \rangle \langle a_{k_3}^\dagger a_{k_2} \rangle \right) \\
 &= \left( \frac{N}{V} \right)^2 - \frac{1}{V^2} \sum_{m=1}^N e^{\frac{2\pi i x}{V} m} \sum_{n=1}^N e^{-\frac{2\pi i x}{V} n} \\
 &= \left( \frac{N}{V} \right)^2 - \frac{1}{V^2} \left( \frac{1 - \cos(2k_F x)}{1 - \cos\left(\frac{2\pi x}{V}\right)} \right). \tag{3.30}
 \end{aligned}$$

Here we used  $\langle a_k^\dagger a_p \rangle = \delta(k, p)$  and applied periodic boundary conditions so that  $k_1 = \frac{2\pi}{V}n$  and  $k_2 = \frac{2\pi}{V}m$  with  $m, n = 1, \dots, V$  and  $k_F = \frac{\pi N}{V}$  with the volume of the system and  $N$  numbers of fermions. In the thermodynamic limit  $N, V \rightarrow \infty$  and  $\frac{N}{V} = \rho_{SF}$  the function equals

$$\langle n_{SF}(x)n_{SF}(0) \rangle = (\rho_{SF})^2 - \frac{1}{2} \left( \frac{1 - \cos(2k_F x)}{\pi^2 x^2} \right). \tag{3.31}$$

The bosonized expression (3.29) is equal to this exact expression apart from the constant  $\rho_{SF}^2 = \left(\frac{k_F}{\pi}\right)^2$ . This is due to the fact that we mapped the spinless fermions on the Dirac fermions in equation (3.7) by adding an infinity in the density of states which in principle would cause the density expression  $n_{SF}$  to be infinite. By point splitting we remove this infinity in  $n_{SF}$ , but as a consequence we are not able to obtain the correct answer for constant value in the operator  $n_{SF}$  or in  $\langle n_{SF}(x)n_{SF}(0) \rangle$ . Apart from this, we find that bosonization characterizes correctly the density density correlations. Let us now continue considering a system of spinful electrons.

## 3.2 The spinful fermion gas

Let us consider a Hamiltonian describing weakly interacting spinful electrons in a one dimensional metal. The kinetic term for this system is of the form

$$H_0 = \sum_{k, \sigma} \varepsilon_k c_\sigma^\dagger(k) c_\sigma(k), \tag{3.32}$$

with  $c_\sigma(k)$  the electron annihilation operator at wave vector  $k$  and for spin  $\sigma \in \{\uparrow, \downarrow\}$  and  $\varepsilon_k = -2t \cos k$ . Similar to the spinless fermion case we linearize the Hamiltonian, giving

$$H_0 = \sum_{\sigma} \sum_{q=\pm k_F} \sum_{k=-\Lambda}^{\Lambda} \left( \frac{\partial \varepsilon}{\partial k} \Big|_q \right) c_\sigma^\dagger(q+k) c_\sigma(q+k), \tag{3.33}$$

and expand the annihilation operator  $c_\sigma(x)$  around the Fermi points

$$c_\sigma(x) = \sum_{q=\pm k_F} \int_{-\Lambda}^{\Lambda} \frac{dk}{2\pi} e^{i(q+k)x} c_\sigma(q+k). \quad (3.34)$$

The left and right mover operators are defined by

$$c_\sigma(x) = e^{ik_F x} \psi_\sigma(x) + e^{-ik_F x} \bar{\psi}_\sigma(x), \quad (3.35)$$

similar to (3.4) and (3.5). It is now easy to show that the Hamiltonian is exactly the spinful Dirac Hamiltonian given by

$$H_0 = -iv_F \sum_{\sigma} \int dx \left[ \psi_{\sigma}^{\dagger}(x) \partial_x \psi_{\sigma}(x) - \bar{\psi}_{\sigma}^{\dagger}(x) \partial_x \bar{\psi}_{\sigma}(x) \right]. \quad (3.36)$$

Finally, we arrive at the following bosonization formulas for the right moving fermions (for  $\sigma = \uparrow, \downarrow$ )

$$\begin{aligned} \psi_{\sigma}(x) &= \frac{\eta_{\sigma}}{\sqrt{2\pi}} e^{-i\sqrt{4\pi}\phi_{\sigma}(x)} \\ \psi_{\sigma}^{\dagger}(x) &= \frac{\eta_{\sigma}}{\sqrt{2\pi}} e^{i\sqrt{4\pi}\phi_{\sigma}(x)}, \end{aligned} \quad (3.37)$$

and similarly for the left movers

$$\begin{aligned} \bar{\psi}_{\sigma}(x) &= \frac{\bar{\eta}_{\sigma}}{\sqrt{2\pi}} e^{i\sqrt{4\pi}\bar{\phi}_{\sigma}(x)} \\ \bar{\psi}_{\sigma}^{\dagger}(x) &= \frac{\bar{\eta}_{\sigma}}{\sqrt{2\pi}} e^{-i\sqrt{4\pi}\bar{\phi}_{\sigma}(x)}. \end{aligned} \quad (3.38)$$

Here we have to include the Klein factors  $\eta_{\sigma}$  and  $\bar{\eta}_{\sigma}$  to guarantee the appropriate anti-commuting relations ( $\{\psi_{\sigma}, \psi_{\sigma'}\} = 0$  for  $\sigma \neq \sigma'$ ). The Klein factors are Hermitian and obey the Clifford algebra

$$\begin{aligned} \{\eta_{\sigma}, \eta_{\sigma'}\} &= \{\bar{\eta}_{\sigma}, \bar{\eta}_{\sigma'}\} = 2\delta_{\sigma\sigma'} \\ \{\eta_{\sigma}, \bar{\eta}_{\sigma'}\} &= 0. \end{aligned} \quad (3.39)$$

The Klein factors disappear if we are considering correlation functions of the form  $\langle O(x)O^{\dagger}(x) \rangle$  [47]. After point splitting of the operators  $J_{\sigma} = \psi_{\sigma}^{\dagger}\psi_{\sigma}$  and  $\bar{J}_{\sigma} = \bar{\psi}_{\sigma}^{\dagger}\bar{\psi}_{\sigma}$  the spinful Dirac equation transforms into

$$\begin{aligned} H_0 &= -2v_F \sum_{\sigma} \int dx \left[ (\partial_x \phi_{\sigma})^2 + (\partial_x \bar{\phi}_{\sigma})^2 \right] \\ &= \frac{v_F}{2} \sum_{\sigma} \int dx \left[ \Pi_{\sigma}^2 + (\partial_x \phi_{\sigma})^2 \right], \end{aligned} \quad (3.40)$$

which is the Hamiltonian for two independent free boson fields.

### 3.3 Bosonizing the interactions terms

Now we turn to the terms describing the interactions of the particles. General speaking, the Hamiltonian describing a two-body interacting between electrons can be written as

$$\begin{aligned}
 H_{int} &= \sum_{\sigma, \sigma'} \sum_x V_{\sigma\sigma'}(x) n_{\sigma}(x) n_{\sigma'}(x) \\
 &= \sum_{\sigma, \sigma', k_1, \dots, k_4} V_{\sigma, \sigma'}(k_1, k_2, k_3) c_{\sigma}^{\dagger}(k_1) c_{\sigma'}^{\dagger}(k_2) c_{\sigma'}(k_3) c_{\sigma}(k_4) \delta\left(\sum_{j=1}^4 k_j\right).
 \end{aligned}
 \tag{3.41}$$

In the low-energy limit, the electrons are restricted to the vicinity of the Fermi points  $k = \pm k_F$  and the scattering processes for these right and left movers fall into four kinematic types illustrated by figure 3.2. They are denoted by forward, backward and Umklapp scattering.

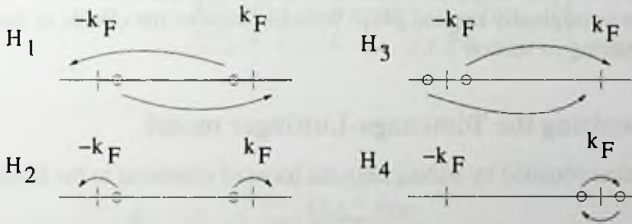


Figure 3.2: The four scattering processes denoted by forward ( $H_2$  and  $H_4$ ), backscattering ( $H_1$ ) and Umklapp ( $H_3$ ) scattering.

Forward scattering describes the process where two particles scatter with a small momentum transfer so that the particles will be moving in the same direction as they were before the collision. So a left (right) mover stays left (right) moving. These collisions can be subdivided into scattering between particles going in the same ( $H_2$ ) or opposite ( $H_4$ ) direction. The  $H_2$  contribution is sometimes denoted by dispersion. In case of backscattering ( $H_1$ ) a right mover becomes a left mover and vice versa. With Umklapp scattering ( $H_3$ ) two right movers become left movers or vice versa. This Umklapp process violates momentum conservation, and is only possible for the half-filled case ( $k_F = \frac{\pi}{2}$ ), in which the momentum violation is equal to a reciprocal lattice vector.

Splitting the Hamiltonian into a charge and spin part  $H_j = H_j^c + H_j^s$  for  $j = 2, 4$ , the

corresponding contributions are equal to

$$\begin{aligned}
 H_1 &= v_F g_1 \sum_{\sigma} \int dx \psi_{\sigma}^{\dagger} \bar{\psi}_{\sigma} \bar{\psi}_{-\sigma}^{\dagger} \psi_{-\sigma}^{\dagger} \\
 H_2^c &= v_F g_{2,c} \int dx (J_{\uparrow} + J_{\downarrow})(\bar{J}_{\uparrow} + \bar{J}_{\downarrow}) \\
 H_2^s &= v_F g_{2,s} \int dx (J_{\uparrow} - J_{\downarrow})(\bar{J}_{\uparrow} - \bar{J}_{\downarrow}) \\
 H_3 &= \frac{v_F}{2} g_3 \sum_{\sigma} \int dx (\psi_{\sigma}^{\dagger} \psi_{-\sigma}^{\dagger} \bar{\psi}_{\sigma} \bar{\psi}_{-\sigma} + h.c.) \\
 H_4^c &= \frac{v_F}{2} g_{4,c} \int dx [(J_{\uparrow} + J_{\downarrow})^2 + (\bar{J}_{\uparrow} + \bar{J}_{\downarrow})^2] \\
 H_4^s &= \frac{v_F}{2} g_{4,s} \int dx [(J_{\uparrow} - J_{\downarrow})^2 + (\bar{J}_{\uparrow} - \bar{J}_{\downarrow})^2], \tag{3.42}
 \end{aligned}$$

with fermionic current operators  $J_{\sigma} = \psi_{\sigma}^{\dagger} \psi_{\sigma}$  and  $\bar{J}_{\sigma} = \bar{\psi}_{\sigma}^{\dagger} \bar{\psi}_{\sigma}$  with  $\psi = \uparrow, \downarrow$ . Here we suppress the  $x$  dependence of the operators.

Let us first consider just the forward scattering  $H_2^{\mu}$  and  $H_4^{\mu}$  ( $\mu = c, s$ ) which together with  $H_0$  defines the Tomonaga-Luttinger model and is the model to which the bosonization method was originally applied [48]. We will consider the effects of backward and Umklapp scattering in section 3.3.3.

### 3.3.1 Bosonizing the Tomonaga-Luttinger model

The Hamiltonian obtained by adding only the forward scattering to the kinetic term,

$$H_{TL} = H_0 + \sum_{\mu=c,s} [H_2^{\mu} + H_4^{\mu}], \tag{3.43}$$

is referred to as the Tomonaga Luttinger model. Using formulas (3.37) and (3.38) the bosonized version of these scattering interactions are easily calculated

$$\begin{aligned}
 H_2^c &= \frac{v_F g_{2,c}}{\pi} \int dx \sum_{\sigma, \sigma'} \partial_z \varphi_{\sigma} \partial_{\bar{z}} \varphi_{\sigma'} = \frac{2v_F g_{2,c}}{\pi} \int dx \partial_z \varphi_c \partial_{\bar{z}} \varphi_c \\
 H_2^s &= \frac{2v_F g_{2,s}}{\pi} \int dx \partial_z \varphi_s \partial_{\bar{z}} \varphi_s \\
 H_4^c &= -\frac{v_F g_{4,c}}{2\pi} \int dx [(\partial_z \varphi_{\uparrow} + \partial_z \varphi_{\downarrow})^2 + (\partial_{\bar{z}} \varphi_{\uparrow} + \partial_{\bar{z}} \varphi_{\downarrow})^2] \\
 &= \frac{v_F g_{4,c}}{\pi} \int dx [(\partial_z \varphi_c)^2 + (\partial_{\bar{z}} \varphi_c)^2] \\
 H_4^s &= -\frac{v_F g_{4,s}}{\pi} \int dx [(\partial_z \varphi_s)^2 + (\partial_{\bar{z}} \varphi_s)^2]. \tag{3.44}
 \end{aligned}$$

Here we combined the boson fields  $\varphi_\uparrow$  and  $\varphi_\downarrow$  into charge and spin components

$$\begin{aligned}\varphi_c &= \frac{1}{\sqrt{2}}(\varphi_\uparrow + \varphi_\downarrow) \\ \varphi_s &= \frac{1}{\sqrt{2}}(\varphi_\uparrow - \varphi_\downarrow).\end{aligned}\quad (3.45)$$

So in boson language the two forward scattering contributions are equal to

$$\begin{aligned}H_2^\mu &= -\frac{v_F g_{2,\mu}}{2\pi} \int dx \left[ \Pi_\mu^2 - (\partial_x \varphi_\mu)^2 \right] \\ H_4^\mu &= \frac{v_F g_{4,\mu}}{2\pi} \int dx \left[ \Pi_\mu^2 + (\partial_x \varphi_\mu)^2 \right].\end{aligned}\quad (3.46)$$

Combining these results the Tomonaga Luttinger Hamiltonian  $H_{TL}$  in (3.43) can be written as

$$H_{TL} = \sum_{\mu=c,s} \frac{v_\mu}{2} \int dx \left[ K_\mu \Pi_\mu^2 + \frac{1}{K_\mu} (\partial_x \varphi_\mu)^2 \right], \quad (3.47)$$

with

$$\begin{aligned}K_\mu &= \sqrt{\frac{\pi - g_{2,\mu} + g_{4,\mu}}{\pi + g_{2,\mu} + g_{4,\mu}}} \\ v_\mu &= v_F \sqrt{\left(1 + \frac{g_{4,\mu}}{\pi}\right)^2 - \left(\frac{g_{2,\mu}}{\pi}\right)^2}.\end{aligned}\quad (3.48)$$

Using rescaled operators,  $\varphi'_\mu = \varphi_\mu / \sqrt{K_\mu}$  and  $\Pi'_\mu = \sqrt{K_\mu} \Pi_\mu$  for  $\mu = c, s$  this Hamiltonian can be written as:

$$H_{TL} = \frac{v_F}{2} \int dx \left[ (\Pi'_\mu)^2 + (\partial_x \varphi'_\mu)^2 \right], \quad (3.49)$$

and has the same form as the free boson Hamiltonian (3.23). So adding forward scattering interactions to the kinetic Hamiltonian  $H_0$  only rescales the free boson operators!

Let us now calculate the charge-charge and spin-spin correlation functions for this Tomonaga-Luttinger model.

### 3.3.2 The correlation functions

Using the bosonization dictionary the density operator  $n_{tot}(x) = n_{\uparrow}(x) + n_{\downarrow}(x)$  can be expressed as

$$\begin{aligned}
 n_{tot}(x) &= \sum_{\sigma} : c_{\sigma}^{\dagger} c_{\sigma} : = \sum_{\sigma} \left[ : \psi_{\sigma}^{\dagger}(x) \psi_{\sigma}(x) : + : \bar{\psi}_{\sigma}^{\dagger}(x) \bar{\psi}_{\sigma}(x) : \right] \\
 &\quad + e^{-2ik_F x} \sum_{\sigma} : \psi_{\sigma}^{\dagger}(x) \bar{\psi}_{\sigma}(x) : + e^{+2ik_F x} \sum_{\sigma} : \bar{\psi}_{\sigma}^{\dagger}(x) \psi_{\sigma}(x) : \\
 &= \sum_{\sigma} \frac{1}{\sqrt{\pi}} \frac{\partial \varphi_{\sigma}}{\partial x} + \frac{e^{-2ik_F x}}{2\pi} \sum_{\sigma} \eta_{\sigma} \bar{\eta}_{\sigma} e^{i\sqrt{4\pi}\varphi_{\sigma}(x)} \\
 &\quad + \frac{e^{2ik_F x}}{2\pi} \sum_{\sigma} \eta_{\sigma} \bar{\eta}_{\sigma} e^{-i\sqrt{4\pi}\varphi_{\sigma}(x)} \\
 &= \sqrt{\frac{2}{\pi}} \frac{\partial \varphi_c}{\partial x} + \mathcal{O}_{CDW}(x) + \mathcal{O}_{CDW}^{\dagger}(x). \tag{3.50}
 \end{aligned}$$

Here  $\mathcal{O}_{CDW}(x)$  and  $\mathcal{O}_{CDW}^{\dagger}(x)$  express respectively the  $e^{-2ik_F x}$  and  $e^{2ik_F x}$  component of  $n_{tot}(x)$ . As in equation (3.24) we obtain a periodic modulation which is referred to as a charge density wave (CDW). The operator  $\mathcal{O}_{CDW}$  can be taken as the order parameter for this wave and in Fourier language can be expressed as

$$\mathcal{O}_{CDW}(q = 2k_F) = \sum_{\sigma, k} \psi_{\sigma}^{\dagger}(k) \bar{\psi}_{\sigma}(k + 2k_F). \tag{3.51}$$

or in real space coordinates

$$\begin{aligned}
 \mathcal{O}_{CDW}(x) &= e^{-2ik_F x} \sum_{\sigma} \psi_{\sigma}^{\dagger}(x) \bar{\psi}_{\sigma}(x) \\
 &= \frac{e^{-2ik_F x}}{2\pi} e^{i\sqrt{2\pi}\varphi_c(x)} \left[ \eta_{\uparrow} \bar{\eta}_{\uparrow} e^{i\sqrt{2\pi}\varphi_s(x)} + \eta_{\downarrow} \bar{\eta}_{\downarrow} e^{-i\sqrt{2\pi}\varphi_s(x)} \right] \\
 &= \frac{1}{\pi} e^{-2ik_F x} e^{i\sqrt{2\pi}\varphi_c(x)} \cos \left[ \sqrt{2\pi}\varphi_s(x) \right]. \tag{3.52}
 \end{aligned}$$

Here we fixed the Klein factor gauge by taking  $\eta_{\uparrow} \bar{\eta}_{\uparrow} = \eta_{\downarrow} \bar{\eta}_{\downarrow} = 1$ . In general the Klein factors disappear from a correlation function of the form  $\langle O(x) O^{\dagger}(0) \rangle$  (see [47]).  $\mathcal{O}_{CDW}$  describes the process where a left mover is annihilated and a right mover is created both near the Fermi surface. This is a two-particle process. But since both an up and a down electron can be located on the same site, we also need to consider the operator

$$\mathcal{O}_{4k_F}(q = 4k_F) = \sum_{\sigma, k} \psi_{\sigma}^{\dagger}(k) \psi_{-\sigma}^{\dagger}(k) \bar{\psi}_{-\sigma}(k + 2k_F) \bar{\psi}_{\sigma}(k + 2k_F). \tag{3.53}$$

Or in real space coordinates

$$\begin{aligned}\mathcal{O}_{4k_F}(x) &= e^{-4ik_F x} \sum_{\sigma} \psi_{\sigma}^{\dagger}(x) \psi_{-\sigma}^{\dagger}(x) \bar{\psi}_{-\sigma}(x) \bar{\psi}_{\sigma}(x) \\ &= e^{-4ik_F x} \frac{1}{2\pi^2} e^{i\sqrt{8\pi}\varphi_c(x)}.\end{aligned}\quad (3.54)$$

And thus we get for the charge-charge correlation function

$$\begin{aligned}\langle n_{tot}(x) n_{tot}(0) \rangle &= \frac{2}{\pi} \langle \partial_x \varphi_c(x) \partial_x \varphi_c(0) \rangle + \left[ \langle \mathcal{O}_{CDW}(x) \mathcal{O}_{CDW}^{\dagger}(0) \rangle + h.c. \right] \\ &\quad + \left[ \mathcal{O}_{4k_F}(x) \mathcal{O}_{4k_F}^{\dagger}(0) + h.c. \right].\end{aligned}\quad (3.55)$$

The first and second contribution can respectively be written as

$$\begin{aligned}\frac{2}{\pi} \langle \partial_x \varphi_c(x) \partial_x \varphi_c(0) \rangle &= \frac{2K_c}{\pi} \langle \partial_x \varphi'_c(x) \partial_x \varphi'_c(0) \rangle = -\frac{K_c}{\pi^2} \frac{1}{x^2} \\ \langle \mathcal{O}_{CDW}(x) \mathcal{O}_{CDW}^{\dagger}(0) \rangle &= \frac{e^{-2ik_F x}}{2\pi^2} \langle e^{i\sqrt{2\pi}[\varphi_c(x) - \varphi_c(0)]} \rangle \langle e^{i\sqrt{2\pi}[\varphi_s(x) - \varphi_s(0)]} \rangle \\ &= \frac{e^{-2ik_F x}}{2\pi^2} \frac{1}{x^{K_c + K_s}} \\ \langle \mathcal{O}_{4k_F}(x) \mathcal{O}_{4k_F}^{\dagger}(0) \rangle &= \frac{1}{(2\pi)^2} \langle e^{i\sqrt{8\pi}[\varphi_c(x) - \varphi_c(0)]} \rangle = \frac{e^{-4ik_F x}}{4\pi^4} \frac{1}{x^{4K_c}},\end{aligned}\quad (3.56)$$

and the charge-charge correlation function (3.27) can therefore be written as

$$\langle n_{tot}(x) n_{tot}(0) \rangle = -\frac{K_c}{\pi^2} \frac{1}{x^2} + \frac{1}{\pi^2} \frac{\cos(2k_F x)}{x^{K_c + K_s}} + \frac{1}{2\pi^4} \frac{\cos(4k_F x)}{x^{4K_c}}.\quad (3.57)$$

Similar to the density  $n_{SF}(x)$  the operator  $S^z(x)$  can be written as

$$\begin{aligned}S^z(x) &= \frac{:n_{\uparrow}(x) - n_{\downarrow}(x):}{2} \\ &= \sqrt{\frac{1}{2\pi}} \partial_x \varphi_s(x) + \mathcal{O}_{SDW,z}(x) + \mathcal{O}_{SDW,z}^{\dagger}(x),\end{aligned}\quad (3.58)$$

with order parameter

$$\mathcal{O}_{SDW,z}(q = 2k_F) = \sum_k \left[ \psi_{\uparrow}^{\dagger}(k) \bar{\psi}_{\downarrow}(k + 2k_F) - \psi_{\downarrow}^{\dagger}(k) \bar{\psi}_{\uparrow}(k + 2k_F) \right].\quad (3.59)$$

Or in space coordinates

$$\begin{aligned}\mathcal{O}_{SDW,z}(x) &= \frac{1}{2} \left[ \psi_{\uparrow}^{\dagger}(x) \bar{\psi}_{\uparrow}(x) - \psi_{\downarrow}(x) \bar{\psi}_{\downarrow}(x) \right] \\ &= \frac{i}{2\pi} e^{-2ik_F x} e^{i\sqrt{2\pi}\varphi_c(x)} \sin \left[ \sqrt{2\pi}\varphi_s(x) \right],\end{aligned}\quad (3.60)$$

where we neglect again the Klein factors. In analogy with the CDW case we find

$$\begin{aligned} \langle S^z(x)S^z(0) \rangle &= \frac{1}{2\pi} \left\langle \frac{\partial\varphi_s(x)}{\partial x} \frac{\partial\varphi_s(0)}{\partial x} \right\rangle + \left[ \langle \mathcal{O}_{SDW,z}(x)\mathcal{O}_{SDW,z}^\dagger(0) \rangle + h.c. \right] \\ \langle \mathcal{O}_{SDW,z}(x)\mathcal{O}_{SDW,z}^\dagger(0) \rangle &= \frac{1}{8\pi^2} e^{-2ik_F x} \langle e^{i\sqrt{2\pi}[\varphi_c(x)-\varphi_c(0)]} \rangle \langle e^{i\sqrt{2\pi}[\varphi_s(x)-\varphi_s(0)]} \rangle \\ &= \frac{1}{8\pi^2} e^{-2ik_F x} \frac{1}{x^{K_c+K_s}} \end{aligned} \quad (3.61)$$

And the spin-spin correlation function becomes

$$\langle S^z(x)S^z(0) \rangle = -\frac{K_s}{4\pi^2} \frac{1}{x^2} + \frac{1}{4\pi^2} \frac{\cos(2k_F x)}{x^{K_c+K_s}}. \quad (3.62)$$

In the upcoming chapters we will discuss the form of this formula and explain the origin of the term proportional to  $\cos(2k_F x)/x^{K_s+K_c}$ .

### 3.3.3 Spin and Charge gap

Let us now examine the effect of the backward scattering and Umklapp scattering. In boson field language the backward scattering interaction term  $H_1$  can be written as

$$H_1 = \frac{v_F g_1}{2\pi^2} \int dx \cos\left[\sqrt{8\pi}\varphi_s(x)\right], \quad (3.63)$$

where we again neglected the Klein factors. If we add the term to the spin part of the free bosonized Hamiltonian (3.40) for  $K_s \neq 1$ , we obtain the sine Gordon model defined as

$$H_{SG} = \frac{v_F}{2} \int dx \left[ \Pi_\sigma^2 + (\partial_x \varphi_s')^2 \right] + \frac{v_F g_1}{2\pi^2} \int dx \cos\left[\sqrt{8\pi} K_s \varphi_s'(x)\right]. \quad (3.64)$$

Studying the renormalization group (RG) flow [49] one can show that for  $K_s = 1$  this cosine term is marginal. If  $|g_1| > 2\pi(K_s - 1)$ , the system flows towards strong coupling indicating that  $g_1$  is marginally relevant. This results in a gap in the spin spectrum. The charges remain gapless. This is described by the Luther-Emery liquid [50]. For  $|g_1| < 2\pi(K_s - 1)$  it flows to  $g_1 = 0$  and is marginally irrelevant. Then the model reduces to a Luttinger liquid. Here both charge and spin excitations are gapless.

Finally, let us discuss Umklapp scattering which is only important when  $2k_F$  is commensurate with the lattice vector. The Umklapp term  $H_3$  can be treated in the same way and yields:

$$H_3 = \frac{v_F g_3}{2\pi^2} \int dx \cos\left[\sqrt{8\pi}\varphi_c(x)\right]. \quad (3.65)$$

Now we can apply the same analysis as used for backward scattering. We simply have to replace  $g_1$  by  $g_3$  and  $K_s$  by  $K_c$ . Thus a charge gap develops if  $|g_3| > 2\pi(K_c - 1)$  and the system is a Mott insulator.

### 3.4 The Hubbard Model

Using bosonization we can analyze the one dimensional Hubbard model. The Hubbard model is defined by the Hamiltonian

$$H = -t \sum_{\sigma} \sum_i (c_{i\sigma}^{\dagger} c_{i+1\sigma} + h.c.) + U \sum_i n_{i\uparrow} n_{i\downarrow}, \quad (3.66)$$

where  $\sigma$  denotes the spin of the electron  $\sigma \in \{\uparrow, \downarrow\}$ . The first term describes the movement of the spinful electrons and the second term represents the local Coulomb repulsion. Using the description of the previous section the Hubbard model can be described by the  $H_{TL} = H_c + H_s$  in (3.47) with  $K_s = 1$  and in the weak coupling limit  $K_c = (1 + \frac{U}{v_F})^{-1} = 1 - \frac{U}{v_F} + \dots$ . Using the Bethe Ansatz wave function described in the next chapter, we can calculate the  $K_c$  more precisely [58] and these results are depicted in figure 3.3. The Coulomb interaction produces a backscattering term proportional to  $U$  similar to the one in (3.64) which can lead to a mass gap term when it becomes relevant. But using the RG flow arguments used in the previous section we find that this cosine is irrelevant for  $U > 0$  and therefore we can neglect it. For  $U < 0$  it becomes relevant where it produces a spin gap. For all  $U$  the charge sector is massless, and there is no gap in creating charge excitations. The system is metallic.

For half filling, that is  $k_F a = \pi/2$ , we cannot neglect the oscillatory terms, and we get an extra Umklapp term, giving also a cosine term by bosonization, giving exactly the reversed situation as for the charge case: The cosine term is irrelevant for any negative  $U$ , but relevant for positive  $U$ . The latter case is called a Mott Hubbard insulator since the gap is created by electron interactions, in combination with lattice commensuration.

### 3.5 Summary

In summary we can conclude that in the Tomonaga Luttinger model but also the sine Gordon Model and the Hubbard Model with respectively positive  $g_1$  and  $U$ , away from half filling, the long-wavelength theory is expressed by the charge and spin correlators according to bosonization

$$\begin{aligned} \langle n_{i\sigma}(x) n_{i\sigma}(0) \rangle &= -\frac{K_c}{(\pi x)^2} + \frac{1}{\pi^2} \frac{\cos(2k_F x)}{x^{K_s + K_c}} + \\ &+ \frac{1}{2\pi^4} \frac{\cos(4k_F x)}{x^{4K_c}} + \dots \\ \langle S^z(x) S^z(0) \rangle &= -\frac{1}{4(\pi x)^2} + \frac{1}{4\pi^2} \frac{\cos(2k_F x)}{x^{K_s + K_c}} + \dots \end{aligned} \quad (3.67)$$

Note again that bosonization is not capable to spot the constant term  $\rho_{i\sigma}^2$  in the correlator  $\langle n_{i\sigma}(x) n_{i\sigma}(0) \rangle$ .

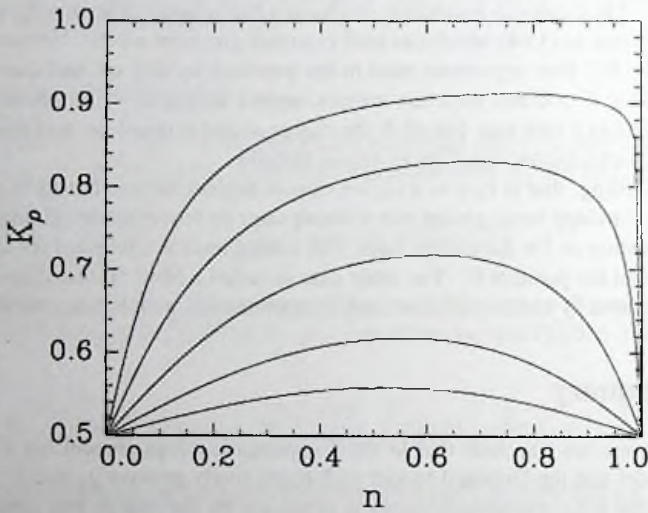


Figure 3.3: The charge stiffness  $K_c$  (here denoted as  $K_\rho$ ) as function of the density  $\rho$  (here  $n$ ) and  $U/t$  where  $U/t = 1, 2, 4, 8, 16$  for the top to bottom curves [58]. The function is discontinuous for the densities  $\rho_{tot} = 0$  and  $\rho_{tot} = 1$ , where  $K_c = 0$ .

## Chapter 4

# The Bethe Ansatz

In this section we will summarize the analytic Bethe Ansatz solution for the Heisenberg model and the Hubbard model [51]. As will turn out, these solutions are an important starting point for defining the topological order discussed in the next chapter.

The Bethe Ansatz technique can be used for so called integrable models. In these systems, not only the total momentum of the particle is conserved, but also the individual momentum of the particles remains unchanged after the collision with other particles. This is a strong requirement which makes the problem solvable. The Bethe Ansatz was first introduced in 1931 by H. Bethe [53] when solving the isotropic Heisenberg model. We will review this solution in section 4.1. As we will see in section 4.2, the solution of this model can be related to the nested Bethe Ansatz solution necessary to solve the Hubbard model. This solution was used by Parola and Sorella [22] to show that the spin spin correlator equals  $\langle S^z(x)S^z(0) \rangle \sim \cos(2k_F x)/x^{K_c+K_s}$ . This is reviewed in section 4.3. Finally we will reinterpret these results and show that it is not correct to view this as an harmonic solid with spin where the elastic coupling is provided by the motion of the charge as was described by Schulz [59]. This analysis will be the basis for our investigation of the topological order in the next chapter.

### 4.1 The Bethe Ansatz for the Heisenberg Model

We will write the Hamiltonian [54] of the antiferromagnetic Heisenberg spin chain of  $L$  sites in the following form

$$\begin{aligned} H &= \sum_{i=1}^L [S_i^x S_{i+1}^x + S_i^y S_{i+1}^y + S_i^z S_{i+1}^z] \\ &= \sum_{i=1}^L \left[ \frac{1}{2} (S_i^+ S_{i+1}^- + S_i^- S_{i+1}^+) + S_i^z S_{i+1}^z \right]. \end{aligned} \quad (4.1)$$

with  $S_j^+$  ( $S_j^-$ ) the raising (lowering) operator working on the spin on site  $j$ . Furthermore we use periodic boundary conditions so that  $\bar{S}_{L+1} = \bar{S}_1$ . Since this Hamiltonian conserves the  $z$ -component  $\sum_{i=1}^L S_i^z$  of the total spin, the eigenfunction of a state with  $N$  down and  $L - N$  up spins can be written as

$$|\psi\rangle = \sum_{x_1 < \dots < x_N} f(x_1, \dots, x_N) S_{x_1}^- \dots S_{x_N}^- |\uparrow \dots \uparrow\rangle, \quad (4.2)$$

with  $x_i$  the positions of the down spins. The spins are ordered so that  $x_1 < \dots < x_N$ . The time-independent Schrödinger equation for  $f(x_1, \dots, x_N)$  is obtained by applying the Hamiltonian to this state  $|\psi\rangle$ . To illustrate how this is done, we start with  $N = 2$ , the case where only 2 of the  $L$  spins are down spins.

#### 4.1.1 The case $N = 2$ : two reversed spins

If the two spins do not collide, that is  $x_1 + 1 \neq x_2$ , the Schrödinger equation for  $f(x_1, x_2)$  is given by

$$\begin{aligned} Ef(x_1, x_2) &= \left[ \frac{1}{2}(\square_1 + \square_2) + \frac{L}{4} - 2 \right] f(x_1, x_2) \\ &= \left[ \frac{1}{2}(\Delta_1 + \Delta_2) + \frac{L}{4} \right] f(x_1, x_2). \end{aligned} \quad (4.3)$$

where  $\square_j - 2$  is the discrete version of the Laplace operator  $\square_j - 2 = \nabla_j^2$  and describes the kinetic energy part for spin  $j$ . For instance  $\square_1 f(x_1, x_2)$  equals

$$\begin{aligned} \square_1 f(x_1, x_2) &= f(x_1 + 1, x_2) + f(x_1 - 1, x_2) \\ &= (\square_1^+ + \square_1^-) f(x_1, x_2). \end{aligned} \quad (4.4)$$

Here  $\square_1^+$  generates a movement of the first down spin of one space to the right and  $\square_1^-$  a movement to the left. The contribution  $\square_1^+ + \square_2^+$  in (4.3) is due to the operator  $\sum_{i=1}^L S_i^+ S_{i+1}^-$  and  $\square_1^- + \square_2^-$  is because of  $\sum_{i=1}^L S_i^- S_{i+1}^+$ . The potential term  $(\frac{L}{4} - 2)f(x_1, x_2)$  in equation (4.3) is caused by  $\sum_{i=1}^L S_i^z S_{i+1}^z$ . This Schrödinger equation (4.3) is a simple Laplace equation which is solved by the usual plane waves

$$f(x_1, x_2) = A e^{ik_1 x_1 + ik_2 x_2}. \quad (4.5)$$

Now consider the situation when the particles collide so that  $x_1 + 1 = x_2$ . 'Before' and 'after'<sup>1</sup> this collision the particles are not adjacent and the solution is a plane wave. So before the collision, the two particles are moving towards each other with momentum  $k_1$  and  $k_2$  described by the solution  $A \exp(ik_1 x_1 + ik_2 x_2)$  as depicted in figure 4.1(a) and after the collision the particles drift away with some momenta  $k'_1$  and  $k'_2$  as described

<sup>1</sup>The terms before and after should not be taken too literally. Since we consider the Laplace equation in the place coordinate  $x$ , the two events before and after the collision take place at the same time.

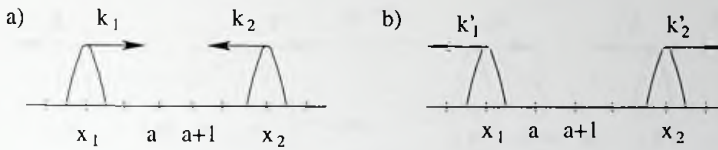


Figure 4.1: Two particles moving (a) towards each other before the collision described by  $A \exp(ik_1x_1 + ik_2x_2)$  and (b) after the collision described by  $B \exp(ik'_1x_1 + ik'_2x_2)$ . The collision takes place at  $x_1 = a, x_2 = a + 1$ . Note that before and after the collision  $x_1 < x_2$ .

by  $B \exp(ik'_1x_1 + ik'_2x_2)$  and depicted in figure 4.1(b). The Bethe Ansatz now consists of assuming that the particles exchange their momenta so that  $k'_1 = k_2$  and  $k'_2 = k_1$  and therefore the wave function equals

$$\begin{aligned}
 f(x_1, x_2) &= A e^{ik_1x_1 + ik_2x_2} + B e^{ik'_1x_1 + ik'_2x_2} \\
 &= A e^{ik_1x_1 + ik_2x_2} + B e^{ik_2x_1 + ik_1x_2} \\
 &= \sum_P A_P e^{i \sum_{j=1}^2 k_{Pj} x_j}.
 \end{aligned} \tag{4.6}$$

Here, the sum is over all the permutations  $P$  of the two particles, so  $A = A_{12}$  with  $I$  the unity permutation and  $B = A_{(12)}$ . Note that, if  $P = (12)$ , then  $P1 = 2$  and  $P2 = 1$ .

The coefficients  $A_I$  and  $A_{(12)}$  are obtained by solving the Schrödinger equation for  $x_1 + 1 = x_2$ . This equation is very similar to (4.3). The only difference is that because the two particles are adjacent, particle 1 and particle 2 cannot move to the right and left so respectively we have to subtract  $\Delta_1^+$  and  $\Delta_2^-$  from respectively  $\Delta_1$  and  $\Delta_2$  in (4.3). Furthermore the energy is increased by one because the particles have now only one neighbor of opposite spin instead of two. So when  $x_1 + 1 = x_2$ , the Schrödinger equation for  $f(x_1, x_2)$  equals

$$\left[ \frac{1}{2} (\Delta_1 + \Delta_2 - \Delta_1^+ - \Delta_2^-) + \frac{L}{4} - 2 + 1 \right] f(x_1, x_2) = E f(x_1, x_2), \tag{4.7}$$

together with the assumption that (4.6) still holds for  $x_1 + 1 = x_2$ , we can determine the ratio between  $A_I$  and  $A_{(12)}$ :

$$\frac{A_{(12)}}{A_I} = - \frac{1 + e^{i(k_1+k_2)} - 2e^{ik_2}}{1 + e^{i(k_1+k_2)} - 2e^{ik_1}}. \tag{4.8}$$

The Bethe Ansatz solution (4.6) can also be interpreted in a different way. To do this we start with an eigenfunction of the form

$$|\psi\rangle = \sum_{x_1, \dots, x_N} f(x_1, \dots, x_N) S_{x_1}^- \dots S_{x_N}^- |\uparrow \dots \uparrow\rangle, \tag{4.9}$$

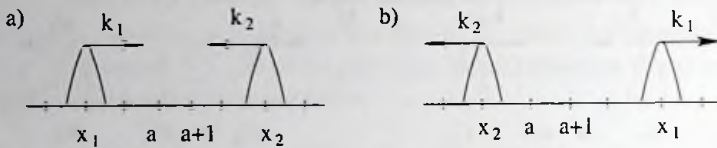


Figure 4.2: The collision event in the second approach. Before the collision (a) the particles are moving toward each other ( $x_1 < x_2$ ) described by the wave function  $A_I \exp(ik_1x_1 + ik_2x_2)$ . The collision only affects the relative phase factor so that after the collision (b) the particles are moving with momenta  $k_1$  and  $k_2$  described  $A_{(12)} \exp(ik_1x_1 + ik_2x_2)$  and  $x_1 > x_2$ .

where the particles are now not ordered, so we have to consider both  $x_1 < x_2$  and  $x_2 < x_1$ . We can also look upon the Bethe Ansatz as the assumption that during a collision the particles move through each other without affecting their momenta and only changing the phase factor of the wave function. So before the collision  $x_1 < x_2$  and the two particles approach each other with momentum  $k_1$  and  $k_2$  described by the solution  $A_I \exp(ik_1x_1 + ik_2x_2)$ . After the collision we have  $x_1 > x_2$  and the wave function is equal to  $A_{(12)} \exp(ik_1x_1 + ik_2x_2)$ . This is depicted in figure 4.2. The function  $f(x_1, x_2)$  can then be written as

$$f(x_1, x_2) = e^{ik_1x_1 + ik_2x_2} [A_I \theta(X_I) + A_{(12)} \theta(X_{(12)})], \quad (4.10)$$

with  $\theta(X_P) = 1$  if  $x_{P1} < x_{P2}$  and  $\theta(X_P) = 0$  if  $x_{P1} > x_{P2}$ . Since the spins are bosonic, the total wave function should be symmetric and we need to symmetrize this solution  $f(x_1, x_2)$  giving

$$\begin{aligned} f(x_1, x_2) &= \mathcal{S} e^{i \sum_{j=1}^2 k_j x_j} \sum_P A_P \theta(X_P) \\ &= \sum_Q e^{i \sum_{j=1}^2 k_j x_{Qj}} \sum_P A_P \theta(X_{QP}) \\ &= \sum_Q \sum_R e^{i \sum_{j=1}^2 k_{Q^{-1}j} x_j} A_{Q^{-1}R} \theta(x_R) \\ &= \sum_P \sum_R e^{i \sum_{j=1}^2 k_{Pj} x_j} A_{PR} \theta(x_R). \end{aligned} \quad (4.11)$$

Here  $\mathcal{S}$  is the symmetrizer, making the solution symmetric by summing over all permutations  $Q$  of the indices  $j$  of place  $x_j$ . If we take the region  $R = I$ , so that  $x_1 < x_2$  we find equation (4.6)

$$f(x_1, x_2) = \sum_P A_P e^{i \sum_{j=1}^2 k_{Pj} x_j}. \quad (4.12)$$

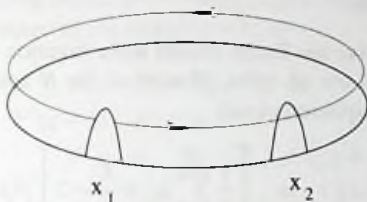


Figure 4.3: Graphical picture of the periodic boundary condition (4.14).

At this point we can introduce the scattering matrix which relates the amplitudes in the two regions  $S^{12}(k_1, k_2)A_I = A_{(12)}$ . So the scattering matrix transforms the wave function  $A_I \exp i(k_1 x_1 + k_2 x_2)$  for  $x_1 < x_2$  before the collision into the wave function  $A_{(12)} \exp i(k_1 x_1 + k_2 x_2)$  for  $x_1 > x_2$  after the collision. From equation (4.7) we find:

$$S^{12}(k_1, k_2) = \frac{A_{(12)}}{A_I} = -\frac{1 + e^{i(k_1+k_2)} - 2e^{ik_2}}{1 + e^{i(k_1+k_2)} - 2e^{ik_1}} = -e^{i\theta(k_1, k_2)}. \quad (4.13)$$

Here  $\theta$  is the phase shift by which the prefactor  $A_I$  is shifted during a collision. Note that the scattering matrix  $S^{12}(k_1, k_2)$  depends on the momenta  $k_1$  and  $k_2$ , but not on the positions  $x_1$  and  $x_2$ .

What remains to be determined are the allowed  $k$ -values in the Bethe Ansatz wave function (4.6). These follow from the periodicity condition on the  $x_j$ , which states

$$f(x_1, x_2) = f(x_2, x_1 + L). \quad (4.14)$$

Note that because the wave function is symmetric, this equation is equal to  $f(x_1, x_2) = f(x_2 + L, x_1)$ . This gives the following equations for the amplitudes  $A_I$  and  $A_{(12)}$

$$\begin{aligned} S^{12}(k_1, k_2)e^{ik_1 L} &= \frac{A_{(12)}}{A_I} e^{ik_1 L} = 1 \\ S^{21}(k_2, k_1)e^{ik_2 L} &= \frac{A_I}{A_{(12)}} e^{ik_2 L} = 1. \end{aligned} \quad (4.15)$$

These equations can be understood as follows. To obtain  $f(x_2, x_1 + L)$  from  $f(x_1, x_2)$  we have to move particle 1 along the chain  $L$  as depicted in figure 4.3. In doing so, the wave function  $A_I \exp i(k_1 + k_2)$  acquires a kinematic term  $\exp(i k_1 L)$  and the scattering matrix from colliding with particle 2 on site  $x_2$ . But in total the procedure of going in this circle should be equal to doing nothing, that is the identity so  $S^{12}(k_1, k_2) \exp(i k_1 L) = 1$  giving the first equation in (4.15). The same can be done for particle 2 giving the second equation in (4.15).

### 4.1.2 General $N$ case

In this section we will derive the Bethe Ansatz wave function in case  $N$  of the  $L$  spins are down spins and  $L - N$  are up spins. If none of the  $N$  spins are adjacent, the time independent Schrödinger equation equals

$$\begin{aligned} Ef(x_1, \dots, x_N) &= \left[ \frac{1}{2} \sum_{j=1}^N \Delta_j + \frac{L}{4} - 2 \right] f(x_1, \dots, x_N) \\ &= \left[ \frac{1}{2} \sum_{j=1}^N \square_j + \frac{L}{4} \right] f(x_1, \dots, x_N), \end{aligned} \quad (4.16)$$

which is again solved by a product of plane waves

$$f(x_1, \dots, x_N) = e^{ik_1 x_1 + \dots + ik_N x_N}. \quad (4.17)$$

Suppose two particles do collide, say  $x_q + 1 = x_{q+1}$ . The Bethe Ansatz states that a collision changes only the phase factor and leaves the momenta unaltered. So before the collision the wave function  $f(x_1, \dots, x_N)$  is equal to  $A_I \exp(ik_1 x_1 + \dots + ik_N x_N)$  and afterwards it is given by the expression  $A_{(q(q+1))} \exp(ik_1 x_1 + \dots + ik_N x_N)$ . The total wave function can be written as

$$f(x_1, \dots, x_N) = e^{\sum_{j=1}^N ik_j x_j} \sum_P A_P \theta(x_P), \quad (4.18)$$

where the sum is over all the permutations  $P$  of the  $N$  spin down sites and  $\theta(x_P) = 1$  only if  $x_{P1} < x_{P2} < \dots < x_{PN}$  and  $\theta(x_P) = 0$  otherwise. The expression has to be symmetrized giving, similar to (4.11)

$$\begin{aligned} f(x_1, \dots, x_N) &= \mathcal{S} e^{i \sum_{j=1}^N k_j x_j} \sum_P A_P \theta(x_P) \\ &= \sum_P \sum_R e^{i \sum_{j=1}^N k_{Pj} x_j} A_{PR} \theta(x_R). \end{aligned} \quad (4.19)$$

If we take the region  $R = I$ , so that  $x_1 < \dots < x_N$  we find

$$f(x_1, \dots, x_N) = \sum_P A_P e^{i \sum_{j=1}^N k_{Pj} x_j}. \quad (4.20)$$

Since  $x_q + 1 = x_{q+1}$ , the Schrödinger equation (4.16) is altered by a term  $(-\square_q^+ - \square_{q+1}^- + 1)f(x_1, \dots, x_N)$ . Using this equation we get the relation between some of the coefficients  $A_P$

$$\begin{aligned} \frac{A_P}{A_{P'}} &= -\frac{1 + e^{ik_{Pq} + k_{P'q}} - 2e^{ik_{Pq}}}{1 + e^{ik_{Pq} + k_{P'q}} - 2e^{ik_{P'q}}} \\ &= -e^{-i\theta(k_{Pq}, k_{P'q})} = S^{q(q+1)}(k_{Pq}, k_{P'q}). \end{aligned} \quad (4.21)$$

which defines the scattering matrix  $S^{q(q+1)}(k_{Pq}, k_{P'q})$ . Here the permutation  $P$  equals  $P'$  except for the interchange of  $Pq$  and  $P(q+1)$ , so

$$\begin{aligned} P'q &= P(q+1) \\ P'(q+1) &= Pq \\ P'j &= Pj \quad \text{if } j \neq q, q+1. \end{aligned} \quad (4.22)$$

So  $P'$  can be written as the product of  $P$  and the 2-cycle  $(Pq \ P(q+1))$ :

$$P' = (Pq \ P(q+1))P. \quad (4.23)$$

One can think of this scattering matrix in (4.21) as describing a collision between the particles on sites  $x_q$  and  $x_{q+1}$  with momenta  $k_{Pq}$  and  $k_{P'q} = k_{P(q+1)}$ . Since every permutation  $P$  can be built up from the identity permutation by a sequence of elementary 2-cycles, the relation (4.21) fixes all the coefficient  $A_P$  in (4.20) up to an overall normalization constant. But we have to be careful here! This sequence of 2 cycles is not unique and therefore could lead to different expressions for certain coefficients  $A_P$ .

For instance, the permutation (132) in case  $N = 3$  can not only be written as  $(132) = (23)(13)(12)I$  but also as  $(132) = (12)(13)(23)I$ . Thus this permutation can be reached by (at least) two different paths of 2-cycles. For the procedure to be consistent these paths must be yield the same result  $A_{(132)}$  when using equation (4.21). This equivalence can be expressed in terms of scattering matrices as

$$S^{12}(k_1, k_2)S^{13}(k_1, k_3)S^{23}(k_2, k_3) = S^{23}(k_2, k_3)S^{13}(k_1, k_3)S^{12}(k_1, k_2), \quad (4.24)$$

which is referred to as the Yang Baxter equation. Similar considerations require that the scattering matrix also needs to satisfy

$$\begin{aligned} S^{ij}(k_i, k_j)S^{ji}(k_j, k_i) &= I \\ S^{ij}(k_i, k_j)S^{mn}(k_m, k_n) &= S^{mn}(k_m, k_n)S^{ij}(k_i, k_j), \end{aligned} \quad (4.25)$$

for  $m, n \neq i, j$ . It can be shown that if the scattering matrix fulfills the Yang Baxter equation together with the relations (4.25), equation (4.21)

$$S^{q(q+1)}(k_{Pq}, k_{P'q}) = \frac{A_P}{A_{P'}}, \quad (4.26)$$

yields for every  $A_P$  a unique value, which proves that the construction (4.20) is consistent [55]. One can demonstrate that the scattering matrix (4.21) obeys these equations and therefore the Bethe Ansatz construction (4.20) for the Heisenberg model is consistent.

So in general, if the  $S$ -matrix derived from the Hamiltonian satisfies the Yang Baxter equation, then the Bethe Ansatz solution for the wave function is consistent and the model is integrable. But how can a model fail to have Bethe Ansatz states? Using the Bethe Ansatz procedure we insist that during collisions the individual momenta of the particles are conserved. This goes beyond energy conservation ( $\sum_k \cos k_j = \text{constant}$ ) or

momentum conservation ( $\sum_j k_j = \text{constant}$ ) and this is a special feature of an integrable system. This feature reflects the fact that the model possesses additional dynamical symmetry, expressed by an infinite number of conservation laws which make the model solvable.

To determine the allowed values for the momenta  $k_j$ , we consider the periodicity conditions, which can be stated as

$$f(x_1, \dots, x_N) = f(x_2, \dots, x_N, x_1 + L). \quad (4.27)$$

This yields  $N$  equations

$$e^{ik_j L} S^{j-1}(k_j, k_{j-1}) \dots S^{j-1}(k_j, k_1) S^{jN}(k_j, k_N) \dots S^{j+1}(k_j, k_{j+1}) = 1, \quad (4.28)$$

for  $j = 1, \dots, N$ . These equations consist of a kinematic part  $\exp(ik_j L)$  and terms expressing the scattering of the particle  $j$  with the  $N - 1$  other particles when the particle  $j$  makes the circle. Since the scattering matrix is a complex number  $S^{jl}(k_j, k_l) = -\exp[i\theta(k_j, k_l)]$ , this equation can be written as

$$e^{ik_j L} \prod_{l=1, l \neq j}^N S^{jl}(k_j, k_l) = e^{ik_j L} (-1)^{N-1} e^{i \sum_{l=1}^N \theta(k_j, k_l)} = 1. \quad (4.29)$$

One can introduce the the so-called rapidity transformation

$$\lambda_j(k_j) = -\frac{1}{2} \cotan\left(\frac{k_j}{2}\right), \quad e^{ik_j} = \frac{2\lambda_j - i}{2\lambda_j + i}, \quad (4.30)$$

to make the scattering matrix depend only on the difference of the velocities  $\lambda_j$  and  $\lambda_l$

$$S^{jl}(k_j, k_l) = \frac{\lambda_j - \lambda_l + i}{\lambda_j - \lambda_l - i} = S^{jl}(\lambda_j - \lambda_l). \quad (4.31)$$

Using these rapidity variables  $\lambda_l$ , the periodicity equation (4.29) simplifies to

$$\left(\frac{2\lambda_l - i}{2\lambda_l + i}\right)^L = -\prod_{j=1}^N \left(\frac{\lambda_l - \lambda_j - i}{\lambda_l - \lambda_j + i}\right). \quad (4.32)$$

If all the  $\lambda$ 's are real, we can simply take the logarithm and we obtain

$$2L \arctan(2\lambda_l) = 2\pi I_l + 2 \sum_{j=1}^N \arctan(\lambda_l - \lambda_j), \quad (4.33)$$

where the  $I_l$  are integers if  $L - N$  is odd and half integers if  $L - N$  is even with

$$|I_l| < \frac{L - N + 1}{2}. \quad (4.34)$$

In the ground state  $N = L/2$  and then all the  $l_i$  are uniquely determined. In the thermodynamic limit the separation between the allowed  $\lambda$ 's vanishes. From equation (4.33) we can derive the distribution density  $\rho(\lambda)$  of solutions  $\lambda$  for the Bethe Ansatz equations.

The equations for the rapidities (4.33) are the most important results of the Bethe Ansatz procedure. Most results are extracted from these equations without referring to the precise form of the corresponding wave function (4.20). For instance, using these equations, we can calculate the ground energy which in terms of the rapidity  $\lambda$  can be written as

$$E = \frac{L}{4} - N \sum_{j=1}^N \cos k_j = \frac{L}{4} - \sum_{j=1}^N \frac{2}{1 + 4\lambda_j^2}. \quad (4.35)$$

In the thermodynamic limit this expression becomes

$$E_0 = \int d\lambda \rho(\lambda) \left( \frac{L}{4} - \frac{2}{1 + 4\lambda^2} \right) = \frac{L}{4} - L \ln 2. \quad (4.36)$$

Excited states can be constructed by taking out several down spins so that a number of possible  $\lambda_i$  states in equation (4.33) is not filled. Furthermore, excited states can also be obtained by looking at complex  $\lambda_j$  in (4.33) [52–54].

## 4.2 The Bethe Ansatz for the Hubbard Model

In the previous section we summarized the solution of the isotropic Heisenberg model using a system of  $N$  interacting particles with no internal structure, whose states are completely determined by the position in the chain as expressed by (4.20). For the Hubbard model we need to construct a system of particles with an internal spin structure where the different spin states get mixed in the process of collision. This requires a generalization of the Bethe Ansatz, the so called nested Bethe Ansatz, as we will explain in this section. The solution was obtained by Lieb and Wu [21] using a method introduced by Yang [56].

Let us start with the Hubbard Hamiltonian

$$H = -t \sum_{\sigma} \sum_{i=1}^L (c_{i\sigma}^* c_{i+1\sigma} + h.c.) + U \sum_{i=1}^L n_{i\uparrow} n_{i\downarrow}, \quad (4.37)$$

where  $L$  is the length of the chain and  $\sigma$  denotes the spin of the electron  $\sigma \in \{\uparrow, \downarrow\}$ . The first term describes the movement of the spinful electrons and the second term represents the Coulomb repulsion. Because the  $z$ -component of the total spin is conserved we can again choose the eigenfunction of the form

$$|F\rangle = \sum_{\sigma_1 \dots \sigma_N} \sum_{1 \leq x_k \leq L} F_{\sigma_1 \dots \sigma_N}(x_1, \dots, x_N) \prod_{i=1}^N c_{x_i, \sigma_i}^{\dagger} |0\rangle, \quad (4.38)$$

where  $c_{x_i, \sigma_i}^\dagger$  creates an electron with spin  $\sigma_i$  on side  $x_i$ . Note that in contrast with the Bethe Ansatz for the Heisenberg model, a permutation is carried out not only on the coordinates of the particles but also on the spins of the electrons.

Now we have to solve the equation  $E|F\rangle = H|F\rangle$ , which amounts to solving  $hF_{\sigma_1 \dots \sigma_N}(x_1, \dots, x_N) = EF_{\sigma_1 \dots \sigma_N}(x_1, \dots, x_N)$  where

$$h = -t \sum_{j=1}^N \Delta_j + U \sum_{j < l} \delta_{n_j n_l}. \quad (4.39)$$

First we will consider the case of two electrons.

### 4.2.1 The case $N = 2$ : two electrons

When the particles are not colliding, that is,  $x_1 \neq x_2$ , the Coulomb interaction vanishes and the equation is solved by plane waves

$$F_{\sigma_1 \sigma_2}(x_1, x_2) = A_{\sigma_1 \sigma_2} e^{i(k_1 x_1 + k_2 x_2)}, \quad (4.40)$$

with  $A_{\sigma_1 \sigma_2}$  a constant. Using the Bethe Ansatz, stating that during a collision the particles move through each other and only the phases of the particles change and not their momenta, the general solution can be written as

$$\begin{aligned} F_{\sigma_1 \sigma_2}(x_1, x_2) &= \mathcal{A} e^{i(k_1 x_1 + k_2 x_2)} [A_{\sigma_1 \sigma_2}(I) \theta(X_I) + A_{\sigma_2 \sigma_1}((12)) \theta(X_{(12)})] \\ &= \mathcal{A} e^{i(k_1 x_1 + k_2 x_2)} [A_I(I) \theta(X_I) + A_{(12)}((12)) \theta(X_{(12)})]. \end{aligned} \quad (4.41)$$

Here  $A_I(I) \exp[i(k_1 x_1 + k_2 x_2)]$  describes the wave function before the collision ( $x_1 < x_2$ ) and  $A_{(12)}((12)) \exp[i(k_1 x_1 + k_2 x_2)]$  is the wave function afterwards ( $x_1 > x_2$ ). Furthermore we use  $A_P(Q)$  as a shorthand for  $A_{\sigma_P \sigma_Q}(Q)$ .  $\mathcal{A}$  is the anticommutator making the expression antisymmetric.

Equation (4.41) shows that there are two unrelated areas,  $x_1 < x_2$  and  $x_2 < x_1$ . We can introduce the scattering matrix  $S^{12}$  relating the amplitude in the two regions  $A_{(12)}((12)) = S^{12} A_I(I)$  which means

$$A_{\sigma_2 \sigma_1}((12)) = \sum_{\xi_1 \xi_2} [S^{12}(k_1, k_2)]_{\sigma_2 \xi_2}^{\sigma_1 \xi_1} A_{\xi_1 \xi_2}(I). \quad (4.42)$$

Note that a general wave function  $A_{\sigma_1 \sigma_2}(I) \exp[i(k_1 x_1 + k_2 x_2)]$  for  $x_1 < x_2$  now can scatter into four different wave functions  $A_{\xi_2 \xi_1}((12)) \exp[i(k_1 x_1 + k_2 x_2)]$  for  $x_1 > x_2$  and  $\xi_i \in \{\uparrow, \downarrow\}$ . Therefore the scattering matrix has in general  $4 \times 4 = 16$  components describing the transition of the 4 different components  $A_{\xi_1 \xi_2}(I)$  into the 4 components  $A_{\sigma_2 \sigma_1}((12))$ . Note that a lot of these components are zero because the spin is conserved during a collision.

Using the Schrödinger equation in case  $x_1 = x_2$  and using the continuity of (4.41), we obtain an expression for the scattering matrix

$$\left[ S^{12}(k_1, k_2) \right]_{\sigma_2 \xi_2}^{\sigma_1 \xi_1} = \frac{(\sin k_1 - \sin k_2) \delta_{\sigma_1 \xi_1} \delta_{\sigma_2 \xi_2} + i \frac{U}{2t} \delta_{\sigma_1 \xi_2} \delta_{\sigma_2 \xi_1}}{\sin k_1 - \sin k_2 + \frac{iU}{2t}}, \quad (4.43)$$

and we find that the scattering matrix depends on the momenta  $k_1$  and  $k_2$ . Using (4.42) we obtain

$$A_{(12)((12))} = \left( \frac{iU/2t}{\sin k_1 - \sin k_2 + \frac{iU}{2t}} \right) A_I(I) + \left( \frac{\sin k_1 - \sin k_2}{\sin k_1 - \sin k_2 + \frac{iU}{2t}} \right) A_{(12)}(I).$$

Generalizing this procedure for  $N$  down spins we obtain

$$\begin{aligned} F_{\sigma_1 \dots \sigma_N}(x_1, \dots, x_N) &= \mathcal{A} e^{i \sum_j k_j x_j} \sum_R A_R(R) \theta(X_R) \\ &= \sum_P (-1)^P e^{i \sum_j k_j x_{Pj}} \sum_R A_{PR}(R) \theta(X_{PR}) \\ &= \sum_P (-1)^P e^{i \sum_j k_{Pj} x_j} \sum_Q A_Q(PQ) \theta(X_Q) \\ &= \sum_P (-1)^P e^{i \sum_j k_{PQj} x_{Qj}} \sum_Q A_Q(PQ) \theta(X_Q) \\ &= \sum_P (-1)^{(P+Q)} e^{i \sum_j k_{Pj} x_{Qj}} \sum_Q A_Q(P) \theta(X_Q). \end{aligned} \quad (4.44)$$

Here  $\theta(X_Q) = 1$  if  $x_{Q1} < \dots < x_{QN}$  and  $\theta(X_Q) = 0$  otherwise. The coefficients  $A_Q(P)$  can be related using the scattering matrix  $S^{q(q+1)}(k_{Pq}, k_{P(q+1)})$  which describes a collision between particle  $q$  and  $q+1$  with momenta  $k_{Pq}$  and  $k_{P(q+1)}$ . Using the Schrödinger equation for  $x_q = x_{q+1}$  and the continuity equation for (4.44), we find

$$\begin{aligned} A_{Q'}(P') &= S^{q(q+1)}(k_{Pq}, k_{P(q+1)}) A_Q(P) \\ &= \frac{(\sin k_{Pq} - \sin k_{P(q+1)}) A_Q(P) + (i \frac{U}{2t}) A_{Q'}(P)}{\sin k_{Pq} - \sin k_{P(q+1)} + i \frac{U}{2t}}. \end{aligned} \quad (4.45)$$

Here  $P'$  is defined as in (4.22).  $Q'$  is defined in the same way and equals  $Q$  except for the interchange of  $Qq$  and  $Q(q+1)$ . So the scattering matrix equals

$$S^{q(q+1)}(k_{Pq}, k_{P(q+1)}) = \frac{(\sin k_{Pq} - \sin k_{P(q+1)}) + i \frac{U}{2t} P Q q Q(q+1)}{\sin k_{Pq} - \sin k_{P(q+1)} + i \frac{U}{2t}}, \quad (4.46)$$

where the permutation operator  $P Q q Q(q+1)$  interchanges the spin labels  $Qq$  and  $Q(q+1)$ . One can prove that this scattering matrix obeys the Yang Baxter equation (4.24) together with the equations (4.25) and thus the Bethe Ansatz construction (4.44) is consistent.

To obtain the allowed values for the momenta, we have to consider the periodicity condition, which can be written as

$$F_{\sigma_1 \dots \sigma_N}(x_1, \dots, x_N) = F_{\sigma_2 \dots \sigma_N, \sigma_1}(x_2, \dots, x_N, x_1 + L). \quad (4.47)$$

Because the wave functions is antisymmetric, this expression is equivalent to a similar expression for the other  $x_j$ . This equation gives rise to  $N$  equations for  $j = 1, \dots, N$ :

$$e^{ik_j N} S^{jj-1}(k_j, k_{j-1}) \dots S^{j1}(k_j, k_1) S^{jN}(k_j, k_N) \dots S^{jj+1}(k_j, k_{j+1}) = 1. \quad (4.48)$$

This equation consists of a kinematic term  $\exp(ik_j N)$  and scattering terms  $S^{jl}$  describing the collision with particle  $l$  when particle  $j$  makes a circle. Note that because  $S^{jl}$  are  $4 \times 4$  matrices they do not really commute and this product is not equal to  $\sum_{l \neq j} S^{jl}(k_j, k_l)$  like in the Heisenberg model where  $S^{jl}(k_j, k_l)$  is just a complex number and therefore commutes.

## 4.2.2 General $N$ case

In deriving equation (4.44) we have not made use of the spin degree of freedom and only considered the movement of the electrons disregarding their spin. To solve the periodicity equation (4.48) and obtain the allowed values for  $k_j$ , we will make use of the symmetries of the wave function with respect to the exchange of spins. This is done in the similar way as was done for the Heisenberg model.

Suppose we have  $M$  down electrons and  $N - M$  electrons whose spins are up. At this point  $A_Q(P)$  is written in the form

$$A_Q(P) = A_{\sigma_{Q1} \dots \sigma_{QN}}(P) = \phi(y_1, \dots, y_M | P). \quad (4.49)$$

Here the numbers  $y_1, \dots, y_M$  are defined to be the positions of the down spins among the spins in the  $N$ -chain  $\sigma_{Q1}, \sigma_{Q2}, \dots, \sigma_{QN}$  in increasing order, that is

$$1 \leq y_1 < y_2 < \dots < y_M \leq N. \quad (4.50)$$

So the  $y_i$  are the positions of the down spins on a lattice where we have squeezed out the holes and  $\phi(y_1, \dots, y_M | P)$  keeps track of the relative position of the up and down spin. So the general equation equals

$$F_{\sigma_1 \dots \sigma_N}(x_1, \dots, x_N) = \sum_P (-1)^{P+Q} e^{i \sum_{j=1}^N k_{Pj} x_{Qj}} \phi(y_1, \dots, y_M | P). \quad (4.51)$$

The solution of  $\phi(y_1, \dots, y_M | P)$  can be obtained in the same manner as the solution for  $f(x_1, \dots, x_N)$  in the previous section, but now we use the periodicity condition (4.48) instead of the Schrödinger equation like (4.16).

First we will examine the case the particles are non-overlapping so that  $y_\alpha + 1 \neq y_{\alpha+1}$ . The solution of the periodicity condition (4.48) is not a product of plane waves like the solution for  $f(x_1, \dots, x_N)$ , but more generally solved by a product of functions  $G_P$

$$\prod_{\alpha=1}^M G_P(\Lambda_\alpha, y_\alpha) = G_P(\Lambda_1, y_1) \dots G_P(\Lambda_M, y_M). \quad (4.52)$$

These solutions  $G_P(\Lambda_\alpha, \gamma_\alpha)$  are characterized by the rapidity  $\Lambda_\alpha$  with

$$G_P(\Lambda_\alpha, \gamma_\alpha) = \prod_{j=1}^{\gamma_\alpha-1} \frac{\sin k_P j - \Lambda_\alpha + i \frac{U}{4t}}{\sin k_P j - \Lambda_\alpha - i \frac{U}{4t}}. \quad (4.53)$$

Now consider what happens if two particles are colliding so that  $\gamma_\alpha + 1 = \gamma_{\alpha+1}$ . Using the Bethe Ansatz which states that the wave function only changes with a phase factor, the general solution for  $\phi(\gamma_1, \dots, \gamma_M | P)$  can be written as (see also (4.11) and (4.20))

$$\begin{aligned} \phi(\gamma_1, \dots, \gamma_M | P) &= \mathcal{S} \left( G_P(\Lambda_1, \gamma_1) \dots G_P(\Lambda_M, \gamma_M) \sum_Q B_Q \theta(Y_Q) \right) \\ &= \sum_{R, Q} B_Q G_P(\Lambda_1, \gamma_{R1}) \dots G_P(\Lambda_M, \gamma_{RM}) \theta(Y_{RQ}) \\ &= \sum_Q B_Q G_P(\Lambda_{Q1}, \gamma_1) \dots G_P(\Lambda_{QM}, \gamma_M), \end{aligned} \quad (4.54)$$

where  $\mathcal{S}$  is the symmetrize operator and  $\theta(Y_P)$  is defined similar to  $\theta(X_Q)$  in (4.44). Furthermore we used that the  $\gamma_j$  are in increasing order.

Using the periodicity condition we obtain the following solution for the rapidities  $\Lambda_\alpha$  in  $G_P(\Lambda_\alpha, \gamma_\alpha)$ .

$$\begin{aligned} e^{ik_j L} &= \prod_{\alpha=1}^M \frac{\Lambda_\alpha - \sin k_j + i \frac{U}{4t}}{\Lambda_\alpha - \sin k_j - i \frac{U}{4t}} \\ \prod_{j=1}^N \frac{\Lambda_\alpha - \sin k_j + i \frac{U}{4t}}{\Lambda_\alpha - \sin k_j - i \frac{U}{4t}} &= - \prod_{\beta=1}^M \frac{(\Lambda_\beta - \Lambda_\alpha) + i \frac{U}{2t}}{(\Lambda_\beta - \Lambda_\alpha) - i \frac{U}{2t}}. \end{aligned} \quad (4.55)$$

Here ( $j = 1, \dots, N$ ) and ( $\alpha = 1, \dots, M$ ). Note that these equations are coupled and therefore difficult to solve.

In summary, the full Bethe Ansatz wave functions for the Hubbard model are generated in two steps. First the charge waves of electrons of unspecified spins characterized by momenta  $k_j$  and describing the positions of the electrons are constructed in equation (4.44). Secondly a number of spin waves characterized by rapidities  $\Lambda_j$  and associated with the position of the down spins of the these electrons over a squeezed lattice, are injected. This procedure is called a (2-step) nested Bethe Ansatz.

From these equation in the thermodynamic limit, one can derive expressions for the distribution densities  $\rho_c(k)$  and  $\rho_s(\Lambda)$  for the solutions. Many results for the Hubbard Model can be extracted using these densities. For instance, the ground state energy is given by

$$E_0 = -2tL \int_{-k_0}^{k_0} dk \rho_c(k) \cos k, \quad (4.56)$$

where the value  $k_0$  is set by the condition

$$\int_{-k_0}^{k_0} dk \rho_c(k) = \frac{N}{L}. \quad (4.57)$$

These expression for the energy will be used to calculate  $K_\rho$  in the next section.

### 4.2.3 Large $U$ limit

Let us now consider the limit when the Coulomb interaction  $U$  is very large. It will turn out that the wave function then simplifies enormously.

In the large  $U$  limit,  $G_P(\Lambda_\alpha, y_\alpha)$  in (4.53) is approximated by

$$G_P(\Lambda_\alpha, y_\alpha) = \prod_{j=1}^{y_\alpha-1} \left( \frac{2\lambda_\alpha - i}{2\lambda_\alpha + i} \right) = \left( \frac{2\lambda_\alpha - i}{2\lambda_\alpha + i} \right)^{y_\alpha-1}, \quad (4.58)$$

with  $\lambda_\alpha = \frac{2\Lambda_\alpha}{U}$ . If we now write  $\exp(ik'_\alpha) = \left( \frac{2\lambda_\alpha - i}{2\lambda_\alpha + i} \right)$  then  $G_P(\Lambda_\alpha, y_\alpha) \sim \exp(ik'_\alpha y_\alpha)$  and  $\phi(y_1, \dots, y_M | P) \sim \sum_R A_R \exp(i \sum_j k'_{Rj} y_j)$  similar to the Bethe Ansatz solution for the Heisenberg chain. Furthermore in this limit the rapidity equations for  $k_j$  and  $\Lambda_\alpha$  (4.55) completely decouple

$$\begin{aligned} e^{ik_j L} &= \prod_{\alpha=1}^M \left( \frac{2\lambda_\alpha - i}{2\lambda_\alpha + i} \right) \\ \left( \frac{2\lambda_\alpha - i}{2\lambda_\alpha + i} \right)^N &= - \prod_{\beta=1}^M \left( \frac{\lambda_\beta - \lambda_\alpha - i}{\lambda_\beta - \lambda_\alpha + i} \right). \end{aligned} \quad (4.59)$$

The first equation reproduces the spectrum of a spinless fermion gas with antiperiodic boundary conditions. The second one is the equation for a Heisenberg chain with periodic boundary conditions.

Thus for  $U$  large the wave function equals

$$\begin{aligned} F_{\sigma_1 \dots \sigma_N}(x_1, \dots, x_N) &= \sum_P (-1)^{P+Q} e^{i \sum_{j=1}^N k_{Pj} x_{Qj}} \sum_R A_R e^{i \sum_{m=1}^M k'_{Rm} y_m} \\ &= \sum_P (-1)^P e^{i \sum_{j=1}^N k_{Pj} x_j} \sum_R A_R e^{i \sum_{m=1}^M k'_{Rm} y_m}, \end{aligned} \quad (4.60)$$

and can be written as the product

$$F_{\sigma_1 \dots \sigma_N}(x_1, \dots, x_N) = \psi_{SF}(x_1, \dots, x_N) \phi_{Heis.}(y_1, \dots, y_M), \quad (4.61)$$

with

$$\begin{aligned} \psi_{SF}(x_1, \dots, x_N) &= \sum_P (-1)^P e^{i \sum_{j=1}^N k_{Pj} x_j} \\ \phi_{Heis.}(y_1, \dots, y_M) &= \sum_R A_R e^{i \sum_{m=1}^M k'_{Rm} y_m}. \end{aligned} \quad (4.62)$$

Here  $x_j$  denote the spatial coordinates of the  $N$  electrons, and the  $y_1, \dots, y_M$  coordinates label the positions of the  $M$  spin down electrons on a squeezed lattice whose sides are  $x_1, \dots, x_N$ . With this notation,  $\phi_{Heis.}(y_1, \dots, y_M)$  is the same function appearing in the Bethe Ansatz wave function of a Heisenberg  $N$ -site chain. Furthermore,  $\psi_{SF}$  is the groundstate wave function of a free spinless Fermi gas with antiperiodic boundary conditions.

Using formula (4.61), we may think of the wave function  $F_{\sigma_1 \dots \sigma_N}(x_1, \dots, x_N)$  as being constructed by two consecutive steps: First distribute the  $N$  electrons arbitrarily over the chain while disregarding their spin as though they were spinless fermions. Secondly, distribute the spins over these electrons like the spins on a Heisenberg chain of  $N$  sites while disregarding the holes in between the electrons.

So for  $U$  large the fundamental excitations of the Hubbard model are not electron-like but are either spinon (carrying spin and no charge) or holons (carrying charge but no spin) form a two-component Luttinger Liquid. These decoupled equation for spin and charge will be used in the next section to calculate the spin-spin correlation function.

### 4.3 Hubbard model spin-spin correlations for large $U$

The previous section showed that when  $U$  is large the distribution of the charge and spin is completely decoupled. The spins of the electrons are independent of the holes that are located in between the electrons. This means that the spin correlations of the doped problem in the large  $U$  limit are identical to those of a Heisenberg spin system, except that the spin system now resides on the 'squeezed' chain obtained by removing all holes situated in between the spins. Parola and Sorella [22] used these notions in their calculation of  $\langle S^z(x)S^z(0) \rangle$ . We will present these calculations in this section. As will turn out in the next chapter, their technique can also be used to calculate the hidden order in the large  $U$  limit.

To calculate this spin-spin correlator, they summed over all possible spin configurations with sites 0 and  $x$  occupied and  $j - 2$  electrons in between. For fixed  $j$ , the spin correlations over the squeezed lattice of length  $j - 1$  for these configurations equals the Heisenberg spin correlation function  $O_{Heis.}(x) = \langle S^z(x)S^z(0) \rangle_{Heis.}$ , and one can write

$$\langle S^z(x)S^z(0) \rangle = \sum_{j=2}^{x+1} P_{SF}^x(j) O_{Heis.}(j-1). \quad (4.63)$$

$P_{SF}^x(j)$  is the probability of finding  $j$  particles in  $[0, x]$  with one electron at 0 and one at  $x$ . So for fixed  $j$ , the spin-spin correlation function factorizes into a charge part  $P_{SF}^x$  and a spin part  $O_{Heis.}(j-1)$ . The Heisenberg spin correlation  $O_{Heis.}(j)$  describes the tendency toward antiferromagnetic long range order. For large separation  $j$

$$O_{Heis.}(j) = (-1)^j f(j) = (-1)^j \Gamma\left(\frac{\log \frac{1}{2}(j)}{j}\right), \quad (4.64)$$

where  $\Gamma$  is a constant [57]. Furthermore the function  $f(j)$  obeys the following inequality for any  $j > j' \geq x$

$$\left| \frac{f(j) - f(j')}{j - j'} \right| \leq M(x) = 2\Gamma \frac{\log^{\frac{1}{2}}(x)}{x^2}. \quad (4.65)$$

In formula (4.63) the function  $P_{SF}^x(j)$  is given by

$$P_{SF}^x(j) = \langle n(0)n(x) \delta \left( \sum_{l=0}^x n(l) - j \right) \rangle_{SF}. \quad (4.66)$$

Here the average is taken over the spinless fermion groundstate. This function  $P_{SF}^x(j)$  is a highly non-local correlation function and it is difficult to calculate, even for the free fermion case. The function is positive definite and as is proven in (3.31), is normalized to

$$\begin{aligned} Z &= \sum_{j=1}^{x+1} P_{SF}^x(j) = \langle n(0)n(x) \rangle_{SF} = \langle n_{SF}(0)n_{SF}(x) \rangle \\ &= \rho_{tot}^2 - \frac{1}{2} \left( \frac{1 - \cos(2k_F x)}{\pi x^2} \right), \end{aligned} \quad (4.67)$$

where  $k_F = \frac{N\pi}{V}$ ,  $\rho_{tot} = \rho_{\uparrow} + \rho_{\downarrow}$  is the average electron density and we took the thermodynamic limit ( $N, L \rightarrow \infty$ ,  $\rho_{tot} = N/L$ ). The first two moments are given by

$$\begin{aligned} \langle r \rangle_x &= \frac{1}{Z} \sum_{j=2}^{x+1} j P_{SF}^x(j) = x\rho_{tot} + 1 \\ \langle r^2 \rangle_x &= \frac{1}{Z} \sum_{j=2}^{x+1} j^2 P_{SF}^x(j) = \langle r \rangle_x^2 + \frac{\ln(x)}{\pi^2}. \end{aligned} \quad (4.68)$$

Note that the averages  $\langle \dots \rangle_x$  are  $x$  dependent.

The results from equation (4.68) show that the function  $P_{SF}^x(j)$  is strongly peaked around  $j \sim \rho_{tot}x$ , which means that a small neighborhood of  $j = \rho_{tot}x$  gives a significant contribution to the spin-spin correlation  $\langle S^z(x)S^z(0) \rangle$  in (4.63). This makes it possible to calculate the asymptotic behavior of the sum (4.63) without knowing the full probability function  $P_{SF}^x(j)$ . To do this, we need the lemma which was used by Parola and Sorella. We present their prove in the next section. We need this prove also to calculate the topological correlator  $O_{top}(x)$  in the limit  $U \rightarrow \infty$  in the next chapter.

### 4.3.1 Lemma

In this section we will prove the following lemma:

**Lemma** The sum  $\sum_{j=2}^{x+1} P_{SF}^x(j)(-1)^j f(j)$  with  $f(j)$  bounded and satisfying (4.65), differs from the sum  $\left[ \sum_{j=2}^{x+1} P_{SF}^x(j)(-1)^j \right] f(\langle r \rangle_x)$  by terms vanishing faster than  $\frac{\log^{\frac{3}{2}}(x)}{x^2}$ .

**Proof** The difference  $R$  between both expressions can be split into two sums  $R = R_1 + R_2$  with

$$\begin{aligned} R_1 &= \sum_{j=2}^{\langle r \rangle_x} P_{SF}^x(j)(-1)^j [f(j) - f(\langle x \rangle_x)] \\ R_2 &= \sum_{j=\langle \frac{r \rangle_x}{2} + 1}^{x+1} P_{SF}^x(j)(-1)^j [f(j) - f(\langle r \rangle_x)]. \end{aligned} \quad (4.69)$$

Since the function  $f(j)$  is bounded, say  $|f(j)| \leq A$ , we find

$$R_1 \leq 2A \sum_{j=2}^{\langle \frac{r \rangle_x}{2}} P_{SF}^x(j). \quad (4.70)$$

Using  $P_{SF}^x(j) \geq 0$ , this sum can easily be bounded using the variance of  $j$

$$\begin{aligned} \sum_{j=2}^{x+1} P_{SF}^x(j)(j - \langle r \rangle_x)^2 &\geq \sum_{j=2}^{\langle \frac{r \rangle_x}{2}} P_{SF}^x(j)(j - \langle r \rangle_x)^2 \\ &\geq (j - \langle r \rangle_x)_{j=\langle \frac{r \rangle_x}{2}} \sum_{j=2}^{\langle \frac{r \rangle_x}{2}} P_{SF}^x(j) \\ &= \frac{\langle r \rangle_x^2}{4} \sum_{j=2}^{\langle \frac{r \rangle_x}{2}} P_{SF}^x(j). \end{aligned} \quad (4.71)$$

And thus, using (4.68):

$$R_1 \leq \frac{8A}{\langle r \rangle_x^2} \left[ \langle r^2 \rangle_x - \langle r \rangle_x^2 \right] = \frac{8A}{(x\rho + 1)^2} \frac{\ln(x)}{\pi^2} \leq \frac{8A}{\rho^2 \pi^2} \frac{\ln(x)}{x^2}, \quad (4.72)$$

we find  $R_1 \leq \text{const.} \frac{\ln^{\frac{3}{2}}(x)}{x^2}$ .

The term  $R_2$  can be bounded using condition (4.65) together with the Schwartz in-

equality stating that for any scalar product  $|y^2| \leq |y|^2$  and so

$$\begin{aligned}
 R_2 &\leq M \left( \frac{\langle r \rangle_x}{2} \right) \sum_{j=\langle r \rangle_x}^{x+1} |j - \langle r \rangle_x| P_{SF}^x(j) \\
 &\leq M \left( \frac{\langle r \rangle_x}{2} \right) \sum_{j=2}^{x+1} |j - \langle r \rangle_x| P_{SF}^x(j) \\
 &\leq M \left( \frac{\langle r \rangle_x}{2} \right) \left( \sum_{j=2}^{x+1} (j - \langle r \rangle_x)^2 P_{SF}^x(j) \right)^{\frac{1}{2}} \\
 &= \frac{2\Gamma \ln^{\frac{1}{2}}\left(\frac{x\rho+1}{2}\right)}{\left(\frac{x\rho}{2}\right)^2} \left( \frac{\rho^2}{\pi^2} \ln(x) \right)^{\frac{1}{2}} \\
 &\leq \text{const.} \frac{\ln(x)}{x^3} \leq \text{const.} \frac{\ln(x)}{x^2}.
 \end{aligned} \tag{4.73}$$

And so we get the desired result.  $\square$

### 4.3.2 Final result

Now we can use the lemma of the previous section to calculate  $\langle S^z(x)S^z(0) \rangle$ . For large distances  $x$ , the spin-spin correlation function (4.63) can be written as

$$\begin{aligned}
 \langle S^z(x)S^z(0) \rangle &= \sum_{j=2}^{x+1} P_{SF}^x(j) O_{Heis.}(j-1) \\
 &= \sum_{j=2}^{x+1} P_{SF}^x(j) (-1)^{j-1} f(j-1) \approx - \sum_{j=2}^{x+1} P_{SF}^x(j) (-1)^j f(j) \\
 &= - \left[ \sum_{j=2}^{x+1} P_{SF}^x(j) (-1)^j \right] f(\langle r \rangle_x) + \mathcal{O} \left( \frac{\ln^{\frac{3}{2}}(x)}{x^2} \right) \\
 &= -C(x) \Gamma \frac{\ln^{\frac{1}{2}}(\rho_{tot}x)}{\rho_{tot}x} + \mathcal{O} \left( \frac{\ln^{\frac{3}{2}}(x)}{x^2} \right),
 \end{aligned} \tag{4.74}$$

where we used  $\langle r \rangle_x = \rho_{tot}x + 1 \approx \rho_{tot}x$  for large distances  $x$  and

$$\begin{aligned}
 C(x) &= \sum_{j=2}^{x+1} P_{SF}^x(j) (-1)^j = \sum_{j=2}^{x+1} \langle n(0)n(x) \delta \left( \sum_{l=0}^x n(l) - j \right) \rangle_{SF} (-1)^j \\
 &= \langle n(0) (-1)^{\sum_{l=0}^x n(l)} n(x) \rangle_{SF} = \langle n_{SF}(0) (-1)^{\sum_{l=0}^x n_{SF}(l)} n_{SF}(x) \rangle.
 \end{aligned} \tag{4.75}$$

As will turn out,  $C(x)$  is also important for the topological correlator calculations for  $U = 0$  which are considered in chapter 6.

In case  $\rho_{tot} = 1$ , the half filled case, Parola and Sorella show that  $C(x) = (-1)^{x+1}$ . When substituted in (4.74) this gives just the Heisenberg spin-spin correlation (4.64), appropriate in the half filled case for large  $U$ :

$$\langle S^z(x)S^z(0) \rangle \sim \Gamma \cos(2k_F x) \frac{\ln^{\frac{1}{2}}(x)}{x} = \Gamma(-1)^x \frac{\ln^{\frac{1}{2}}(x)}{x}. \quad (4.76)$$

Here  $k_F = \frac{\pi\rho_{tot}}{2} = \frac{\pi}{2}$ .

For quarter filling  $\rho_{tot} = \frac{1}{2}$ , Parola and Sorella demonstrate that for large  $x$ ,  $C(x)$  equals

$$C(x) = -\frac{A^2 \cos(2k_F x)}{\sqrt{2} x^{\frac{1}{2}}}, \quad (4.77)$$

where again  $k_F = \frac{\pi\rho_{tot}}{2} = \frac{\pi\rho_{SF}}{2}$  where  $A = 0.645002448$ . So at quarter filling  $\rho_{tot} = \frac{1}{2}$ , the long range behavior of the spin-spin correlation function equals

$$\langle S^z(x)S^z(0) \rangle = A^2 \sqrt{2} \Gamma \frac{\cos(2k_F x)}{\rho x^{\frac{3}{2}}} \ln^{\frac{1}{2}}(x/2) + \mathcal{O}\left(\frac{\ln^{\frac{3}{2}}(x)}{x^2}\right). \quad (4.78)$$

Furthermore, Parola and Sorella argued, although they do not rigorously prove this, that  $C(x) \sim \cos(2k_F x)/x^{\frac{1}{2}}$  for all  $\rho \neq 1$  away from half filling and thus  $\langle S^z(x)S^z(0) \rangle = \cos(2k_F x)/x^{\frac{3}{2}}$  in the large  $U$  limit. In chapter 6 we numerically calculate  $C(x)$  for several fillings away from half filling and verified that this assumption is indeed correct. (See equation (6.16).)

### 4.3.3 Interpretation

In this last part of this section, we will summarize the results that we obtained so far. Also we reinterpret the data and show that the usual explanation as is presented by Schulz [59] is not valid. The analysis we present is the basis for our investigation of the topological order in the next chapter.

Let us start by comparing the lattice expressions equations (4.76) and (4.78) with the general bosonization results of chapter 3 in equation (3.67),  $\langle S^z(x)S^z(0) \rangle \sim \cos(2k_F x) / x^{K_s + K_c}$ . By  $SU(2)$  symmetry, in both cases  $K_s = 1$ . And thus we find  $K_c = 0$  and  $K_c = \frac{1}{2}$  which are appropriate for respectively the half and quarter filled cases. The deviation of the charge stiffness  $K_c$  for  $\rho_{tot} = 1$  is due to Umklapp processes, which are present only at half filling and enhance the antiferromagnetic correlations. These results are in agreement with values for the charge stiffness obtained by numerically [58] solving the Bethe Ansatz (4.55) as shown in figure 3.3. The function  $K_c(\rho_{tot})$  is discontinuous for  $\rho_{tot} = 0$  and  $\rho_{tot} = 1$  where  $K_c = 0$ .

It has been claimed by Schulz [59] that the result  $\langle S^z(x)S^z(0) \rangle \sim \cos(2k_F x)/x^{K_s + K_c}$  can be explained using the idea that the system can be seen as a harmonic solid with a

spin at each site where the elastic coupling between the sites is provided by the motion of the holes. In this picture the spins are 'surfing' on charge waves. This interpretation is wrong! For let us calculate the spin-spin correlation function using this approach.

In this continuum approximation, the spin density equals

$$\vec{S}(x) = \sum_m \vec{S}_{Heis.}(m) \delta(x - x_m), \quad (4.79)$$

where we sum over all the electrons. Using the hypothesis about the harmonic motion of the electrons,  $x_m$  can be written as  $x_m = R_m + u_m$ , where  $R_m = \frac{m}{\rho}$  is the average electron of the  $m$ -th electron and  $u_m$  is the displacement to this position. Using some algebra the correlation function can be written as

$$\langle \vec{S}(x) \cdot \vec{S}(0) \rangle \sim \int dq \sum_{m,m'} e^{-iqx} \langle \vec{S}_{Heis.}(m) \cdot \vec{S}_{Heis.}(m') \rangle e^{iq(R_m - R_{m'})} \langle e^{iq(u_m - u_{m'})} \rangle. \quad (4.80)$$

Here, the average over  $u_m$  has a powerlaw behavior

$$\langle e^{iq(u_m - u_{m'})} \rangle \approx |m - m'|^{-\alpha(q)}, \quad (4.81)$$

with  $\alpha(q) \sim q^2$ . The  $q$  integration in (4.80) is dominated by the term  $q \approx \pi\rho = 2k_F$  and thus, using the Heisenberg correlation function (4.64), we obtain

$$\begin{aligned} \langle \vec{S}(x) \cdot \vec{S}(0) \rangle &\approx \int dq \sum_{m,m'} e^{iq(R_m - R_{m'} - x)} \langle \vec{S}_{Heis.}(m) \cdot \vec{S}_{Heis.}(m') \rangle |m - m'|^{-\alpha(2k_F)} \\ &\approx \int dq \sum_{m,m'} e^{iq(\frac{m}{\rho} - \frac{m'}{\rho} - x)} \frac{(-1)^{m-m'}}{|m - m'|^{1+\alpha(2k_F)}} \\ &= \frac{\cos(\pi\rho x) \ln^{\frac{1}{2}}(\rho x)}{(\rho x)^{1+\alpha(2k_F)}} = \frac{\cos(2k_F x)}{(\rho x)^{1+\alpha(2k_F)}} \ln^{\frac{1}{2}}(\rho x). \end{aligned} \quad (4.82)$$

In comparing this result with the bosonization result  $\langle S^z(x) S^z(0) \rangle \sim \cos(2k_F x)/x^{K_s + K_c}$ , Schulz claims that  $\alpha(2k_F) = K_c$ . This is of course tempting, but also incorrect. Using a similar calculation one can show that  $\langle n_{Tot}(x) n_{Tot}(0) \rangle \sim 1/x^{\alpha(2k_F)}$ . But in the limit  $U \rightarrow \infty$  the particles behave like spinless fermions and  $\langle n_{Tot}(x) n_{Tot}(0) \rangle \sim 1/x^{4K_c} = 1/x^2$  with  $K_c = 1/2$ . And so one finds  $\alpha(2k_F) = 4K_c$  and not  $\alpha(2k_F) = K_c$ , like Schulz claimed. Using this correct identification, the spin-spin correlation (4.82) yields  $\langle \vec{S}(x) \cdot \vec{S}(0) \rangle = \cos(2k_F x)/x^{K_s + 4K_c}$ . This is indeed the result for spins that are surfing on charge waves since it is the product of charge and spin decay. But it is clearly not equal to the results for the Hubbard model.

So although the spin and charge degree of freedom are decoupled, the spin-spin correlation function is not simply the product of the charge and spin correlator. The reason for this can be best explained using equation (4.74) for the staggered magnetization

$M^z(x) = (-1)^x S^z(x)$  which yields

$$\begin{aligned}
 \langle M^z(x) M^z(0) \rangle &= \sum_{j=2}^{x+1} P_{SF}^x(j) (-1)^x \langle S^z(j-1) S^z(0) \rangle_{Heis.} \\
 &= \sum_{j=2}^{x+1} \langle n_{tot}(x) \delta \left( \sum_{l=0}^x n_{tot}(l) - j \right) n_{tot}(0) \rangle (-1)^{x+j-1} f(j-1) \\
 &\approx \langle n_{tot}(x) \rangle (-1)^{\sum_{j=1}^{x-1} (1-n_{tot}(j))} \langle n_{tot}(0) \rangle \langle S^z(\rho_{tot}x) S^z(0) \rangle_{par.Heis.} \\
 &\sim -(-1)^x C(x) f(x\rho_{tot}) = \frac{\cos[(2k_F - \pi)x] \frac{1}{x}}{\sqrt{x}} \\
 &= \frac{\cos[(2k_F - \pi)x]}{x^{K_c + K_s}} \tag{4.83}
 \end{aligned}$$

with  $\langle S^z(x) S^z(0) \rangle_{par.Heis.} = f(x)$  the Heisenberg correlator without the staggering term defined by (4.64). From this formula it can be seen that the alternating sign of the Heisenberg chain gets entangled in the function  $P_{SF}^x(j)$ , describing the charge. Because of this,  $\langle S^z(x) \cdot S^z(0) \rangle \sim -C(x) f(x\rho_{tot})$  instead of the simply being proportional to  $\sum_{j=2}^{x+1} P_{SF}^x(j) f(x\rho_{tot}) = \langle n_{tot}(x) n_{tot}(0) \rangle f(\rho_{tot}x) = \langle n_{tot}(x) n_{tot}(0) \rangle \langle S^z(x) \cdot S^z(0) \rangle_{par.Heis.}$  which is the product of the spin and charge decay with  $\langle S^z(x) \cdot S^z(0) \rangle_{par.Heis.}$ . We would obtain this result if the Heisenberg spins would be parallel. In that case the spin-spin correlations would yield

$$\begin{aligned}
 \langle M^z(x) M^z(0) \rangle_{aligned} &= \sum_{j=2}^{x+1} P_{SF}^x(j) (-1)^x \langle S^z(j-1) S^z(0) \rangle_{Heis.} \\
 &= \sum_{j=2}^{x+1} \langle n_{tot}(x) \delta \left( \sum_{l=0}^x n_{tot}(l) - j \right) n_{tot}(0) \rangle (-1)^x f(j-1) \\
 &\approx (-1)^x \langle n_{tot}(x) n_{tot}(0) \rangle \langle S^z(\rho_{tot}x) S^z(0) \rangle_{par.Heis.} \\
 &\sim \frac{(-1)^x \rho_{tot} \frac{1}{x}}{\sqrt{x}} = \frac{(-1)^x}{x^{K_c + K_s}} \tag{4.84}
 \end{aligned}$$

and the spin correlator is the product of the charge and spin correlations. We can also explain this result using the elementary excitations of the Luttinger Liquid, the spinon and the holon.

Figure 4.4 shows the spinon and holons in the configuration described in the introduction and depicted in figure 1.1, only now for the staggered magnetization  $M^z(x) = (-1)^x S^z(x)$ . Clearly both the spinon and the holon cause a kink in the staggered magnetization. Note that when using the staggered magnetization the spinon is a fluctuation in an effectively parallel spin Heisenberg system as can be seen from figure 1.1. The fluctuation of the kink attached to the spinon causes the ferromagnetic like algebraic decay in the function  $f(\rho_{tot}x) = 1/(\rho x)^{K_s}$  in formula (4.83). The fluctuation of the kink

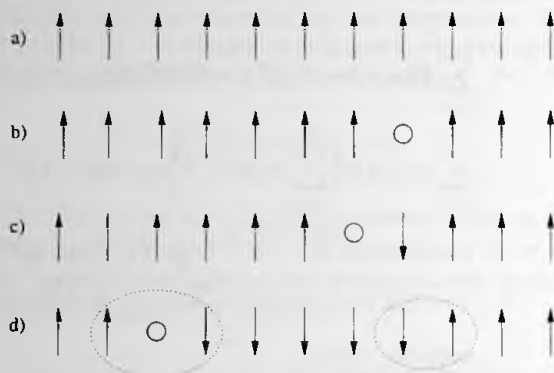


Figure 4.4: The staggered magnetization  $M^z(x) = (-1)^x S^z(x)$  for the spin configurations depicted in figure 1.1. Both spinon and the holon give rise to a kink in this operator.

attached to the holon is responsible for the algebraic decaying term

$$\langle n_{tot}(x) (-1)^{\sum_{j=1}^{x-1} (1-n_{tot}(j))} n_{tot}(0) \rangle = \frac{1}{\sqrt{x}} = \frac{1}{x^{K_c}} \quad (4.85)$$

in (4.83). So in calculating the staggered spin-spin correlation function both the spinon and the holon have a contribution with respectively a term  $1/x^{K_s}$  and  $1/x^{K_c}$ . So the kink caused by the holons the simple order of the spins is obscured and  $\langle S^z(x) S^z(0) \rangle \sim \cos(2k_F x) / x^{K_c + K_s}$ .

In the next chapter we will show how to untangle the obscuring effect of the charge and to reach the internal spin-spin correlations.

## Chapter 5

# Sublattice Parity Order

After having studied the general structure of Luttinger Liquids using bosonization and the Bethe Ansatz wave function for the Hubbard model, we are ready to turn to the main subject of this thesis, sublattice parity topological order in Luttinger Liquids which are represented by the Hubbard model with positive Coulomb repulsion  $U$ .

Sublattice parity order in the Hubbard model is most convincingly in the limit of strong interactions,  $U \rightarrow \infty$ . In this limit the wave function factorizes into a spin and a charge part, which on close inspection hints at the existence of the hidden order. In this chapter we will prove that in the limit of large  $U$  the Hubbard model has (quasi) sublattice parity order by showing that the topological correlator  $\langle S^z(x) (-1)^{\sum_{j=1}^{x-1} n_{\text{tot}}(j)} S^z(0) \rangle$  decays like a Heisenberg spin correlator.

We start by reinterpreting the Bethe Ansatz wave function in the limit  $U \rightarrow \infty$  introduced in the previous chapter.

### 5.1 Sublattice parity order for $U \rightarrow \infty$

As was summarized in chapter 4, the Bethe Ansatz wave function for the Hubbard model simplifies significantly in the special case that  $U$  is very large ( $U \rightarrow \infty$ ) [19, 20]. In this limit the charge and spin degrees of freedom decouple and the multi-electron wave function  $\psi$  factorizes into a spin and a charge component

$$\psi(x_1, \dots, x_N; y_1, \dots, y_M) = \psi_{SF}(x_1, \dots, x_N) \psi_{Heis.}(y_1, \dots, y_M). \quad (5.1)$$

The charge part  $\psi_{SF}$  represents the wave function of non-interacting spinless fermions where the coordinates  $x_i$  denote the positions of the  $N$  electrons. The spin part  $\psi_{Heis.}$  is identical to the wave function of a chain of Heisenberg spins interacting via an antiferromagnetic nearest neighbor exchange. As the total spin is conserved, the wave function  $\psi_{Heis.}$  is completely determined by the  $M$  positions of the up spins corresponding to the coordinates  $y_j$ ,  $j = 1, \dots, M$ . The surprise is that the coordinates  $y_j$  do not refer to the original Hubbard chain with length  $L$ , but instead to a new space: a lattice of length

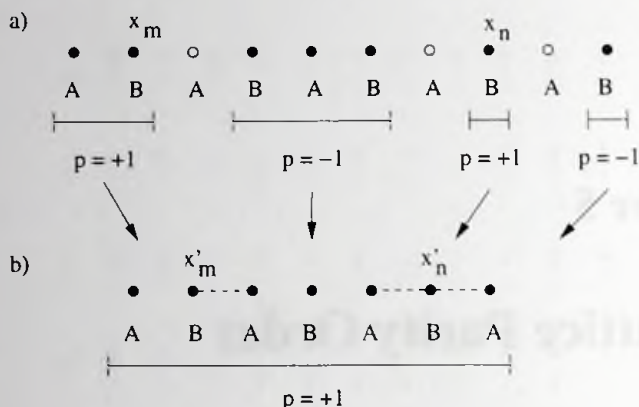


Figure 5.1: The emergence of the  $Z_2$  sublattice parity field in the geometrical squeezing operation demonstrated for a certain configuration in full space (a) and its related spin configuration in spin space (b). The open circles represent unoccupied sites, the holes. The black dots refer to occupied sites in both the full lattice (figure a) and the squeezed lattice (figure b). The unsqueezing can be parametrized by binding the holes to flips in the  $Z_2$  valued sublattice parity field. In squeezed space, the distance between the spins on positions  $x_m$  and  $x_n$  is  $x'_n - x'_m$ .

$M$  constructed from the sites at coordinates  $x_1, x_2, \dots, x_M$  given by the positions of the charges in a configuration with amplitude  $\psi_{SF}$ . This illustrates that although the factorization property (5.1) gives a precise meaning to the notion of spin-charge separation, charge and spin are actually not quite independent from each other.

The construction of the wave function in this manner is based on a geometrical structure similar to the one encountered in general relativity. There the presence of mass influences the metric connected to a particle. In our case the holes change the metric observed by the spins compared to the metric attached to an external observer, for instance an experimentalist. Let us visualize this for a representative example (See figure 5.1).

Consider  $N$  electrons on a chain with  $L$  sites where  $N < L$ . In the full Hubbard chain a charge configuration contributes an amplitude  $\psi_{SF}$  to the wave function. These charges are depicted in figure 5.1a as black dots with coordinates  $x_i$ , where  $i = 1, \dots, N$ . An external observer would say that the relevant distance between the two spins  $m$  and  $n$  is  $x_n - x_m$ . However, the spin system is confronted with a different internal space, the so called squeezed space. This space is obtained from the full space by removing the holes together with the sites where the holes are located, substituting the hole and its site with an antiferromagnetic exchange between the sites neighboring the hole. So in spin space the distance between the two spins equals  $x'_n - x'_m$ . This distance is smaller than  $x_n - x_m$  because the spins of the electrons are independent of the holes that are located in between the electrons.

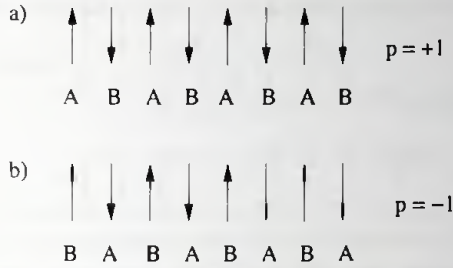


Figure 5.2: The subdivision of an antiferromagnetic Heisenberg chain into  $A$  and  $B$  sublattices according to a sublattice parity  $p = +1$  and  $p = -1$ .

As in general relativity, the physics is derived from relations between the different reference frames, but the geometry involved in the Woynarovich-Ogata-Shiba case is obviously much simpler than the geometry of fundamental space-time. This simplification makes it possible to parametrize matters in terms of a simple gauge theory. Let us compare the internal and external space: in which regard are the full chain and the squeezed chain different?

First of all, as already noted, squeezing changes the distances between spins. This can be parametrized by a simple dilation: a distance  $x$  between two spins measured in the full chain becomes a distance  $\rho_{tot}x$  in the squeezed chain with  $\rho_{tot} = N/L$  equal to the total electron density.

Another difference between the full chain and the squeezed chain is expressed by the sublattice parity which has to do with the notion of bipartiteness. A lattice is called bipartite when it can be subdivided into two sublattices  $A$  and  $B$ , such that all sites on the  $A$  sublattice are neighbored by  $B$  sublattice sites and vice versa. This division can be done in two ways ( $\dots - A - B - A - B \dots$  and  $\dots - B - A - B - A \dots$ , see figure 5.2) defining a  $Z_2$  valued quantity  $p = \pm 1$ , which we refer to as 'sublattice parity'. The Heisenberg spin system in the squeezed space is a quantum antiferromagnet and it is as such sensitive to the geometrical property of bipartiteness. Now consider the sublattice parity. A redefinition in this system of  $p = 1$  and  $p = -1$  is just a global shift of the coordinates by one lattice site and does not carry any consequences; it is a pure gauge degree of freedom.

However, sublattice parity becomes important in the mapping of squeezed space into full space. To examine this, let us fix the gauge in squeezed space, by choosing a particular sublattice parity, let say  $p = +1$  (see figure 5.1) and consider what happens when it is unsqueezed. In the process of unsqueezing, together with the holes, the lattice sites themselves are inserted. These lattice sites cause the sublattice parity to flip sign every time a hole is passed, which is referred to as the ordering of the sublattice parity. So the squeezing operation can be parametrized by attaching a sublattice parity flip to every hole. Due to the sublattice parity flips attached to the holes, the simple order of the internal spin is obscured by the presence and motion of the holes and yield a spin-

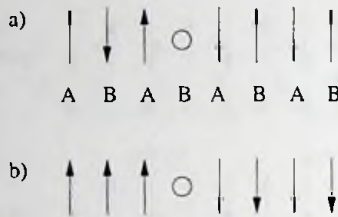


Figure 5.3: A spin configuration with a sublattice parity flip caused by a hole (a) and its staggered magnetization (b). The sublattice parity flip causes a kink in the staggered magnetization.

spin correlator equal to  $\langle S^z(x)S^z(0) \rangle \sim \cos(2k_F x)/x^{K_s+K_c}$ , as was described in the last section of the previous chapter.

## 5.2 Probing the internal spin-spin correlations

Is it possible to untangle these fluctuations due to the charge motion and can we recover the order of the internal spin system by observing the full Hubbard chain? Or to put it differently: can we define a correlation function acting on the full Hubbard chain which can measure the ‘true’ internal spin correlations associated with squeezed space?

To construct such an operator, we first turn to the staggered magnetization  $\bar{M}(x) = (-1)^x \bar{S}(x)$ . As is shown in figure 5.3, a sublattice parity flip due to a hole is equal to a kink in the staggered magnetization  $M^z(x)$ . This indicates that the damage done by a hole on the staggered spin due to the sublattice parity flip can simply be repaired by multiplying every spin to the left of the hole by  $-1$ . Therefore, we restore the original sublattice parity in the full space by looking at the altered staggered spin operator  $(M')^z$  defined by

$$(M')^z(x) = M^z(x)(-1)^{\sum_{j=-\infty}^{x-1} h(j)} = M^z(x)(-1)^{\sum_{j=-\infty}^{x-1} (1-n_{\text{tot}}(j))}, \quad (5.2)$$

where  $h(j) = 1 - n_{\text{tot}}(j)$  is the number of holes on site  $j$  and the charge operator  $n_{\text{tot}}(j) = n_{\uparrow}(j) + n_{\downarrow}(j)$  taking the values 0, 1 and 2 for an empty-, singly- and doubly occupied site, respectively. The operator  $(-1)^{(1-n_{\text{tot}}(j))}$  takes the value  $+1$  for a singly occupied spin site while it is  $-1$  for a hole or doubly occupied site. By multiplying these values on the interval  $0 < j < x$  all the minus signs associated with the sublattice parity flips are removed from the spin correlations. We can use this operator  $(M')^z$  to measure the true internal spin correlation associated with squeezed space. For

instance the spin-spin correlations function measured in squeezed space is given by

$$\begin{aligned}
 O_{top}(x) &= \langle (M')^z(x) (M')^z(0) \rangle \\
 &= \langle M^z(x) (-1)^{\sum_{j=0}^{x-1} (1-n_{tot}(j))} M^z(0) \rangle \\
 &= -\langle S^z(x) (-1)^{\sum_{j=1}^{x-1} n_{tot}(j)} S^z(0) \rangle.
 \end{aligned} \tag{5.3}$$

A comparable correlation function was also used to find a similar hidden order in Haldane spin-1 chains, as was described by den Nijs and Rommelse [18].

Although the string operator  $(-1)^{\sum_{j=1}^{x-1} (1-n_{tot}(j))}$  is non-local, it can be evaluated straightforwardly in the limit  $U \rightarrow \infty$  using the techniques introduced by Parola and Sorella which were discussed in chapter 4. They used  $\langle S^z(x) S^z(0) \rangle = \sum_{j=2}^{x+1} P_{SF}^x(j) O_{Heis.}(j-1)$  to calculate the spin-spin correlation function, where  $O_{Heis.}$  is the spin-spin correlator of the Heisenberg chain, while the expression  $P_{SF}^x(j) = \langle n_{SF}(x) n_{SF}(0) \delta(\sum_{l=0}^x n_{SF}(l) - j) \rangle_{SF}$  is the probability of finding  $j$  spinless fermions in the interval  $[0, x]$ . Using this they showed that  $\langle S^z(x) S^z(0) \rangle \sim \cos(2k_F x) / x^{K_s + K_c}$ . Using the same principle we find

$$\begin{aligned}
 O_{top}(x) &= -\langle S^z(0) (-1)^{\sum_{j=1}^{x-1} n(j)} S^z(x) \rangle \\
 &= -\sum_{j=2}^{x+1} P_{SF}^x(j) (-1)^{j-2} O_{Heis.}(j-1) \\
 &= \sum_{j=2}^{x+1} P_{SF}^x(j) f(j) \\
 &= \left[ \sum_{j=2}^{x+1} P_{SF}^x(j) \right] f(x \rho_{tot}) + \mathcal{O} \left( \frac{\ln^{\frac{3}{2}}(x)}{x^2} \right) \\
 &= \langle n_{SF}(x) n_{SF}(0) \rangle \frac{\Gamma}{\rho_{tot} x} \ln^{\frac{1}{2}}(\rho_{tot} x) + \mathcal{O} \left( \frac{\ln^{\frac{3}{2}}(x)}{x^2} \right) \\
 &= \Gamma \frac{\rho_{tot}}{x} \ln^{\frac{1}{2}}(\rho_{tot} x) + \mathcal{O} \left( \frac{\ln^{\frac{3}{2}}(x)}{x^2} \right).
 \end{aligned} \tag{5.4}$$

Here we used equation (3.31) from the chapter 3. So the asymptotically exact result is  $O_{top}(x) = \Gamma \frac{\rho_{tot}}{x} \ln^{1/2}(\rho_{tot} x)$ .

To get the spin correlations in the internal squeezed space, we have to correct for the fact that the density of staggered spin in full space is reduced by a factor  $\rho_{tot}$  as compared to squeezed space while in addition distances are measured by  $x/\rho_{tot}$  instead of  $x$ . After rescaling,  $O_{top}^{scaled}(x) = \frac{1}{x} \ln^{1/2}(x)$  which is indeed the behavior of the staggered spin correlation function of a Heisenberg spin chain at large distances. So in the limit  $U \rightarrow \infty$  the topological operator  $O_{top}(x)$  enables us to reach the spin space and calculate the spin spin correlation in the internal spin system.

In the study of the Haldane spin-1 chain by den Nijs and Rommelse, the topological correlator gave a finite result with  $O_{top} = C \neq 0$  for large distances  $x$  [18]. But in the Hubbard model the spins have a continuous symmetry, instead of the discrete  $Z_2$  Ising symmetry of the internal spin space of the Haldane chain, and so, according to the Mermin Wagner theory [12], our system has no long range order and we find  $O_{top}(x) = 0$  in (5.4) for large distances  $x$ . How should we interpret this result?

Let us consider the well known asymptotic behavior of the 'normal' staggered spin correlations for the Hubbard chain and large  $U$ , which is given by

$$O_M(x) = \langle M^z(x)M^z(0) \rangle \sim \frac{\cos[(2k_F - \pi)x]}{x^{K_s + K_c}} \quad (5.5)$$

What matters is that the algebraic decay of  $O_M(x)$  is more rapid than that of the topological correlator  $O_{top}(x)$  in (5.4). This is because the direct spin correlations as measured by equation (5.5) are sensitive to the kinks attached to the holes which are disorder events for the spin correlator. This adds an additional algebraic decay to the spin correlations  $\sim 1/x^{K_c}$  as was described in the last section of chapter 4. In the topological correlator  $O_{top}(x)$ , the charge string operator  $(-1)^{\sum_{j=0}^{x-1} n_{tot}(j)}$  removes the kinks attached to the holes and therefore measures the algebraic decay  $1/x^{K_s}$  of the spin correlations as they exist in the squeezed chain. Note that in this process the spin correlation have turned into those of an effectively parallel spin system.

The extra decaying term  $1/\sqrt{x}$  is closely related to the fact that the internal spin system has antiferromagnetic interactions. Because of the fact that the internal spin correlations alternate with  $\langle S^z(x)S^z(0) \rangle_{Heis.} \sim \frac{(-1)^x}{x}$ , the normal spin-spin correlations do not just get diluted with a factor  $n_0$ , but produce a decaying term  $1/\sqrt{x}$  when we inject the Heisenberg chain with holes.

Another way to say this is that in the Hubbard chain the sublattice parity is ordered, which means that the sublattice parity changes sign every time a hole is passed. Using the topological correlator  $O_{top}(x)$ , the original sublattice parity from the spin sector is restored by the string operator  $(-1)^{\sum_{j=0}^{x-1} n_{tot}(j)}$ . And because of this, apart from some scaling effects,  $O_{top}(x)$  calculates the spin-spin correlations in the squeezed space.

Note that in principle this kind of hidden order can also occur in systems defined on a continuum instead of on a lattice. For the construction of the wave function described in (5.1) can also be applied on a continuum. But since the sublattice parity can only be defined on a lattice, we would not refer to it as the sublattice parity order. On a continuum, the order would be characterized by the property that neighboring spins have antiferromagnetic interactions independent of the distance between them. Only the interpretation of the topological correlator described in section 5.1 is now not completely appropriate anymore and we have to change it. For instance in a continuum, it is not true that the holons and spinons simply cause kinks in the staggered magnetization  $M^z(x) = (-1)^x S^z(x)$ . On the other hand, the expression for the staggered spin correlator (4.83) is still valid. So also for continuous  $x$ , we obtain an extra decaying term  $1/\sqrt{x}$  caused by the antiferromagnetic staggering in the internal spin system and represented by the  $(-1)^{\sum_{j=1}^{x-1} n_{tot}(j)}$  in the term  $\langle n_{tot}(x)(-1)^{\sum_{j=1}^{x-1} (1-n_{tot}(j))} n_{tot}(0) \rangle$  in (4.83). To remove these minus signs we have to multiply the function with  $(-1)^{\sum_{j=1}^{x-1} (1-n_{tot}(j))}$  similar

to what we did for the lattice limit which yields the expression  $-\langle S^z(x)(-1)^{\sum_{j=1}^{x-1} n_{tot}(j)} S^z(0) \rangle$ . Now the term  $(-1)^{\sum_{j=1}^{x-1} n_{tot}(j)}$  can be interpreted as removing the internal anti-ferromagnetic staggering in the internal spin system and making the spins parallel. And thus by calculating  $O_{top}(x)$  we obtain the product

$$O_{top}(x) = \langle n_{tot}(x)n_{tot}(0) \rangle \langle S^z(x)S^z(0) \rangle_{Heis..} \quad (5.6)$$

This interpretation is not only valid on a continuum, but also on a lattice.

In the next two chapters we will calculate the topological correlator  $O_{top}(x)$  for  $U = 0$  and for intermediate Coulomb repulsion  $U > 0$ . These calculations will show that for all  $U \geq 0$ ,  $O_{top}(x) \sim 1/x^{K_s} = 1/x$ .



## Chapter 6

# Sublattice parity order for $U = 0$

The calculations presented in the previous chapter all refer to the specific situation of the strong coupling Hubbard model, and the generality of this  $Z_2$  topological order is a-priori unclear. Is this only restricted to the strongly coupled case? In this chapter we consider the limit where the Coulomb interactions completely vanish and the system is described by a spinful fermion gas on the lattice. For this  $U = 0$  case we calculate the topological correlator  $O_{top}(x)$  numerically. Remarkably, these calculations will show that also under these conditions the sublattice parity is ordered.

### 6.1 Introduction

To see whether the sublattice parity is ordered we have to consider the topological correlator  $O_{top}(x)$  defined in equation (5.3). For zero Coulomb interactions  $U = 0$ , the Hubbard model is described by a spinful fermion gas. In that case, the up and down electrons completely decouple, and this simplifies the calculation of  $O_{top}(x)$  considerably. Using  $S^z(y) = \frac{1}{2}(n_\uparrow(y) - n_\downarrow(y))$  and  $n_{tot}(y) = (n_\uparrow(y) + n_\downarrow(y))$  the topological correlator can be written as

$$\begin{aligned} O_{top}(x) &= -\langle S^z(x)(-1)^{\sum_{j=1}^{x-1} n_{tot}(j)} S^z(0) \rangle = \\ &= -\frac{1}{4} \langle n_\uparrow(x)(-1)^{\sum_{j=1}^{x-1} n_\uparrow(j)} n_\uparrow(0) \rangle \langle (-1)^{\sum_{j=1}^{x-1} n_\downarrow(j)} \rangle \\ &= -\frac{1}{4} \langle n_\downarrow(x)(-1)^{\sum_{j=1}^{x-1} n_\downarrow(j)} n_\downarrow(0) \rangle \langle (-1)^{\sum_{j=1}^{x-1} n_\uparrow(j)} \rangle \\ &+ \frac{1}{4} \langle n_\uparrow(x)(-1)^{\sum_{j=1}^{x-1} n_\uparrow(j)} \rangle \langle n_\downarrow(0)(-1)^{\sum_{j=1}^{x-1} n_\downarrow(j)} \rangle \\ &+ \frac{1}{4} \langle n_\downarrow(x)(-1)^{\sum_{j=1}^{x-1} n_\downarrow(j)} \rangle \langle n_\uparrow(0)(-1)^{\sum_{j=1}^{x-1} n_\uparrow(j)} \rangle. \end{aligned} \tag{6.1}$$

This expression contains several averages in which there is only one sort of particle that is either up or down. Therefore, in the calculation, it suffices to consider spinless fermions with density  $n_{SF}(j)$  so that the topological correlator equals

$$\begin{aligned} O_{top} = & - \langle S^z(x) (-1)^{\sum_{j=1}^{x-1} n_{top}(j)} S^z(0) \rangle = \\ & - \frac{1}{2} \langle n_{SF}(x) (-1)^{\sum_{j=1}^{x-1} n_{SF}(j)} n_{SF}(0) \rangle \langle (-1)^{\sum_{j=1}^{x-1} n_{SF}(j)} \rangle \\ & + \frac{1}{2} \langle n_{SF}(x) (-1)^{\sum_{j=1}^{x-1} n_{SF}(j)} \rangle \langle n_{SF}(0) (-1)^{\sum_{j=1}^{x-1} n_{SF}(j)} \rangle. \end{aligned} \quad (6.2)$$

It follows that the topological operator  $O_{top}$  in (6.1) can be expressed in the spinless fermion correlators  $\langle (-1)^{\sum_{j=1}^{x-1} n_{SF}(j)} \rangle$ ,  $\langle n_{SF}(x) (-1)^{\sum_{j=1}^{x-1} n_{SF}(j)} \rangle$  and the average  $\langle n_{SF}(x) (-1)^{\sum_{j=1}^{x-1} n_{SF}(j)} n_{SF}(0) \rangle$ . In the next section we describe the method for the numerical calculation of these expressions.

## 6.2 Spinless fermion numerics

As shown in equation (6.1), the topological correlator  $O_{top}(x)$  can be expressed in the spinless fermion correlators  $\langle (-1)^{\sum_{j=1}^{x-1} n_{SF}(j)} \rangle$ ,  $\langle n_{SF}(x) (-1)^{\sum_{j=1}^{x-1} n_{SF}(j)} \rangle$  and  $\langle n_{SF}(x) (-1)^{\sum_{j=1}^{x-1} n_{SF}(j)} n_{SF}(0) \rangle$ . Let us start by considering the expression  $\langle (-1)^{\sum_{j=1}^{x-1} n_{SF}(j)} \rangle$ . Using periodic boundary conditions, this expression can be written as

$$\begin{aligned} \langle (-1)^{\sum_{j=1}^{x-1} n_{SF}(j)} \rangle &= \langle k_N \dots k_1 | (-1)^{\sum_{j=1}^{x-1} n_{SF}(j)} | k_1 \dots k_N \rangle \\ &= \sum_{x_1 \dots x_N} \sum_{y_1 \dots y_N} \langle 0 | a_{x_N} \dots a_{x_1} (-1)^{\sum_{j=1}^{x-1} n_{SF}(j)} a_{y_1}^\dagger \dots a_{y_N}^\dagger | 0 \rangle \\ &\quad \times \left( \frac{1}{V} \right)^N e^{-ik_1 x_1 - \dots - ik_N x_N} e^{ik_1 y_1 + \dots + ik_N y_N} \\ &= \sum_{x_1 \dots x_N} \sum_{y_1 \dots y_N} \langle 0 | a_{x_N} \dots a_{x_1} a_{y_1}^\dagger \dots a_{y_N}^\dagger | 0 \rangle \\ &\quad \times \left( \frac{1}{V} \right)^N e^{-ik_1 x_1 - \dots - ik_N x_N} e^{ik_1 y_1 + \dots + ik_N y_N} \\ &\quad \times \prod_{j=1}^N [1 - 2\theta(y_j - 1)\theta(r - 1 - y_j)]. \end{aligned} \quad (6.3)$$

Here  $|k_1 \dots k_N\rangle$  indicates the ground state. The product term on the last line equals  $-1$  when  $y_j \in [1, x-1]$  and  $1$  otherwise, taking into account the result of the factor

$(-1)^{\sum_{j=1}^{x-1} n_{SF}(j)}$ . Part of this sum can be written as

$$\begin{aligned} \frac{1}{V} \sum_y e^{iy(p-k)} [1 - 2\theta(y-1)\theta(x-1-y)] &= \frac{1}{V} \sum_y e^{iy(p-k)} - \frac{2}{V} \sum_{y=1}^{x-1} e^{iy(p-k)} \\ &= \delta(p, k) - \frac{2}{V} \frac{e^{i(p-k)x} - e^{i(p-k)}}{e^{i(p-k)} - 1} \\ &= \delta^*(p, k), \end{aligned} \quad (6.4)$$

where we introduced the altered delta function  $\delta^*(p, k)$ . Using this function, the expression (6.3) can be expressed as the determinant of a  $N \times N$  matrix made of  $\delta^*(k_i, k_j)$  functions

$$\langle (-1)^{\sum_{j=1}^{x-1} n_{SF}(j)} \rangle = \det \begin{pmatrix} \delta^*(k_1, k_1) & \delta^*(k_2, k_1) & \cdots & \delta^*(k_N, k_1) \\ \delta^*(k_1, k_2) & \delta^*(k_2, k_2) & \cdots & \delta^*(k_N, k_2) \\ \delta^*(k_1, k_3) & \delta^*(k_2, k_3) & \cdots & \delta^*(k_N, k_3) \\ \vdots & \vdots & \ddots & \vdots \\ \delta^*(k_1, k_N) & \delta^*(k_2, k_N) & \cdots & \delta^*(k_N, k_N) \end{pmatrix}. \quad (6.5)$$

This is similar to calculating  $\langle 1 \rangle = \langle k_N, \dots, k_1 | k_1, \dots, k_N \rangle$ , which is of course 1, and equals the determinant of a similar  $N \times N$  matrix

$$\langle 1 \rangle = \det \begin{pmatrix} \delta(k_1, k_1) & \delta(k_2, k_1) & \cdots & \delta(k_N, k_1) \\ \delta(k_1, k_2) & \delta(k_2, k_2) & \cdots & \delta(k_N, k_2) \\ \delta(k_1, k_3) & \delta(k_2, k_3) & \cdots & \delta(k_N, k_3) \\ \vdots & \vdots & \ddots & \vdots \\ \delta(k_1, k_N) & \delta(k_2, k_N) & \cdots & \delta(k_N, k_N) \end{pmatrix}. \quad (6.6)$$

only now consisting of normal  $\delta(k_i, k_j)$  functions.

Secondly, we consider  $\langle n_{SF}(x) (-1)^{\sum_{j=1}^{x-1} n_{SF}(j)} \rangle = \langle (-1)^{\sum_{j=1}^{x-1} n_{SF}(j)} n_{SF}(0) \rangle$ . Similar to equation (6.3) this is equal to

$$\begin{aligned} \langle n_{SF}(x) (-1)^{\sum_{j=1}^{x-1} n_{SF}(j)} \rangle &= \langle k_N \dots k_1 | n_{SF}(x) (-1)^{\sum_{j=1}^{x-1} n_{SF}(j)} | k_1 \dots k_N \rangle \\ &= \left( \frac{1}{V} \right)^N \sum_{x_1 \dots x_N} \sum_{y_1 \dots y_N} \langle 0 | a_{x_N} \dots a_{x_1} a_x^\dagger a_x a_{y_1}^\dagger \dots a_{y_N}^\dagger | 0 \rangle \\ &\quad \times e^{-ik_1 x_1 - \dots - ik_N x_N} e^{ik_1 y_1 + \dots + ik_N y_N} \\ &\quad \times \prod_{j=1}^N [1 - 2\theta(y_j - 1)\theta(r - 1 - y_j)]. \end{aligned} \quad (6.7)$$

This can be written as the determinant of the  $(N + 1) \times (N + 1)$  matrix

$$\begin{pmatrix} 0 & \frac{e^{ik_1x}}{\sqrt{V}} & \frac{e^{ik_2x}}{\sqrt{V}} & \cdots & \frac{e^{ik_Nx}}{\sqrt{V}} \\ \frac{e^{-ik_1x}}{\sqrt{V}} & \delta^*(k_1, k_1) & \delta^*(k_2, k_1) & \cdots & \delta^*(k_N, k_1) \\ \frac{e^{-ik_2x}}{\sqrt{V}} & \delta^*(k_1, k_2) & \delta^*(k_2, k_2) & \cdots & \delta^*(k_N, k_2) \\ \vdots & \vdots & \vdots & \ddots & \vdots \\ \frac{e^{-ik_Nx}}{\sqrt{V}} & \delta^*(k_1, k_N) & \delta^*(k_2, k_N) & \cdots & \delta^*(k_N, k_N) \end{pmatrix}. \quad (6.8)$$

Again, if we replace the redefined delta function  $\delta^*(k_i, k_j)$  in this matrix by a normal delta function, we obtain an expression for the normal density  $\langle n_{SF}(x) \rangle = \langle n_{SF}(0) \rangle = \frac{1}{V} \sum_{k_1} e^{-ik_1x} e^{-ik_2x} = \frac{1}{V} \sum_{m=1}^N = \frac{N}{V}$ , where we used that  $k_1 = \frac{2\pi m}{V}$  with  $m = 1, \dots, V$ .

Finally we consider  $\langle n_{SF}(x) (-1)^{\sum_{j=1}^{x-1} n_{SF}(j)} n_{SF}(0) \rangle$ . This average can be expressed as the determinant of the  $(N + 2) \times (N + 2)$  matrix

$$\begin{pmatrix} 0 & 0 & \frac{1}{\sqrt{V}} & \frac{1}{\sqrt{V}} & \cdots & \frac{1}{\sqrt{V}} \\ 0 & 0 & \frac{e^{ik_1x}}{\sqrt{V}} & \frac{e^{ik_2x}}{\sqrt{V}} & \cdots & \frac{e^{ik_Nx}}{\sqrt{V}} \\ \frac{1}{\sqrt{V}} & \frac{e^{-ik_1x}}{\sqrt{V}} & \delta^*(k_1, k_1) & \delta^*(k_2, k_1) & \cdots & \delta^*(k_N, k_1) \\ \frac{1}{\sqrt{V}} & \frac{e^{-ik_2x}}{\sqrt{V}} & \delta^*(k_1, k_2) & \delta^*(k_2, k_2) & \cdots & \delta^*(k_N, k_2) \\ \vdots & \vdots & \vdots & \vdots & \ddots & \vdots \\ \frac{1}{\sqrt{V}} & \frac{e^{-ik_Nx}}{\sqrt{V}} & \delta^*(k_1, k_N) & \delta^*(k_2, k_N) & \cdots & \delta^*(k_N, k_N) \end{pmatrix}. \quad (6.9)$$

If we replace the redefined delta function  $\delta^*(k_i, k_j)$  by a normal delta function  $\delta(k_i, k_j)$ , we obtain an expression for  $\langle n_{SF}(x) n_{SF}(0) \rangle = \left(\frac{N}{V}\right)^2 - \frac{1}{V^2} \sum_{m=1}^N e^{i2\pi x m} \sum_{p=1}^N e^{-i2\pi x p}$  which is calculated in (3.31) in chapter 3.

A Fortran program was used to calculate the expression for the correlation functions  $\langle (-1)^{\sum_{j=1}^{x-1} n_{SF}(j)} \rangle$ ,  $\langle n_{SF}(x) (-1)^{\sum_{j=1}^{x-1} n_{SF}(j)} \rangle$  and  $\langle n_{SF}(x) (-1)^{\sum_{j=1}^{x-1} n_{SF}(j)} n_{SF}(0) \rangle$  in respectively (6.5), (6.8) and (6.9) for various fermion densities  $\rho_{SF}$ . Careful analysis of this data, obtained via the determinant of (6.5) demonstrates that away from the density  $\rho_{SF} = 1$ ,

$$\langle (-1)^{\sum_{j=1}^{x-1} n_{SF}(j)} \rangle = \frac{A^2 \sqrt{2} \cos\left(\frac{\pi(x-1)N}{V}\right)}{\sqrt{\sin\left(\frac{\pi N}{V}\right)} \sqrt{\frac{V}{\pi} \sin\left(\frac{\pi(x-1)}{V}\right)}}. \quad (6.10)$$

Figure 6.1 displays the results for  $\rho_{SF} = \frac{N}{V} = 0.1$  with  $N = 20$  and  $V = 200$  together with this analytic expression (6.10). Furthermore, figure 6.2 displays the numerical data for the prefactor of  $\langle (-1)^{\sum_{j=1}^{x-1} n_{SF}(j)} \rangle$  normalized to 1 for  $\rho_{SF} = \frac{N}{V} = 0.5$ , which is equal to  $\langle (-1)^{\sum_{j=1}^{x-1} n_{SF}(j)} \rangle \sqrt{\frac{V}{\pi} \sin\left(\frac{\pi(x-1)}{V}\right)} / (A^2 \sqrt{2} \cos\left(\frac{\pi(x-1)N}{V}\right))$ , together with the function  $\frac{1}{\sqrt{\sin(\pi \rho_{SF})}}$  for several values for  $\rho_{SF}$  in between 0 and 1. Also here  $N = 20$  and  $V = 200$ .

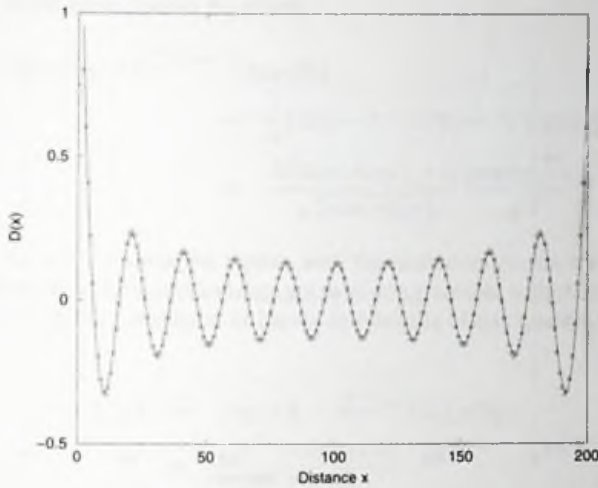


Figure 6.1: Numerical data for the function  $D(x) = \langle (-1)^{\sum_{j=0}^x n_{SF}(j)} \rangle$  using equation (6.5) together with the analytical prediction in equation (6.10) and a density  $\rho_{SF} = \frac{N}{V} = 0.1$ . Here  $N = 20$  and  $V = 200$ . Note that in these calculations periodic boundary conditions were used.

Taking the thermodynamic limit  $V \rightarrow \infty$ ,  $\frac{N}{V} \rightarrow \rho_{SF}$  the function in (6.10) will go to

$$\langle (-1)^{\sum_{j=1}^{x-1} n_{SF}(j)} \rangle = \frac{A^2 \sqrt{2}}{\sqrt{\sin(\pi \rho_{SF})}} \frac{\cos(\pi \rho_{SF}(x-1))}{\sqrt{x-1}}. \quad (6.11)$$

This is in agreement with calculations done by Parola and Sorella, discussed in chapter 4. They showed that for  $\rho_{SF} = \frac{1}{2}$  the asymptotic form of  $D(x)$  is

$$D(x) = \langle (-1)^{\sum_{j=0}^x n_{SF}(j)} \rangle = A^2 \sqrt{2} \frac{\cos(\frac{\pi(x+1)}{2})}{\sqrt{x+1}}, \quad (6.12)$$

with  $A = 0.645002448$  [22]. Our numeric result in (6.11) is expressing the generalization of this result for densities away from  $\rho_{SF} = \frac{1}{2}$  and  $\rho_{SF} = 1$ .

The averages  $\langle n_{SF}(x) (-1)^{\sum_{j=1}^{x-1} n_{SF}(j)} \rangle$  and  $\langle n_{SF}(x) (-1)^{\sum_{j=1}^{x-1} n_{SF}(j)} n_{SF}(0) \rangle$  can be related to the expression for  $D(x) = \langle (-1)^{\sum_{j=0}^x n_{SF}(j)} \rangle$ . For instance, using  $n_{SF}(j) =$

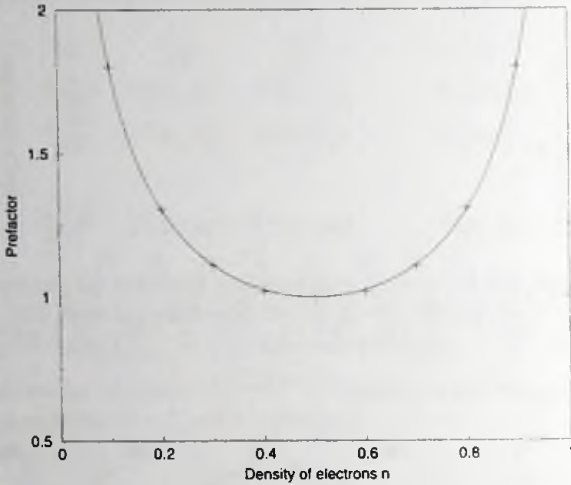


Figure 6.2: The points indicate the numerical value of the prefactor of the function  $D(x) = \langle (-1)^{\sum_{j=0}^x n_{SF}(j)} \rangle$  normalized to 1 for  $n = \rho_{SF} = \frac{N}{V} = 0.5$  with  $V = 200$ . The solid line represents the function  $\frac{1}{\sqrt{\sin(\pi\rho_{SF})}}$ .

$\frac{1}{2} [1 - (-1)^{n_{SF}(j)}]$  for  $j = x$  we get

$$\begin{aligned}
 & \langle n_{SF}(x) (-1)^{\sum_{j=1}^{x-1} n_{SF}(j)} \rangle \\
 &= \langle (-1)^{\sum_{j=1}^{x-1} n_{SF}(j)} n_{SF}(0) \rangle = \frac{D(x-2) - D(x-1)}{2} \\
 &= \frac{A^2}{\sqrt{2 \sin(\pi\rho_{SF})}} \left( \frac{\cos(\pi\rho_{SF}x) [\cos(\pi\rho_{SF}) - 1] + \sin(\pi\rho_{SF}x) \sin(\pi\rho_{SF})}{\sqrt{x}} \right) \\
 &= \text{sign}[\cos(\pi\rho_{SF}) - 1] \frac{A^2 \sqrt{1 - \cos(\pi\rho_{SF})} \cos(\pi\rho_{SF}x - K)}{\sqrt{\sin(\pi\rho_{SF})} \sqrt{x}}, \quad (6.13)
 \end{aligned}$$

where the constant  $K$  is given by

$$K = \arctan \left( \frac{\sin(\pi\rho_{SF})}{\cos(\pi\rho_{SF}) - 1} \right) \quad (6.14)$$

Furthermore, in the same manner we obtain

$$\begin{aligned}
 \langle n_{SF}(x)(-1)^{\sum_{j=1}^{x-1} n_{SF}(j)} n_{SF}(0) \rangle & \\
 &= \frac{1}{4} [D(x-2) - 2D(x-1) + D(x)] \\
 &= \frac{A^2(\cos(\pi\rho_{SF}) - 1) \cos(\pi\rho_{SF}x)}{\sqrt{2} \sin(\pi\rho_{SF}) \sqrt{x}}. \quad (6.15)
 \end{aligned}$$

Although we will not show the figures with the numerical results for these expressions, it turned out that our numerical data are in good agreement with these results. This is in agreement with the calculation of Parola and Sorella of this quantity for  $\rho_{SF} = \frac{1}{2}$ , where

$$\begin{aligned}
 C(x) &= \langle n_{SF}(x)(-1)^{\sum_{j=0}^{x-1} n(j)} n_{SF}(0) \rangle \\
 &= -\frac{A^2 \cos(\pi\rho_{SF}x)}{\sqrt{2} \sqrt{x}}, \quad (6.16)
 \end{aligned}$$

as was described in chapter 4. The result in (6.15) expresses the generalization of this result for densities away from  $\rho_{SF} = \frac{1}{2}$  and  $\rho = 1$ .

### 6.3 Final result spinful case

Inserting all the different spinless fermion averages calculated in the previous section in equation (6.1), we find for the spinful topological expression

$$\begin{aligned}
 O_{top}(x) &= -\langle S^z(x)(-1)^{\sum_{j=1}^{x-1} n_{tot}(j)} S^z(0) \rangle \\
 &= -\frac{1}{8} [D(x-2)D(x) - D(x-1)^2] \\
 &= \frac{A^4 \sin(\pi\rho_{SF})}{4 \frac{V}{\pi} \sin(\frac{\pi x}{V})} \approx \frac{A^4 \sin(\pi\rho_{SF})}{4x} = \frac{A^4 \sin(k_F)}{4x} \\
 &= \frac{A^4 \sin(\pi\rho_{tot}/2)}{4x}, \quad (6.17)
 \end{aligned}$$

where  $\rho_{SF} = \rho_{tot}/2 = (\rho_{\uparrow} + \rho_{\downarrow})/2$ . Note that  $2k_F = \pi\rho_{tot} = \pi \frac{2N_{SF}}{V}$  and so  $k_F = \frac{\pi N_{SF}}{V} = \pi\rho_{SF}$ .

Figure 6.3 shows the numeric data for  $O_{top}(x)$  using the determinant expression of equation (6.5), (6.8) and (6.9) for  $\rho_{tot} = 2N_{SF}/V = 0.2$  and  $V = 200$ . The data is in good agreement with the analytic expression in (6.17). The algebraic decay is clearly in log-log plot of these data in figure 6.4. Here the string correlator function  $\langle S^z(x)(-1)^{\sum_{j=1}^{x-1} n_{tot}(j)} S^z(0) \rangle$  is calculated for the densities  $\rho_{tot} = 0.2$ ,  $\rho_{tot} = 0.6$  and  $\rho_{tot} = 1$ .

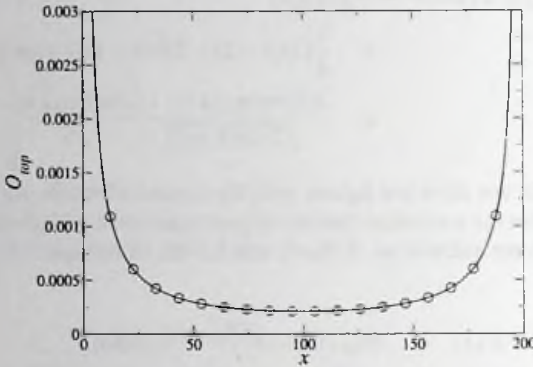


Figure 6.3: The function  $O_{top} = -\langle S^z(x)(-1)^{\sum_{j=1}^{x-1} n_{tot}(j)} S^z(0) \rangle$  for  $U = 0$  calculated numerically using determinant formulas (6.5), (6.8) and (6.9). Here  $\rho_{tot} = 2N_{SF}/V = 0.2$  and  $V = 200$ . The drawn line is the analytic solution in equation (6.17).

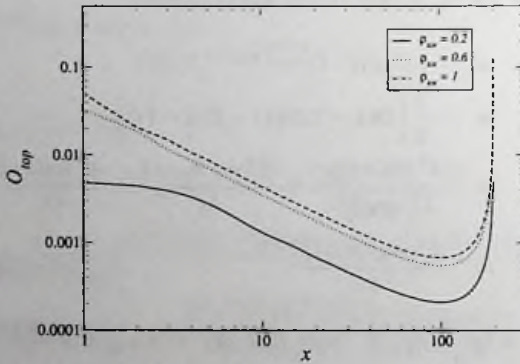


Figure 6.4: The function  $O_{top} = -\langle S^z(x)(-1)^{\sum_{j=1}^{x-1} n_{tot}(j)} S^z(0) \rangle$  for  $\rho_{tot} = 0.2$ ,  $\rho_{tot} = 0.6$  and  $\rho_{tot} = 1$ , shown in a log-log plot. The algebraic decay in equation (6.17) is displayed as a straight line.

So we can conclude that for  $U = 0$  the topological correlator probes the internal spin spin correlations with  $O_{top}(x) \sim 1/x$  for large distances  $x$ , indicating that the sublattice parity is ordered.

It is remarkable that even in the limit of zero Coulomb interactions the sublattice parity is ordered. Before giving an explanation for these results, we will investigate in the next chapters the sublattice parity order for finite intermediate  $U > 0$ . Since the Luttinger model is solved by bosonization, we will first try to apply this method to do this.



## Chapter 7

# The failures of Bosonization

After proving the existence of the (quasi) sublattice parity order for the Hubbard model in the limits  $U = 0$  and  $U \rightarrow \infty$ , we would like to use bosonization to investigate this hidden order for intermediate  $U \geq 0$ . Although this technique is defined on a continuum, a hidden order similar to the sublattice parity order can occur, as was pointed out in the end of chapter 5. But in this chapter we will demonstrate that despite triumphant success in many other arenas, the method of bosonization does not correctly represent the string operators in the lattice Luttinger liquid described in the previous sections, which gives rise to an incorrect behavior of the correlation functions. As we will show, this is partly because in going from a lattice to a continuum the technique generates the wrong continuum limit for these operators. But as we will indicate, this is not the only problem and we conclude that bosonization cannot be trusted when calculating these string operators.

We will start this chapter by giving some examples of where things go wrong.

### 7.1 Examples of where things go wrong

A first example of this failure of bosonization can be seen by considering the expectation value of the string correlator itself. To obtain an expression for it using bosonization, we first represent this function as a cosine with

$$\langle (-1)^{\sum_{j=0}^x n_{\text{tot}}(j)} \rangle = \langle \cos \left[ \pi \sum_{j=0}^x n_{\text{tot}}(j) \right] \rangle \rightarrow \langle \cos \left[ \pi \int_0^x dy n_{\text{tot}}(y) \right] \rangle. \quad (7.1)$$

Here we took the continuum limit. According to the bosonization dictionary, the total charge density is given by  $n_{\text{tot}}(y) = \sqrt{\frac{2}{\pi}} \frac{\partial \varphi_c}{\partial x}(y) + \mathcal{O}_{CDW}(y) + \mathcal{O}^\dagger_{CDW}(y)$ , where the charge density operator  $\mathcal{O}_{CDW}(y) = e^{-2ik_F y} e^{i\sqrt{2\pi}\varphi_c(y)} \cos[\sqrt{2\pi}\varphi_s(y)]$ . Using these expressions, it follows that on average  $\langle (-1)^{\sum_{j=0}^x n_{\text{tot}}(j)} \rangle \sim \langle e^{i\sqrt{2\pi}(\varphi_c(x) - \varphi_c(0))} \rangle = 1/x^{K_c}$ .

Since bosonization can only probe the non-zero wave vectors of the density operator  $n_{tot}(x)$ , this expression is only valid up to multiplicative factors of order  $\cos(\pi x \rho_{tot})$ .

On the other hand, because on the lattice

$$(-1)^{n_{tot}(j)} \equiv (-1)^{n_{\uparrow}(j)+n_{\downarrow}(j)} = (-1)^{n_{\uparrow}(j)-n_{\downarrow}(j)} \equiv (-1)^{2S^z(j)}, \quad (7.2)$$

we might as well use  $\langle (-1)^{\sum_{j=0}^x n_{tot}(j)} \rangle = \langle \cos[2\pi \sum_{j=0}^x S^z(j)] \rangle$ . Because in bosonization  $2S^z(x) = \sqrt{\frac{2}{\pi}} \frac{\partial \varphi_s}{\partial x}(x) + \mathcal{O}_{SDW}(x) + \mathcal{O}_{SDW}^\dagger(x)$ , we obtain

$$\langle (-1)^{\sum_{j=0}^x n_{tot}(j)} \rangle_{BOS.} \sim \frac{1}{x^{K_s}}. \quad (7.3)$$

For  $U = 0$ , the modulus  $K_s = K_c$  and the two expressions are the same, but away from this point  $K_s \neq K_c$  and bosonization runs into a paradox: depending on the way one calculates  $\langle (-1)^{\sum_{j=0}^x n_{tot}(j)} \rangle$ , one obtains different, mutually exclusive answers. As will be shown in the next chapter, DMRG calculations prove that for positive  $U$  this function equals

$$\langle (-1)^{\sum_{j=0}^x n_{tot}(j)} \rangle = \frac{B_s}{x^{K_s}} + \frac{B_c \cos(2k_F x)}{x^{K_c}}, \quad (7.4)$$

and apparently the two ways of calculating the operator in bosonization recover part of the correct answer.

A similar problem occurs when one uses bosonization to calculate the expectation value of the string operator  $(-1)^{2\sum_{j=0}^x n_{tot}(j)}$ . On the lattice this operator is just the identity operator. But according to bosonization its expectation value decays like

$$\langle (-1)^{2\sum_{j=0}^x n_{tot}(j)} \rangle = \langle \cos[2\pi \sum_{j=0}^x n_{tot}(j)] \rangle = \frac{1}{x^{4K_c}} \neq 1. \quad (7.5)$$

These examples show that the usual bosonization description can yield incorrect expressions for certain string operators. What is going on?

## 7.2 Why does bosonization fail?

To explain why bosonization fails to describe these string operators, let us take a closer look at the principles of the technique, starting with the bosonization of spinless fermions as was described in chapter 3.

Using bosonization we write the number operator  $n_{SF}(y)$  as a bosonic operator. On the lattice, the number operator  $n_{SF}(y)$  is integer valued. A site is either empty or occupied corresponding with respectively charge quantum number 0 and 1. In bosonization this discrete valued operator is approximated by a continuous function  $\varphi(y)$  with  $n_{SF}(y) = -\frac{1}{\sqrt{\pi}} \partial_x \varphi(y)$ , or equivalently  $\int_0^x dy n_{SF}(y) = -\frac{1}{\sqrt{\pi}} [\varphi(x) - \varphi(0)]$ . The operators  $n_{SF}(y)$  and  $\sum_{j=0}^x n_{SF}(j)$  for the discrete lattice configuration of spinless

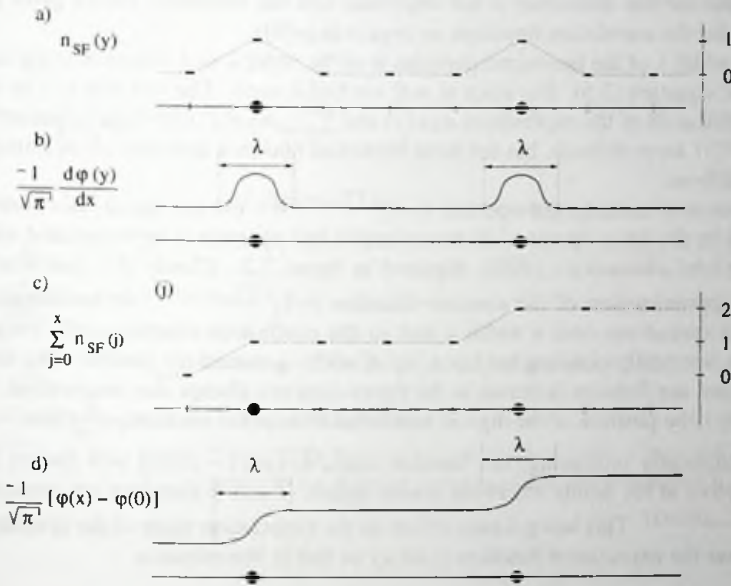


Figure 7.1: These figures show the principle of bosonization of spinless fermions. The spinless fermions are indicated as black dots. The first two figures display the density operator  $n_{SF}(y)$  on a lattice (a) and its continuous version  $-\frac{1}{\sqrt{\pi}} \frac{\partial \varphi(y)}{\partial x}$  obtained via bosonization (b). The last set of figures show the accumulated electron density  $\sum_{j=0}^x n_{SF}(j)$  and its continuous bosonized version  $-\frac{1}{\sqrt{\pi}} [\varphi(x) - \varphi(0)]$ . On a lattice, the particles are located on a single point while in the bosonized version the particles have acquired a width  $\lambda$ . Although we have drawn  $\lambda$  of finite length in reality  $\lambda = \infty$ . Note that the function on a lattice theory is only defined on the lattice points. The dashed lines is added to a guide to the eye.

fermions depicted in figure 7.1a and 7.1c are approximated with the continuous functions  $-\frac{1}{\sqrt{\pi}}\partial_x\varphi(y)$  and  $\frac{1}{\sqrt{\pi}}[\varphi(x)-\varphi(0)]$  in respectively figure 7.1b and 7.1d.

The main difference between the lattice operators and their bosonized continuum counterpart is that on the lattice, the fermions are located at single points whereas in the bosonized description, the fermions are spread out continuously around this point and the particles have acquired a width  $\lambda$  as indicated in figure 7.1. For the long wavelength scale behavior this difference is not important and the bosonized theory gives proper answers for the correlation functions as  $\langle n_{SF}(x)n_{SF}(0) \rangle$ .

The width  $\lambda$  of the bosonized particles is of the order  $\lambda = \frac{1}{m}$  where  $m$  is the mass in the Dirac equation (3.6). But since  $m = 0$  we find  $\lambda = \infty$ . The fact that  $\lambda = \infty$  makes the identification of the expressions  $n_{SF}(y)$  and  $\sum_{j=0}^x n_{SF}(j)$  with their bosonized form in figure 7.1 more difficult, but the most important notion is that they are in principle of the same form.

Let us now consider the operator  $(-1)^{2\sum_{j=0}^x n_{SF}(j)}$ . On the lattice, this operator is identical to the unity operator. In bosonization this operator is approximated with the operator  $\cos[\sqrt{4\pi}(\varphi(x)-\varphi(0))]$ , depicted in figure 7.2. Clearly this function is not a good approximation of the constant function  $(-1)^{2\sum_{j=0}^x n_{SF}(j)}$ . In bosonization the charge is spread out over a width  $\lambda$  and so the continuous function  $\cos[\sqrt{4\pi}(\varphi(x)-\varphi(0))]$  is not totally constant but has a dip of width  $\lambda$  around the particle. The fact that  $\lambda = \infty$  and not finite as is drawn in the figure does not change this observation. If one increases  $\lambda$  the position of the dip can somewhat change but because  $-\frac{2}{\sqrt{\pi}}[\varphi(x)-\varphi(0)]$  is monotonically increasing, the function  $\cos[\sqrt{4\pi}(\varphi(x)-\varphi(0))]$  will always have a dip centered at the points where the cosine equals -1 and is therefore not constant like  $(-1)^{2\sum_{j=0}^x n_{SF}(j)}$ . This has a drastic effect on the expectation value of the operator. The dip causes the expectation function to decay so that in bosonization

$$\langle (-1)^{2\sum_{j=0}^x n_{SF}(j)} \rangle_{BOS} = \frac{1}{x^2}. \quad (7.6)$$

In other words, in bosonization the operator  $(-1)^{2\sum_{j=0}^x n_{SF}(j)}$  is treated as the operator  $(-1)^{\sum_{j=0}^x \tilde{n}_{SF}(j)}$  with  $\tilde{n}_{SF}(j)$  the density of spinless fermions with  $\tilde{n}_{SF}(j) = 2n_{SF}(j)$ . But since the charge is a continuous variable, the function is not constant like it would be on a lattice and causes a dip on the location of the spinless fermions. Why does this happen?

We want to approximate an operator defined on a lattice with a continuous function defined on the continuum. This means that we have to construct a continuation of this operator. But there are infinitely many ways to make such a continuation. The bosonization procedure is designed to generate the proper continuation for the density operator  $n_{SF}(y)$ . But using this description, it selects the wrong continuum limit for the function  $(-1)^{2\sum_{j=0}^x n_{SF}(j)}$ .

A similar problem occurs for the string operator  $(-1)^{\sum_{j=0}^x n_{tor}(j)}$  for spinful electrons in (7.1). Figure 7.3 depicts this function for a selected electron configuration together with the bosonized version  $\cos[\sqrt{2\pi}(\varphi_c(x)-\varphi_c(0))]$  used in equation (7.3). One can clearly see a discrepancy between the lattice expression and the bosonized continuation.

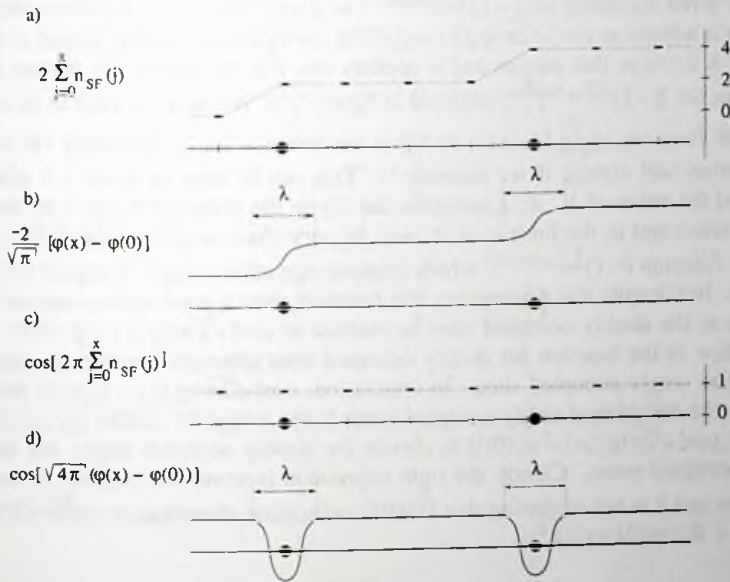


Figure 7.2: In straightforward bosonization the constant sum  $(-1)^{2\sum_{j=0}^x n_{SF}(j)}$  depicted in figure c, is approximated by the continuous  $\cos[\sqrt{4\pi}(\varphi(x) - \varphi(0))]$  in d, which clearly is not constant and yields incorrect long wave length behavior. In reality  $\lambda = \infty$  and is not finite as drawn in the figure. But for every  $\lambda > 0$  the function  $\cos[\sqrt{4\pi}(\varphi(x) - \varphi(0))]$  has a dip centered at the points where the cosine equals -1 and is therefore not constant like  $(-1)^{2\sum_{j=0}^x n_{SF}(j)}$ .

The bosonized function has a dip of width  $\lambda$  around a doubly occupied site, which is not present on the lattice expression. So  $\cos[\sqrt{2\pi}(\varphi_c(x) - \varphi_c(0))]$  is not the proper continuum limit for the operator  $(-1)^{\sum_{j=0}^x n_{tot}(j)}$ . Although  $\lambda = \infty$ , we used a finite  $\lambda$  in this picture. But since the function  $-\sqrt{\frac{2}{\pi}}(\varphi_c(x) - \varphi_c(0))$  is monotonically increasing for every  $\lambda > 0$ , the function  $\cos[\sqrt{2\pi}(\varphi_c(x) - \varphi_c(0))]$  has always an extra dip centered at the point where the cosine equals -1 due to a doubly occupied site compared to  $(-1)^{\sum_{j=0}^x n_{tot}(j)}$  for the configuration drawn in figure 7.3.

Now write the string as  $\langle (-1)^{\sum_{j=0}^x n_{tot}(j)} \rangle = \langle (-1)^{2\sum_{j=0}^x S^z(j)} \rangle$ . In bosonization this function is written as  $\cos[\sqrt{2\pi}(\varphi_s(x) - \varphi_s(0))]$ , see figure 7.4. Again instead of  $\lambda = \infty$  we took  $\lambda$  finite in this picture and it appears that this function is the correct continuum limit for  $\langle (-1)^{\sum_{j=0}^x n_{tot}(j)} \rangle$  depicted in figure 7.3b. But now we have to be careful! Since the function  $-\sqrt{\frac{2}{\pi}}[\varphi_s(x) - \varphi_s(x)]$  is not monotonically increasing the form of the function will change if we increase  $\lambda$ ! This can be seen in figure 7.5 where we increased the value of  $\lambda$ . As  $\lambda$  increases the dip in the cosine in figure 7.4d and 7.5d will decrease and in the limit  $\lambda \rightarrow \infty$  will be very close to unity. This is in contrast with the function  $(-1)^{\sum_{j=1}^x n_{tot}(j)}$  which changes sign after a singly occupied site in figure 7.5c. But despite this discrepancy this function gives a good approximation for the function at the doubly occupied sites in contrast to  $\cos[\sqrt{2\pi}(\varphi_c(x) - \varphi_c(0))]$ : There are no dips in the function for doubly occupied sites although now the function fails to describe singly occupied sites. In conclusion,  $\cos[\sqrt{2\pi}(\varphi_c(x) - \varphi_c(0))]$  describes properly the behavior of singly occupied states but is wrong for doubly occupied states whereas  $\cos[\sqrt{2\pi}(\varphi_s(x) - \varphi_s(0))]$  is correct for doubly occupied states, but fails for singly occupied states. Clearly the right expression is some combination of both expressions and it is not surprising that DMRG calculation show that  $\langle (-1)^{\sum_{j=0}^x n_{tot}(j)} \rangle = B_s/x^{K_s} + B_c \cos(2k_F x)/x^{K_c}$ .

### 7.3 Bosonizing using the proper continuum limit

So we can conclude that, although the bosonization procedure is correct for the density correlator  $\langle n_{tot}(x)n_{tot}(0) \rangle$ , the bosonization procedure selects the wrong continuum limit for averages like  $\langle (-1)^{2\sum_{j=0}^x n_{SF}(j)} \rangle$  and bosonization fails. On the other hand, it is not true that bosonization generates the wrong continuum limit for every string operator. In this section we present some spinless fermion operators for which bosonization is expected to generate the proper continuum limit. But as will turn out, even in this case, the method is not able to generate correct expressions.

For instance, consider the string operator for spinless fermions  $(-1)^{\sum_{j=0}^x n_{SF}(j)} = \cos[\pi \sum_{j=0}^x n_{SF}(j)]$ . In bosonized form this function equals  $\cos[\sqrt{\pi}(\varphi(x) - \varphi(0))]$ . These operators are depicted in figure 7.6. Now because for spinless fermions two particles cannot be on the same site, we do not run into the problem that we encountered before in calculating  $\langle (-1)^{\sum_{j=0}^x n_{tot}(j)} \rangle$  and here bosonization does generate the proper continuum limit. What is the average of this operator?

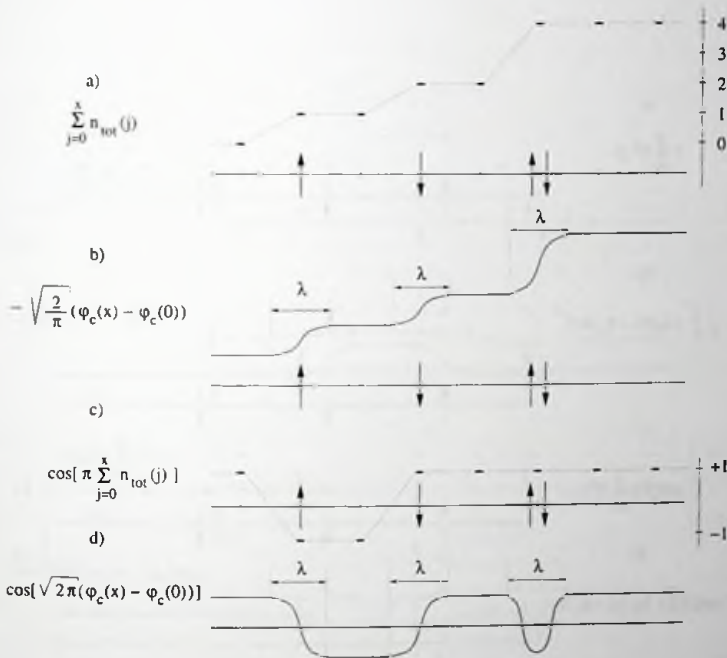


Figure 7.3: Picture a and b show respectively the sum  $\sum_{j=0}^x n_{tot}(j)$  and its bosonized version  $-\sqrt{\frac{2}{\pi}}(\varphi_c(x) - \varphi_c(0))$ . Using the normal bosonization procedure, the function  $\cos[\pi \sum_{j=0}^x n_{tot}(j)]$  in figure c is approximated by  $\cos[\sqrt{2\pi}(\varphi_c(x) - \varphi_c(0))]$  which is depicted in figure d. Here we again took  $\lambda$  finite instead of  $\lambda = \infty$ . But since  $\cos[\sqrt{2\pi}(\varphi_c(x) - \varphi_c(0))]$  is monotonically increasing for these configurations,  $\cos[\sqrt{2\pi}(\varphi_c(x) - \varphi_c(0))]$  will have two dips, one too many as compared to the function  $\cos[\pi \sum_{j=0}^x n_{tot}(j)]$  in figure c due to the doubly occupied site. Clearly this is not the proper continuum limit in the case that two particles can be on the same site.

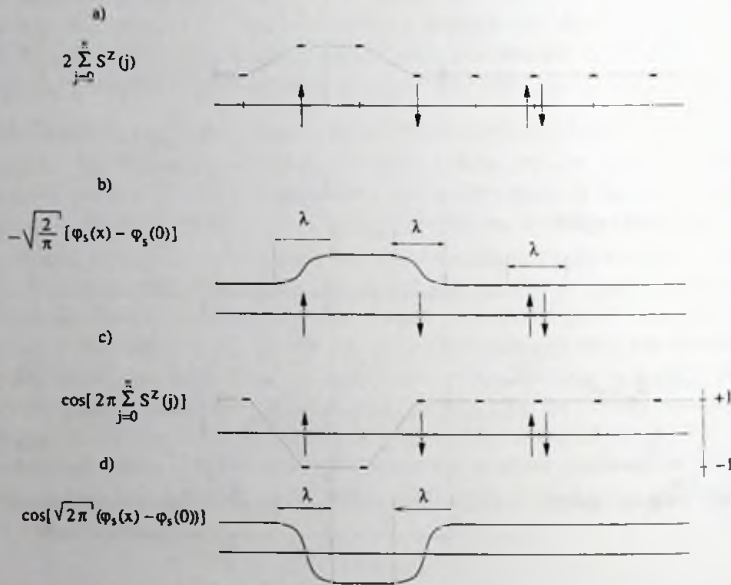


Figure 7.4: Instead of the function  $\cos[\sqrt{2\pi}(\varphi_c(x) - \varphi_c(0))]$ , we can use  $\cos\sqrt{2\pi}[\varphi_s(x) - \varphi_s(0)]$  depicted in figure d to approximate  $(-1)^{\sum_{j=0}^x n_{101}(j)} = (-1)^{\sum_{j=0}^x 2S^z(j)}$  in figure c. It appears that this function is the correct continuum limit for  $\cos[\pi \sum_{j=0}^x n_{101}(j)] = \cos[2\pi \sum_{j=0}^x S^z(j)]$  depicted in figure c. But as can be seen in figure 7.5, this operator fails for singly occupied states when we increase  $\lambda$ .

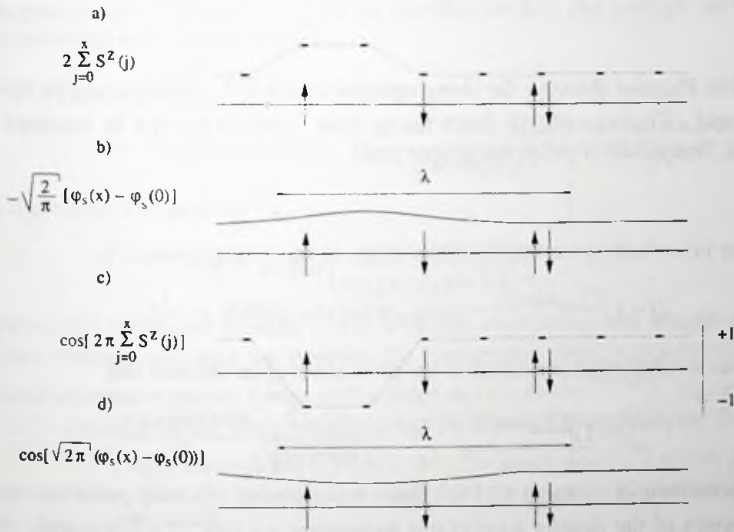


Figure 7.5: Pictures showing  $\cos[\sqrt{2\pi}(\varphi_s(x) - \varphi_s(0))]$  as an approximation for  $(-1)^{\sum_{j=0}^x n_{SF}(j)}$  as also was done in figure 7.4 only now with a larger width  $\lambda$  of the particles. Figure d shows that for larger  $\lambda$  the function  $\cos[\sqrt{2\pi}(\varphi_s(x) - \varphi_s(0))]$  is not the proper continuum limit for  $(-1)^{\sum_{j=0}^x 2S^z(j)} = (-1)^{\sum_{j=0}^x n_{SF}(j)}$ . In figure b and d we only depicted the width  $\lambda$  of the down spin particle in the middle.

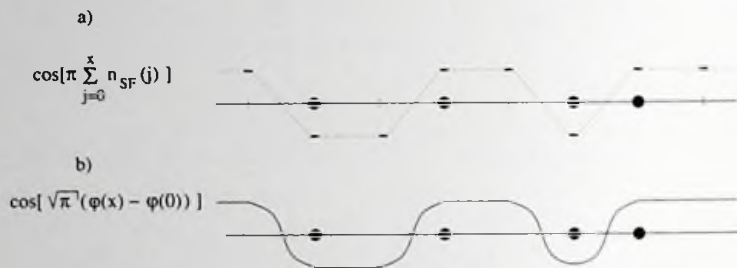


Figure 7.6: Pictures showing the string operator  $\cos[\pi \sum_{j=0}^x n_{SF}(j)]$  and its bosonized version  $\cos[\sqrt{\pi}(\varphi(y) - \varphi(z))]$ . Since the spinless fermions can not be localized on the same site, bosonization yields the proper limit.

Using bosonization we find for the average of this string operator is

$$\langle (-1)^{\sum_{j=0}^x n_{SF}(j)} \rangle \sim \langle \cos[\sqrt{\pi}(\varphi(x) - \varphi(0))] \rangle = \frac{1}{\sqrt{x}}. \quad (7.7)$$

The numeric calculation presented in the previous chapter showed that

$$\langle (-1)^{\sum_{j=0}^{x-1} n_{SF}(j)} \rangle = \frac{A^2 \sqrt{2}}{\sqrt{\sin(\pi \rho_{SF} x)}} \frac{\cos(\pi \rho_{SF} x)}{\sqrt{x}}, \quad (7.8)$$

as was presented in equation (6.11). Since bosonization can only probe the non-zero wave vectors of the density  $n_{SF}(x)$  this expression  $\langle (-1)^{\int_0^x n_{SF}(y) dy} \rangle$  is only valid up to multiplicative factors of order  $\cos(\pi \rho_{SF} x)$  and so we can conclude that bosonization yields the correct powerlaw decay in (7.8) although it does not yield the prefactor  $A^2 \sqrt{2} / \sqrt{\sin(\pi \rho_{SF})}$ .

We can also calculate the expression  $\langle n_{SF}(x) (-1)^{\sum_{j=1}^{x-1} n_{SF}(j)} \rangle$ . In principle, like with the average  $\langle (-1)^{\sum_{j=1}^{x-1} n_{SF}(j)} \rangle$ , bosonization yields the proper continuum limit for this average. In bosonization this expression is

$$\begin{aligned} \langle n_{SF}(x) \cos \left[ \sum_{j=1}^{x-1} n_{SF}(j) \right] \rangle = & \\ & - \frac{1}{2\sqrt{\pi}} \left( \langle \partial_x \varphi(x) e^{i\sqrt{\pi}[\varphi(x) - \varphi(0)]} \rangle + \langle \partial_x \varphi(x) e^{-i\sqrt{\pi}[\varphi(x) - \varphi(0)]} \rangle \right) \\ & + \left( \frac{e^{-2ik_F x}}{2\pi} e^{i\sqrt{4\pi}\varphi(x)} e^{i\sqrt{\pi}(\varphi(x) - \varphi(0))} + h.c. \right) \\ & + \left( \frac{e^{+2ik_F x}}{2\pi} e^{-i\sqrt{4\pi}\varphi(x)} e^{-i\sqrt{\pi}(\varphi(x) - \varphi(0))} + h.c. \right). \end{aligned} \quad (7.9)$$

To simplify this expression, we use

$$\begin{aligned} \langle \partial_x \varphi(x) e^{i\sqrt{\pi}(\varphi(x)-\varphi(0))} \rangle &= \frac{1}{i\sqrt{\pi}} \frac{d}{dx} \langle e^{i\sqrt{\pi}(\varphi(x)-\varphi(0))} \rangle \\ &= -\langle \partial_x \varphi(x) e^{-i\sqrt{\pi}(\varphi(x)-\varphi(0))} \rangle, \end{aligned} \quad (7.10)$$

and we obtain

$$\langle n_{SF}(x) (-1)^{\sum_{j=0}^{x-1} n_{SF}(j)} \rangle_{BOS} = 0. \quad (7.11)$$

Note that because of normal ordering we can neglect the last two expressions in (7.9). As was pointed out in equation (6.13) of the previous section, this average can be linked to the expression in (7.8) which yields

$$\begin{aligned} \langle n_{SF}(x) (-1)^{\sum_{j=1}^{x-1} n_{SF}(j)} \rangle \\ = \text{sign}(\cos(\pi\rho_{SF}) - 1) \frac{A^2 \sqrt{1 - \cos(\pi\rho_{SF})} \cos(\pi\rho_{SF}x - K)}{\sqrt{\sin(\pi\rho_{SF})} \sqrt{x}}, \end{aligned} \quad (7.12)$$

where the constant  $K$  is given by

$$K = \arctan \left( \frac{\sin(\pi\rho_{SF})}{\cos(\pi\rho_{SF}) - 1} \right). \quad (7.13)$$

Comparing the bosonized formula (7.11) with this expression, one should remember that since bosonization does not describe the background density  $\rho_{SF}$  in  $n_{SF}(x)$ , the bosonized expression misses a term of the order  $\rho_{SF} \langle (-1)^{\sum_{j=1}^{x-1} n_{SF}(j)} \rangle$ . The expression in (7.12) is precisely of this form because it can be obtained by multiplying the average  $\langle (-1)^{\sum_{j=1}^{x-1} n_{SF}(j)} \rangle$  with the constant  $g(\rho_{SF}) = A^2 \sqrt{1 - \cos(\pi\rho_{SF})} / \sqrt{2}$  which is of order  $\rho_{SF}$ . On the other hand, the bosonization result does not describe the shift of the cosine with the constant  $K$ .

Using the same principles, we can also calculate  $\langle n_{SF}(x) (-1)^{\sum_{j=1}^{x-1} n_{SF}(j)} n_{SF}(0) \rangle$  which in bosonization after normal ordering can be written as

$$\begin{aligned} \langle n_{SF}(x) (-1)^{\sum_{j=1}^{x-1} n_{SF}(j)} n_{SF}(0) \rangle_{BOS} = \\ + \left( \frac{1}{\pi} \langle \partial_x \varphi(x) e^{i\sqrt{\pi}(\varphi(x)-\varphi(0))} \partial_x \varphi(0) \rangle + h.c. \right) \\ + \left( \frac{e^{-2ik_F x} e^{i\sqrt{4\pi}(\varphi(x)-\varphi(0))}}{2\pi} e^{i\sqrt{\pi}(\varphi(x)-\varphi(0))} + h.c. \right) \\ + \left( \frac{e^{-2ik_F x} e^{i\sqrt{4\pi}(\varphi(x)-\varphi(0))}}{2\pi} e^{-i\sqrt{\pi}(\varphi(x)-\varphi(0))} + h.c. \right). \end{aligned} \quad (7.14)$$

The first part can be calculated using

$$\begin{aligned} \langle \partial_x \varphi(x) e^{i\sqrt{\pi}(\varphi(x)-\varphi(y))} \partial_y \varphi(y) \rangle &= \frac{1}{\pi} \frac{d}{dx} \frac{d}{dy} \langle e^{i\sqrt{\pi}(\varphi(x)-\varphi(y))} \rangle \\ &= \frac{-3}{4\pi(x-y)^{\frac{5}{2}}}, \end{aligned} \quad (7.15)$$

and so

$$\begin{aligned}
 & \langle n_{SF}(x)(-1)^{\sum_{j=1}^{x-1} n_{SF}(j)} n_{SF}(0) \rangle_{BOS} \\
 &= -\frac{3}{4\pi^2 x^{\frac{5}{2}}} + \frac{\cos(2k_F x)}{\pi} \langle e^{i3\sqrt{\pi}(\varphi(x)-\varphi(0))} \rangle + \frac{\cos(2k_F x)}{\pi} \langle e^{i\sqrt{\pi}(\varphi(x)-\varphi(0))} \rangle \\
 &= -\frac{3}{4\pi^2} \frac{1}{x^{\frac{5}{2}}} + \frac{\cos(2k_F x)}{\pi} \left( \frac{1}{x^{\frac{1}{2}}} + \frac{1}{x^{\frac{9}{2}}} \right). \tag{7.16}
 \end{aligned}$$

So for large  $x$  the bosonization calculation yields

$$\langle n_{SF}(x)(-1)^{\sum_{j=1}^{x-1} n_{SF}(j)} n_{SF}(0) \rangle_{BOS} \rightarrow \frac{\cos(2k_F x)}{\pi \sqrt{x}}. \tag{7.17}$$

Again this operator can be linked to expression (7.8) which yields (see (6.15))

$$\langle n_{SF}(x)(-1)^{\sum_{j=1}^{x-1} n_{SF}(j)} n_{SF}(0) \rangle_{NUM} = \frac{A^2(\cos(\pi\rho_{SF}) - 1) \cos(\pi\rho_{SF}x)}{\sqrt{2}\sqrt{\sin(\pi\rho_{SF})} \sqrt{x}}. \tag{7.18}$$

The bosonization result and the exact result look very similar and it seems that bosonization generates the correct answer. But we have to be careful here! Note that since bosonization does not describe the background density  $\rho_{SF}$  in  $n_{SF}(x)$ , the result in (7.17) misses a term of  $\rho_{SF}^2 \langle (-1)^{\sum_{j=1}^{x-1} n_{SF}(j)} \rangle$ . In comparison with (7.12) our first guess for this missing term would be

$$g(\rho_{SF})^2 \langle (-1)^{\sum_{j=1}^{x-1} n_{SF}(j)} \rangle = \frac{A^2(\cos(\pi\rho_{SF}) - 1) \cos(\pi\rho_{SF}x)}{\sqrt{2}\sqrt{\sin(\pi\rho_{SF})} \sqrt{x}}. \tag{7.19}$$

But this expression exactly equals (7.18)! So it is not clear what to think about the bosonized expression (7.17). Although it has the same powerlaw decay as the numeric calculated expression (7.18), it is probably not referring to it because (7.18) can be completely described by the missing term  $g(\rho_{SF})^2 \langle (-1)^{\sum_{j=1}^{x-1} n_{SF}(j)} \rangle$ . On the other hand, we are only guessing the expression of the missing terms of order  $\rho_{SF}^2 \langle (-1)^{\sum_{j=1}^{x-1} n_{SF}(j)} \rangle$ . So maybe the bosonized expression (7.17) together with this unknown missing terms are describing (7.12). So it is not completely clear what is happening here.

We see that even in the case that we use the proper continuum limit for the expressions  $\langle (-1)^{\sum_{j=1}^{x-1} n_{SF}(j)} \rangle$ ,  $\langle n_{SF}(x)(-1)^{\sum_{j=1}^{x-1} n_{SF}(j)} \rangle$  and  $\langle n_{SF}(x)(-1)^{\sum_{j=1}^{x-1} n_{SF}(j)} n_{SF}(0) \rangle$  in bosonization we are still missing important contributions. This is because bosonization is handicapped due to the fact that it cannot track down the background component  $\rho_{SF}$  of the charge density  $n_{SF}(x)$ . Therefore we have to be very careful when using bosonization for such expressions.

## 7.4 Bosonizing the hidden order string correlator

From the previous sections we conclude that bosonization can yield incorrect results even when we take the proper continuum limit. Being warned by this, let us consider the

hidden order string correlator  $\langle S^z(x)(-1)^{\sum_{j=1}^{x-1} n_{tot}(j)} S^z(0) \rangle$  and see what bosonization has to say about this expression.

We already observed in section 7.1 that we can either use  $\cos[\sqrt{2\pi}(\varphi_c(x) - \varphi_c(0))]$  or  $\cos[\sqrt{2\pi}(\varphi_s(x) - \varphi_s(0))]$  to approximate the product  $(-1)^{\sum_{j=1}^{x-1} n_{tot}(j)}$ . We also noticed that the first expression is correct for singly occupied states and fails for doubly occupied states, while  $\cos[\sqrt{2\pi}(\varphi_s(x) - \varphi_s(0))]$  is correct for doubly occupied states and is incorrect for singly occupied states. But since  $S^z(x)$  and  $S^z(0)$  are zero for doubly occupied states, it is correct to use the expression  $\cos[\sqrt{2\pi}(\varphi_s(x) - \varphi_s(0))]$  as the continuum bosonized version for  $(-1)^{\sum_{j=1}^{x-1} n_{tot}(j)}$  in this string operator. And so the topological correlator  $O_{top}(x)$  can be written as

$$\begin{aligned} O_{top}(x) &= -\langle S^z(x)(-1)^{\sum_{j=1}^{x-1} n_{tot}(j)} S^z(0) \rangle = \\ &\left( \frac{1}{4\pi} \langle \partial_x \varphi_s(x) e^{i\sqrt{2\pi}(\varphi_c(x) - \varphi_c(0))} \partial_x \varphi_s(0) \rangle + h.c. \right) \\ &\left( \frac{e^{-2ik_F x}}{8\pi^2} \langle e^{i\sqrt{2\pi}(\varphi_c(x) - \varphi_c(0))} e^{-i\sqrt{2\pi}(\varphi_c(x) - \varphi_c(0))} \rangle \langle e^{-i\sqrt{2\pi}(\varphi_s(x) - \varphi_s(0))} \rangle + h.c. \right) \\ &\left( \frac{e^{2ik_F x}}{8\pi^2} \langle e^{-i\sqrt{2\pi}(\varphi_c(x) - \varphi_c(0))} e^{-i\sqrt{2\pi}(\varphi_c(x) - \varphi_c(0))} \rangle \langle e^{-i\sqrt{2\pi}(\varphi_s(x) - \varphi_s(0))} \rangle + h.c. \right). \end{aligned} \quad (7.20)$$

And these contributions equal

$$\begin{aligned} O_{top}(x) &= -\langle S^z(x)(-1)^{\sum_{j=1}^{x-1} n_{tot}(j)} S^z(0) \rangle = \\ &-\frac{1}{4\pi^2} \frac{1}{x^2 + K_c} - \frac{1}{4\pi^2} \frac{\cos(2k_F x)}{x^{K_s}} - \frac{1}{4\pi^2} \frac{\cos(2k_F x)}{x^{K_s + 4K_c}}. \end{aligned} \quad (7.21)$$

So for large distances the bosonized expression equals

$$\langle S^z(x)(-1)^{\sum_{j=1}^{x-1} n_{tot}(j)} S^z(0) \rangle = \frac{\cos(2k_F x)}{x^{K_s}}. \quad (7.22)$$

Because bosonization does not describe the background density  $\rho_{tot}$  in  $n_{tot}(x)$  the oscillatory term in (7.22) should not be taken too seriously. Furthermore since  $\rho_{\uparrow} = \rho_{\downarrow}$ , the constant background term in  $S^z(x)$  is zero, and we do not run into missing terms like we did when calculating expressions like  $\langle n_{SF}(x)(-1)^{\sum_{j=1}^{x-1} n_{SF}(j)} \rangle$  and  $\langle n_{SF}(x)(-1)^{\sum_{j=1}^{x-1} n_{SF}(j)} n_{SF}(0) \rangle$ . This result indicates that the sublattice parity is ordered. But as was described in the previous section, the procedure of bosonization can generate incorrect results for string operators, even when the proper continuum limit is obtained.

So from these results it is still unclear whether the sublattice parity is ordered or not. In the next section we will turn to numeric DMRG calculations to resolve this question.

[The text in this section is extremely faint and illegible. It appears to be a multi-paragraph discussion, possibly containing mathematical notation or technical details related to the chapter's title. The content is too blurry to transcribe accurately.]

## Chapter 8

# DMRG calculations

In this chapter we will analyze the numeric calculations performed by McCulloch to resolve the ambiguity in the bosonization results for the topological correlation functions found in the previous chapter. Using the Density Matrix Renormalization Group (DMRG) algorithm, the sublattice parity order in the Hubbard model for finite Coulomb repulsion  $U$  was investigated. In this regime it is difficult to calculate the topological correlator  $O_{top}(x)$  from the Bethe Ansatz solution. Furthermore, we will also discuss the DMRG calculations of the averages of some other functions, which are needed in chapter when explaining the obtained results.

Before presenting the results of the DMRG calculation, we give a quick introduction of the technique in general.

### 8.1 Introduction

The Density Matrix Renormalization Group (DMRG) algorithm was introduced by White in 1992 [62]. It evolved from Wilson's famous Numerical Renormalization Group approach [63], although the resulting algorithm owes very little to the renormalization group idea. In fact, the name 'DMRG' is a historical misnomer and the algorithm is essentially a direct diagonalization of a truncated Hilbert space, and there is no scaling transformation or any renormalization group flow as such. DMRG is conceptually similar to exact diagonalization, or similar pure variational calculation where the number of variational parameters is rather large.

In exact diagonalization, one directly constructs the Hamiltonian matrix for the lattice system and diagonalizes it using some numerical diagonalization algorithm, usually the Lanczos algorithm [64] or similar. The problem with this approach is that the dimension of the Hilbert space increases exponentially with the lattice size. For example, the Hubbard model requires four basis states per site; hence the full Hilbert space of an  $L$ -site lattice contains  $4^L$  states. Even with sophisticated numerical techniques, diagonalizing such a matrix for a reasonably large value of  $L$  (say, around 20 or so) rapidly becomes impractical. A solution for this is provided by the DMRG method.

The DMRG algorithm is based around an approximation whereby the lattice system is split into two parts, called the left block and the right block (denoted  $A$  and  $B$  here) and the basis in each block is then truncated. The wave function is written in the basis of the tensor product of the two-block basis (usually called the superblock basis),

$$|\Psi\rangle = \sum_{a=1}^{N_A} \sum_{b=1}^{N_B} \psi_{ab} |a\rangle \otimes |b\rangle, \quad (8.1)$$

where the dimension of the left block is  $N_A$  and the dimension of the right block is  $N_B$ . The essential approximation is to reduce the dimension of the blocks, such that the wave function is affected in the smallest possible way. To see how this works, we construct the basis states in the left block that are the most important in the representation of the wave function. Let  $|\phi\rangle$  be an arbitrary state in the left block basis,

$$|\phi\rangle = \sum_{a=1}^{N_a} \phi_a |\alpha\rangle. \quad (8.2)$$

The weight of this state in the superblock wave function is simply the trace over the environment block of  $\langle\phi|\Psi\rangle = \sum_{ab} \phi_a \psi_{ab} \langle b|$ ,

$$W(|\phi\rangle) = \sum_{a=1}^{N_a} \sum_{b=1}^{N_b} \phi_a \psi_{ab}. \quad (8.3)$$

We now calculate the expansion coefficients  $\phi_a$  such that  $W(|\phi\rangle)$  is a maximum, subject to the constraint that  $\langle\phi|\phi\rangle = 1$ . This can be done simply with Lagrange multipliers, giving the result that

$$\phi_{a'} = \lambda \sum_a \rho_{a'a} \phi_a, \quad (8.4)$$

where  $\lambda$  is a maximum and  $\rho_{a'a}$  is the reduced density-matrix,

$$\rho_{a'a} = \sum_{b=1}^{N_b} \psi_{a'b} \psi_{ab}^*. \quad (8.5)$$

Hence the important states required in the system basis are the eigenstates of the reduced density-matrix that have largest eigenvalue.

Using this result, we construct the simplest form of DMRG, the so-called infinite-size algorithm [62]. In this scheme, a single lattice site is added to each of the left and right blocks at each iteration; thus the length of the superblock  $L$  grows by two sites at a time. Prior to the first iteration, the left and right blocks each consist of a single site. The iterations are started by adding a single site to each block and forming the superblock as the tensor product of the resulting two blocks. In the usual graphical notation, this is given by the first line of figure 8.1. Here, solid rectangles indicate

truncated blocks with at most  $m$  basis states and open circles indicate bare sites. The ground state wave function of the superblock is found using a matrix diagonalization algorithm, for example the Lanczos or Davidson algorithms [64]. From this, the reduced density-matrix in (8.5) is constructed and the truncation to  $m$  basis states is performed as described in the previous paragraph. This is done for the left and right blocks separately. New sites are then added to each block and the process is repeated. This is called the infinite-size algorithm because it is commonly supposed that the limit of a large number of iterations corresponds to taking the thermodynamic limit to an infinite lattice size. It must be remembered however, that infinite-size DMRG only converges to the exact ground state in the limit  $m \rightarrow \infty$  and this limit must be taken before the limit  $L \rightarrow \infty$ .

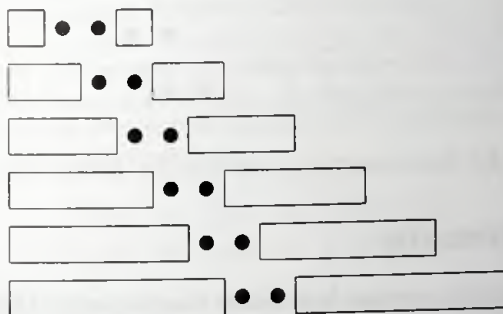


Figure 8.1: Schematic form of the infinite-size DMRG algorithm. Open rectangles represent truncated blocks, solid circles are bare lattice sites.

If one is interested in calculating accurately the properties of a system of some specific size, then it is possible to significantly improve upon the accuracy of the infinite-size algorithm. Constructing an  $L$  site system using the infinite-size algorithm requires the construction of blocks of all sizes  $2, 3, \dots, L/2$ . In the infinite-size algorithm these smaller blocks are not needed and can be discarded on the next iteration. However, the overall system size can be maintained at  $L$  if we take the next left block to be size  $L/2 + 1$  and the right block to be the block from the previous iteration, of size  $L/2 - 1$ . This procedure can be carried further, so that the  $n$ 'th iteration uses a left block of size  $L/2 + n$  and a right block of size  $L/2 - n$ . Once the right block gets small enough that it can be represented exactly (ie. when the dimension of the Hilbert space becomes less or equal to  $m$ ), the direction of iteration is reversed. This is illustrated schematically in figure 8.2. Many 'sweeps' can be performed over the system, so that the target state is iteratively improved.

The DMRG calculations presented here make all use of the  $SO(4)$  symmetry in the Hubbard model. We describe this application in the next section.

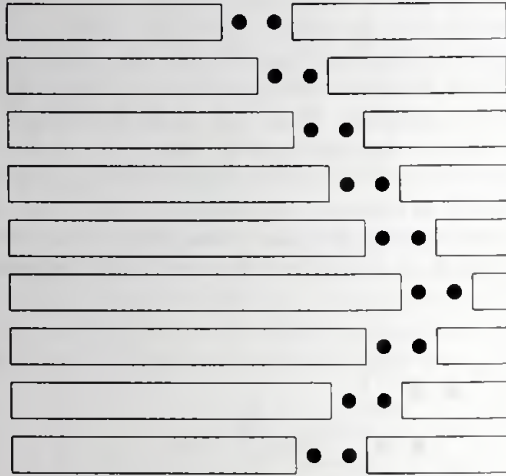


Figure 8.2: Schematic form of the finite-size DMRG algorithm.

## 8.2 $SO(4)$ Symmetry

The DMRG calculations presented here utilizes the non-Abelian DMRG algorithm developed by McCulloch and Gulácsi [65]. This algorithm makes use of the celebrated Wigner-Eckart theorem [66] to reduce substantially the dimension of the Hilbert space, thus increasing the accuracy of the calculation. This also has implications for the types of quantities that can be measured using the algorithm. We will now briefly sketch the main principles of this algorithm.

Consider the matrix elements of some operator  $O^k$ , which transforms as the  $D(k)$  irreducible representation of for instance  $SU(2)$  (ie.  $k = 0$  scalar,  $k = 1$  vector etc.). We can denote the matrix elements of the  $l^{\text{th}}$  component of  $O^k$  by

$$\langle j' m'(\alpha') | O_l^k | j m(\alpha) \rangle, \quad (8.6)$$

where  $j', j$  are the total spin,  $m', m$  are the corresponding projections onto the  $z$ -axis, and  $(\alpha'), (\alpha)$  are labels to distinguish different basis states that have the same  $(j, m)$  quantum numbers. The Wigner-Eckart theorem states that the matrix elements can be factorized into a product of two factors, a purely geometric component, given by the Clebsch-Gordan coefficients, and a factor that is independent of the projection quantum numbers, called the reduced matrix element. Thus,

$$\langle j' m'(\alpha') | O_l^k | j m(\alpha) \rangle = C_{m' m l}^{j' j k} \times \langle j'(\alpha') || O^k || j(\alpha) \rangle. \quad (8.7)$$

The reduced matrix element is denoted with the unusual notation  $\langle j'(\alpha') || O^k || j(\alpha) \rangle$  to indicate that it acts in a different Hilbert space, and the algebra of reduced basis states  $|| j(\alpha) \rangle$  is different to that of ordinary kets and requires special treatment.

The significance of this theorem is that the single 'reduced' operator  $O^k$  acts on a different Hilbert space to the full operator  $O_f^k$ . In particular, all  $2k + 1$  components  $O_f^k$  can be recovered given knowledge of just  $O^k$ , and the dimension of the Hilbert space has been reduced from  $\sum_j (2j + 1)$  to  $\sum_j 1$ .

For example, consider the spin operator itself acting on a single spin  $j$ . The full Hilbert space comprises the  $2j + 1$  states  $|-j\rangle, |-j + 1\rangle, \dots, |j\rangle$ , therefore the spin operator  $\bar{S}$  requires  $3 \times (2j + 1)^2$  matrix elements to fully specify. But, since the spin operator transforms according to the  $s = 1$  vector representation of  $SU(2)$ , the matrix elements factorize into the product of a Clebsch-Gordan coefficient and a single reduced matrix element  $\langle j' || \bar{S} || j \rangle$ . In the specific case of the Hubbard model, we can see that the original 4-state basis is reduced to three states, since the two states  $|\uparrow\rangle$  and  $|\downarrow\rangle$  can be replaced by a single spin  $1/2$  multiplet  $|\frac{1}{2}\rangle$ . Note that the spin operator cannot distinguish between an empty and a doubly occupied site, and therefore we cannot use this symmetry to make a further reduction of these two states.

But for the Hubbard model, in addition to using the  $SU(2)$  symmetry leading to (8.7), we can use another symmetry to reduce the basis states. This is the so-called pseudospin found by Yang and Zhang [67]. To obtain this symmetry, one notices that the Hubbard Hamiltonian introduced in equation (4.37) is invariant under a particle-hole transformation of the eg. down spins only,

$$\begin{aligned} c_{\downarrow}^{\dagger}(j) &\rightarrow \bar{c}_{\downarrow}^{\dagger}(j) = (-1)^j c_{\downarrow}(j), \\ c_{\downarrow}(j) &\rightarrow \bar{c}_{\downarrow}(j) = (-1)^j c_{\downarrow}^{\dagger}(j). \end{aligned} \quad (8.8)$$

The staggered phase ensures that the hopping term connecting nearest-neighbor sites is preserved. More generally, the hopping term remains invariant if and only if the lattice is bipartite, with hopping only from one partition of lattice sites to the other partition.

Since the Hamiltonian is invariant under the transformation equation (8.8), for any operator  $X$  that commutes with  $H$ , the image under the transformation,  $\bar{X}$ , must also commute with  $H$ . In particular, this applies to the operators  $S^+$ ,  $S^-$  and  $S^z$ . This is useful because the image of these operators under the transformation equation (8.8) results in a new set of operators generating an additional  $SU(2)$  symmetry,

$$\begin{aligned} I^+(j) &= \bar{S}^+(j) = (-1)^j c_{\uparrow}^{\dagger}(j) c_{\downarrow}^{\dagger}(j), \\ I^-(j) &= \bar{S}^-(j) = (-1)^j c_{\downarrow}(j) c_{\uparrow}(j), \\ I^z(j) &= \bar{S}^z(j) = \frac{1}{2} [n_{\uparrow}(j) + n_{\downarrow}(j) - 1]. \end{aligned} \quad (8.9)$$

The pseudospin operators  $I^+$ ,  $I^-$ ,  $I^z$  all mutually commute with  $S^+$ ,  $S^-$  and  $S^z$ , which means that the 6 quantities generate the algebra  $SU(2) \times SU(2)$ , which is locally isomorphic to  $SO(4)$ .

The additional  $SU(2)$  symmetry label means that there are now two spin indices on every operator and basis state, which we write as  $(s, i)$  for spin  $s$  and pseudospin  $i$ . On a single site of the Hubbard model, pseudospin symmetry places the empty- and double-occupied states into a multiplet of degree 2, with pseudospin  $1/2$  and spin zero. The singly-occupied states in the spin  $1/2$  multiplet have zero pseudospin. This is indicated in the table 8.1. These two multiplets have the quantum numbers of the holon and spinon

	$s$	$s^z$	$i$	$i^z$
0	0	0	+1/2	-1/2
$ \uparrow\downarrow\rangle$	0	0	+1/2	+1/2
$ \uparrow\rangle$	+1/2	-1/2	0	0
$ \downarrow\rangle$	+1/2	+1/2	0	0

Table 8.1: The eigenvalues  $s, s^z, i$  and  $i^z$  for the operators  $S, S^z, I$  and  $I^z$  for the zero and doubly occupied site 0 and  $|\uparrow\downarrow\rangle$  and the two single occupied sites  $|\uparrow\rangle$  and  $|\downarrow\rangle$ . Note that using only the  $(s, i)$  coordinates, we can not distinguish between the non and doubly occupied sites, and the two single occupied sites.

respectively [68]. The two reduced basis states can be conveniently denoted  $||s\rangle, ||h\rangle$  for the spinon and holon respectively.

Now we can use the Wigner-Eckart theory to reduce the dimension of the Hilbert space. Instead of a  $SU(2)$  symmetry in (8.6) we have a  $SO(4)$  symmetry where  $j$  and  $m$  are replaced by the pairs  $(s, i)$  and  $(s^z, i^z)$  respectively and we retrieve a reduced matrix element similar to (8.7) which only depends on the eigenvalues  $(s, i)$ . So this method is designed to calculate operators which are  $SO(4)$  symmetric and commute with the generators  $\vec{S}$  and  $\vec{I}$ . One can show that the total number operator  $n_{tot}$  does not commute with the pseudospin  $[n_{tot}, I] \neq 0$ , and it is rather inconvenient to obtain correlation function like  $\langle n_{tot}(x)n_{tot}(0) \rangle$ . Instead, we must use the unfamiliar (but equivalent) total pseudospin correlation  $\langle I(x)I(0) \rangle$ . This is not the case for the operator for single occupied sites  $n_s$  for which  $[n_s, I] = 0$ . This operator is defined by  $n_s(x) = 1$  for a single occupied site and  $n_s(x) = 0$  for a doubly or non occupied site.

### 8.3 Specifications of the DMRG calculations

For all the calculations presented in this chapter, the finite-size algorithm was used exclusively. For a finite-size calculation, one would prefer to use periodic boundary conditions, as this ought to give the best scaling to the thermodynamic limit. However, it was noted quite early [69, 70] that using periodic boundary conditions in DMRG result in a loss of accuracy. Thus open boundary conditions are strongly preferred.

The charge and spin density fluctuations caused by open boundary conditions can be interpreted as generalized Friedel oscillations. If the oscillations remain finite in the thermodynamic limit then the oscillation corresponds to a charge density wave (CDW). More commonly, they decay with power-law behavior, with an exponent related to the density correlation exponent [71]. The advantage of measuring Friedel oscillations over correlation functions is that the former requires only single-site expectation values which are less susceptible to numerical error than two-point correlation functions, in large part due to the slower decay; the exponent governing the decay being half that of a two-point correlation function. However, the relationship between Friedel oscillations and topological correlation functions is less transparent. Thus, rather than using Friedel oscillations we explicitly construct the correlation functions and perform a direct fit. This

actually works quite well for the topological correlation functions as they generically decay slower than two-point correlation functions anyway.

To reduce the effect of the open boundary conditions, we used a relatively large system size (1000 sites) large enough to achieve a truncation length of the order of 200-300 lattice constants. In this way meaningful results can be obtained from a simple curve fit to obtain the desired exponents.

## 8.4 Outline of the DRMG calculations

Before considering the topological correlator, we will calculate the average of some other functions which we need in the upcoming chapter, when we review the results.

First we focus on the calculation of the quantity  $D_s(x) = \langle (-1)^{\sum_{j=0}^{x-1} n_{tot}(j)} \rangle$  for the Hubbard model. Amongst other things, this function has served in the previous chapter as an evidence in demonstrating that bosonization cannot be trusted when calculating non-local string correlators like  $O_{top}(x)$ .

After this, we investigate the correlators  $\langle n_s(x) \rangle$  and  $\langle n_s(x) (-1)^{\sum_{j=1}^{x-1} n_s(j)} n_s(0) \rangle$  with  $n_s(x)$  the density operator for single occupied sites. As is shown in the next chapter, these operators are very important in explaining the origin of the sublattice parity order.

We end the chapter by describing the DRMG results for the topological correlator  $O_{top}(x)$ .

## 8.5 Calculating $D_s(x)$

In this section we consider the correlation function  $D_s(x) = \langle (-1)^{\sum_{j=1}^x n_{tot}(j)} \rangle$  for spinful fermions for several total densities  $\rho_{tot}$  and Coulomb interactions  $U \geq 0$ . These results were already used in the previous chapter when we proved that bosonization cannot be trusted when calculating non local string correlators like  $O_{top}(x)$ . We can calculate the function  $D_s(x)$  analytically in two limits, namely  $U = 0$  and  $U \rightarrow \infty$ .

For  $U = 0$ , the up and down electrons decouple and the function can be calculated using spinless fermions and formula (6.11). But note that here we use  $\rho_{SF} = \rho_{tot}/2 = k_F/\pi$  and so we find

$$\begin{aligned}
 D_s(x) &= \langle (-1)^{\sum_{j=1}^x n_{tot}(j)} \rangle = \langle (-1)^{\sum_{j=1}^x n_{SF}(j)} \rangle^2 \\
 &= \frac{2A^4 \cos(\pi x \rho_{SF})^2}{\sin(\pi \rho_{SF}) x} \\
 &= \frac{2A^4 \cos(\frac{\pi x \rho_{tot}}{2})^2}{\sin(\frac{\pi \rho_{tot}}{2}) x} \\
 &= \frac{A^4}{\sin(\frac{\pi \rho_{tot}}{2})} \left( \frac{1 + \cos(2k_F x)}{x} \right). \tag{8.10}
 \end{aligned}$$

Furthermore, for  $U \rightarrow \infty$  the electrons behave like spinless fermions and there are no double occupied sites. In that case, the function can be written as

$$\begin{aligned} D_s(x) &= \langle (-1)^{\sum_{j=1}^x n_{tot}(j)} \rangle = \langle (-1)^{\sum_{j=1}^x n_{SF}(j)} \rangle \\ &= \frac{A^2 \sqrt{2}}{\sqrt{\sin(\pi \rho_{tot})}} \frac{\cos(\pi x \rho_{tot})}{\sqrt{x}} \\ &= \frac{A^2 \sqrt{2}}{\sqrt{\sin(\pi \rho_{tot})}} \frac{\cos(2k_F x)}{\sqrt{x}}, \end{aligned} \quad (8.11)$$

with the density  $\rho_{SF} = \rho_{tot} = \frac{2k_F}{\pi}$  and  $A = 0.645002448$ . Here we used again formula (6.11) which was proven in the previous chapter.

Since  $\langle (-1)^{\sum_{j=1}^x n_{tot}(j)} \rangle = \langle (-1)^{\sum_{j=1}^x n_s(j)} \rangle$  we can use the  $SO(4)$  DMRG algorithm to calculate it. The results indicate that away from half filling this function can be fitted with the function

$$D_s(x) = \langle (-1)^{\sum_{j=1}^x n_{tot}(j)} \rangle = \frac{B_s}{x^{g_1}} + \frac{B_c \cos(2k_F x)}{x^{g_2}}. \quad (8.12)$$

It is found that  $g_1 = 1$ , independent of the parameters and can be identified with  $K_s = 1$ . The values for  $g_2$  are displayed in figure 8.4, right under the figure 8.3 of the charge stiffness  $K_c$ , as it was obtained by Schulz in [58]. The two show a similar shape and we conclude that  $g_2$  matches  $K_c$ . So according to DMRG calculations

$$D_s(x) = \langle (-1)^{\sum_{j=1}^x n_{tot}(j)} \rangle = \frac{B_s}{x^{K_s}} + \frac{B_c \cos(2k_F x)}{x^{K_c}}. \quad (8.13)$$

The prefactors  $B_s$  and  $B_c$  are displayed in the figure 8.5 and 8.6 for different values of the density  $\rho_{tot}$  and Coulomb repulsion  $U$ . The analytic expression in (8.10) shows that for  $U = 0$ ,  $B_s = A^4 / \sin(\frac{\pi \rho_{tot}}{2})$ . We displayed this curve in figure 8.5, and it is in good agreement with the DMRG results. Furthermore, upon increasing the Coulomb repulsion  $U$ , the prefactor  $B_s$  rapidly goes to zero. Again this is in agreement with the result in (8.11) for  $U \rightarrow \infty$ , since it does not have a spin decaying term proportional to  $1/x^{K_s}$ .

The analytic expression in (8.10) and (8.11) indicate that  $B_c = A^4 / \sin(\pi \rho_{tot}/2)$  and  $B_c = A^2 \sqrt{2} / \sqrt{\sin(\pi \rho_{tot})}$  for respectively  $U = 0$  and  $U \rightarrow \infty$  and we plotted these curves in figure 8.6. These figures show that the numerical data for  $B_c$  are slightly too high compared to the analytic values. On the other hand, the values for the exponent  $g_2$  in figure 8.4 are a bit too low and since they appear like  $B_c/x^{g_2}$  this is at least consistent.

## 8.6 Calculating $\rho_s = \langle n_s(x) \rangle$

As we will see in the next chapter, it is convenient to have an expression for the correlator  $\langle n_s(x) \rangle$ . As stated before,  $n_s(x)$  is the density operator for singly occupied electrons and is defined as  $n_s(x) = 1$  for a single occupied site and  $n_s(x) = 0$  for a double or non-occupied site. In formula

$$n_s(x) = n_{\uparrow}(x) + n_{\downarrow}(x) - 2n_{\uparrow}(x)n_{\downarrow}(x). \quad (8.14)$$

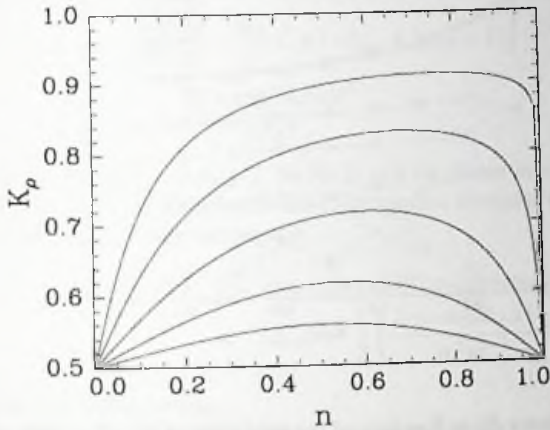


Figure 8.3: The charge stiffness  $K_c$  (here denoted as  $K_\rho$ ) as function of the density  $n = \rho_{tot}$  for  $U/t = 1, 2, 4, 8, 16$  for the top to bottom curves.

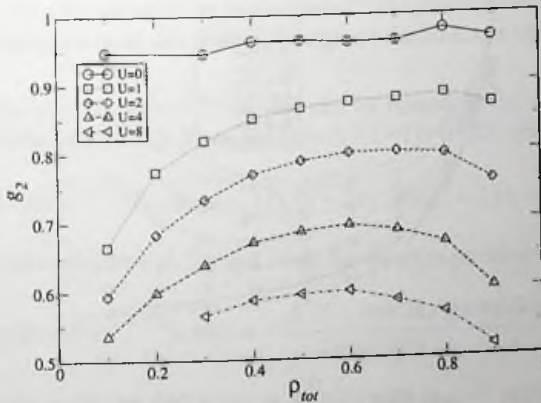


Figure 8.4: The exponent  $g_2$  as measured from formula (8.12) using DMRG calculations. The exponent  $g_2$  matches the charge stiffness  $K_c$  displayed in figure 8.3.

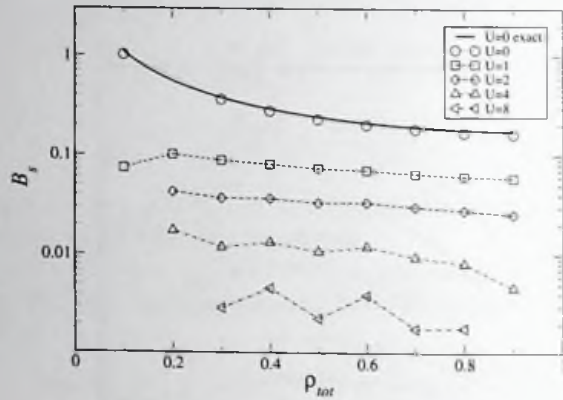


Figure 8.5: The prefactor  $B_s$  as function of the total density  $\rho_{tot}$  for different values of  $U$  together with the analytical curve for  $U = 0$ . Upon increasing  $U$ , the function decays rapidly to zero.

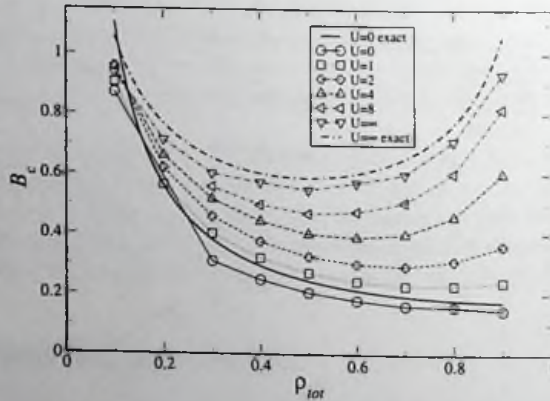


Figure 8.6: The prefactor  $B_c$  as function of the total density  $\rho_{tot}$  for different values of  $U$  together with the analytical curve for  $U = 0$  and  $U \rightarrow \infty$ .

The density  $\rho_s = \langle n_s(x) \rangle$  can be obtained by calculating the correlator  $\langle n_s(x)n_s(0) \rangle$ . For  $U = 0$  the up and down electron decouple into independent spinless fermion particles and we obtain

$$\begin{aligned} \langle n_s(x)n_s(0) \rangle &= 2\rho_{SF}^2 + (2 - 8\rho_{SF})\langle n_{SF}(x)n_{SF}(0) \rangle + 4\langle n_{SF}(x)n_{SF}(0) \rangle^2 \\ &= \rho_{tot}^2 \left(1 - \frac{\rho_{tot}}{2}\right)^2 + (-\rho_{tot}^2 + 2\rho_{tot} - 1) \left(\frac{1 - \cos(2k_F x)}{\pi^2 x^2}\right) \\ &\quad + \frac{(1 - \cos(2k_F x))^2}{\pi^4 x^4}. \end{aligned} \quad (8.15)$$

Here we have used that  $\rho_{SF} = \rho_{tot}/2$ . So for  $U = 0$  we obtain  $\rho_s = \rho_{tot}(1 - \rho_{tot}/2)$ .

In the limit  $U \rightarrow \infty$  the electrons behave like spinless fermions with  $n_s(x) \rightarrow n_{SF}(x)$  with  $\rho_{SF} = \rho_{tot}$  and the correlator equals

$$\begin{aligned} \langle n_s(x)n_s(0) \rangle &= \langle n_{SF}(x)n_{SF}(0) \rangle \langle n_{SF}(x)n_{SF}(0) \rangle \\ &= (\rho_{tot})^2 - \frac{1}{2} \left(\frac{1 - \cos(2k_F x)}{\pi^2 x^2}\right). \end{aligned} \quad (8.16)$$

So in this limit we find  $\rho_s = \rho_{tot}$ .

Now we turn to DMRG calculations to calculate the density  $\rho_s = \langle n_s(x) \rangle$  for different densities  $\rho_{tot}$  and Coulomb repulsion  $U$ . These results are depicted in figure 8.7 together with the analytic results for  $U = 0$  and  $U \rightarrow \infty$ .

## 8.7 Calculating $\langle n_s(x)(-1)^{\sum_{j=1}^{x-1} n_s(j)} n_s(0) \rangle$

In this section we will calculate  $\langle n_s(x)(-1)^{\sum_{j=1}^{x-1} n_s(j)} n_s(0) \rangle$ . As will be demonstrated in the next chapter, we need this average to explain the structure of the spin correlator  $\langle S^z(x)S^z(0) \rangle$ .

The function  $\langle n_s(x)(-1)^{\sum_{j=1}^{x-1} n_s(j)} n_s(0) \rangle$  can be related to the correlation function  $D_s(x)$  calculated in section 8.5. Since  $n_s(j) = (1 - (-1)^{n_s(j)})/2$ , one can write

$$\langle n_s(x)(-1)^{\sum_{j=1}^{x-1} n_s(j)} n_s(0) \rangle = \frac{1}{4} [D_s(x-2) - 2D_s(x-1) + D_s(x)]. \quad (8.17)$$

For  $U = 0$ ,  $D_s(x)$  is given by (8.10) and using the above expression we find

$$\langle n_s(x)(-1)^{\sum_{j=1}^{x-1} n_s(j)} n_s(0) \rangle = -\frac{A^4(1 - \cos(2k_F)) \cos(2k_F x)}{2 \sin(\frac{\pi \rho_{tot}}{2}) x}. \quad (8.18)$$

In the limit  $U \rightarrow \infty$ , we find  $n_s(x) \rightarrow n_{SF}(x)$  with  $\rho_{tot} \rightarrow \rho_{SF}$  and the expression can be written as

$$\begin{aligned} \langle n_s(x)(-1)^{\sum_{j=1}^{x-1} n_s(j)} n_s(0) \rangle &\rightarrow \langle n_{SF}(x)(-1)^{\sum_{j=1}^{x-1} n_{SF}(j)} n_{SF}(0) \rangle \\ &= -\frac{A^2(1 - \cos(\pi \rho_{tot})) \cos(2k_F x)}{\sqrt{2} \sin(\pi \rho_{tot}) \sqrt{x}}. \end{aligned} \quad (8.19)$$

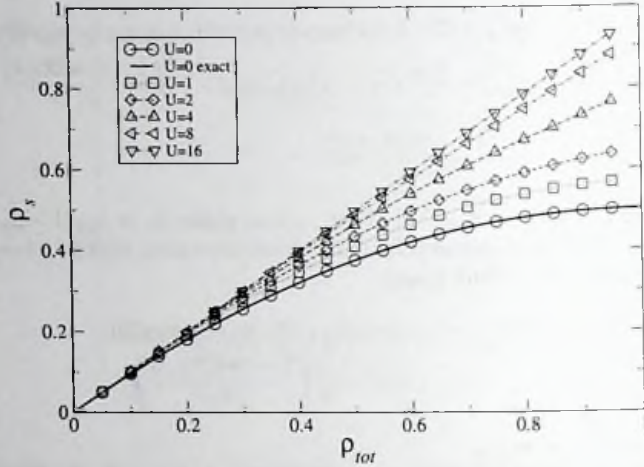


Figure 8.7: The density  $\rho_s$  of single occupied sites as a function of the total density  $\rho_{tot}$  for various values of the Coulomb repulsion  $U$ .

as was already calculated in equation (6.15). Note that  $2k_F = \pi \rho_{tot} = \pi \rho_S F$ .

For intermediate  $U \geq 0$ , the DMRG calculations presented in section 8.5 showed that  $D_s(x) = B_s/x^{K_c} + B_c \cos(2k_F x)/x^{K_c}$  and using (8.17) we find

$$\begin{aligned} \langle n_s(x) (-1)^{\sum_{j=1}^{x-1} n_s(j)} n_s(0) \rangle &= -\frac{B_c(1 - \cos(2k_F)) \cos(2k_F x)}{2 x^{K_c}} \\ &= -\frac{Q_c \cos(2k_F x)}{x^{K_c}}, \end{aligned} \quad (8.20)$$

with  $B_c$  calculated in figure 8.6 and  $Q_c = B_c(1 - \cos(2k_F))/2$ . We also calculated the correlator  $\langle n_s(x) (-1)^{\sum_{j=1}^{x-1} n_s(j)} n_s(0) \rangle$  using DMRG. The results are consistent with equation (8.20) and show that

$$\langle n_s(x) (-1)^{\sum_{j=1}^{x-1} n_s(j)} n_s(0) \rangle = -\frac{F_c \cos(2k_F x)}{x^h}. \quad (8.21)$$

The results for  $Q_c$  and  $F_c$  are depicted in figure 8.8 together with the analytic result for  $U = 0$  and  $U = \infty$ . The values for  $h$  are displayed in figure 8.9 and match the charge stiffness  $K_c$  from figure 8.3. And thus

$$\langle n_s(x) (-1)^{\sum_{j=1}^{x-1} n_s(j)} n_s(0) \rangle = -\frac{F_c \cos(2k_F x)}{x^{K_c}}. \quad (8.22)$$

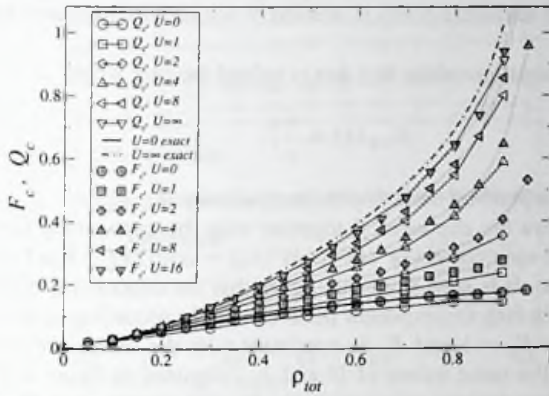


Figure 8.8: The prefactor  $F_c$  and  $Q_c$  in respectively (4.21) and (8.21) as function of the total density  $\rho_{tot}$  for different values of  $U$  together with the analytical curve for  $U = 0$  and  $U \rightarrow \infty$ .

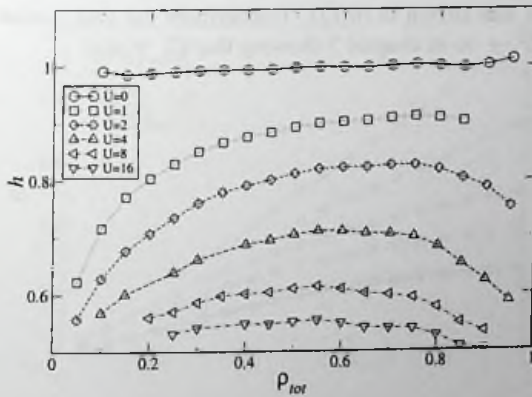


Figure 8.9: The exponent  $h$  as measured from formula (8.21) using DMRG calculations. The exponent  $h$  matches the charge stiffness  $K_c$  displayed in figure 8.3.

## 8.8 Calculating the correlator $O_{top}(x)$

Finally, we turn to the calculation of the topological correlator  $O_{top}(x)$  to resolve the question whether the sublattice parity is ordered or not for intermediate Coulomb repulsion  $U \geq 0$ .

The numeric calculations show that this is indeed the case where

$$O_{top}(x) = \frac{G_s}{x^f}, \quad (8.23)$$

with  $G_s$  a constant depending on  $U$  and the total density  $\rho_{tot}$ .

Figure 8.10 shows the exponent  $f$  together with the exponent  $\eta$  for the standard two point staggered spin correlator  $\langle M^z(0)M^z(x) \rangle \sim \cos[(2k_F - \pi)x]/x^\eta$  for various interaction strengths. It is seen from this figure that the exponent  $\eta$  depends strongly on the parameters. In fact, the exponent behaves exactly according to the expectations:  $\eta = K_s + K_c$  where  $K_s = 1$  and  $K_c$  is consistent with the values previously obtained by Schulz [58] for the same values of  $U$  and  $\rho_{tot}$  depicted in figure 4.4 in chapter 4. we find no other characteristic momenta in the Fourier transform of  $O_{top}(x)$  which is already reminiscent of the staggered spin correlator of a Heisenberg chain. This is further amplified by our finding that the exponent  $\eta_{top}$  does not depend on the microscopic parameters at all. In fact, for all parameters the exponent of the topological correlator  $\eta_{top} = 1 = K_s$ . Hence, regardless the values of  $U$  and  $\rho$  the long distance behavior of the topological correlator is indistinguishable from the spin-spin correlator of a Heisenberg chain, demonstrating that the Hubbard model indeed carries the sublattice parity topological order fully for all values  $U \geq 0$ .

In figure 8.11 we depicted the numerical data for the prefactor  $G_s$  of the topological correlator  $O_{top}(x)$  together with the analytical result for  $U = 0$  where  $G_s = A^4 \sin(\pi\rho_{tot}/2)/4$  as was shown in (6.17). Furthermore the data is also in agreement with our results for  $U \rightarrow \infty$  in chapter 5 showing that  $G_s \sim \rho_{tot}$ .

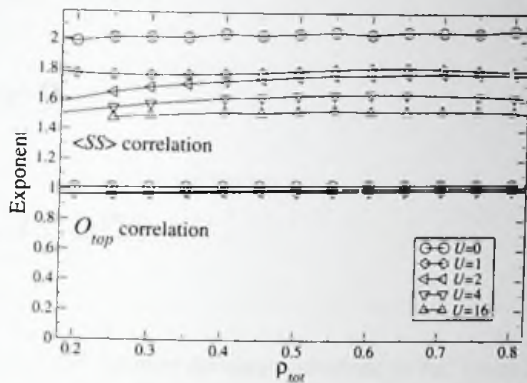


Figure 8.10: Exponents of the spin-spin correlation,  $\eta$ , (top) and the topological correlation,  $f$ , (bottom) as a function of electron filling, for various values of interaction  $U$ .

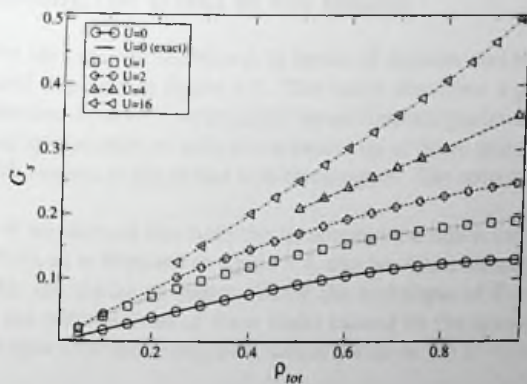


Figure 8.11: The prefactor  $G_s$  of the topological correlator  $O_{top}(x)$  from equation (8.23).

*[The following text is extremely faint and illegible due to the low resolution of the scan. It appears to contain several paragraphs of text and possibly some mathematical equations or diagrams.]*

## Chapter 9

# Conclusions

In this chapter we will interpret the results obtained so far. From the previous chapters we conclude that for all Coulomb repulsions  $U \geq 0$ , the topological correlator  $O_{top}(x)$  in the Hubbard model measures the internal spin-spin correlations with  $O_{top}(x) \sim 1/x^{K_s}$ . From this one can be shown that the one dimensional Hubbard model spin charge separation is controlled by the sublattice parity. In this chapter we will describe the ordering of this  $Z_2$  topological order parameter in terms of the elementary collective excitations of a Luttinger model, the spinon and holon. We noticed already that the correlator  $O_{top}(x)$  can be seen as removing the effect of the holons. In this chapter we introduce the correlator  $O_{top(holon)}(x)$  which removes the effect of the spinons.

### 9.1 Removing the effect of the holons

The concept of spin charge separation in terms of spinons and holons was introduced in chapter 1 and depicted in figure 1.1. The holon describes a pure charge excitation and is characterized by a hole surrounded by antiferromagnetically aligned spins. The spinon is a pure spin excitation with two adjacent up or down spins, which has an excess spin  $\pm 1/2$  with respect to the initial antiferromagnet. The spinon and holon can move separately.

In chapter 4 we showed that both the spinon and the holon cause a kink in the staggered spin  $M^z(x)$ , as is depicted in figure 4.4, can be characterized by a  $Z_2$  topological order parameter, the sublattice parity. Using the technique of Parola and Sorella [22], we calculated the contributions of these kinks caused by the spinons and holons to the staggered spin-spin correlation function, which yields in the  $U \rightarrow \infty$  limit

$$\begin{aligned} \langle M^z(x)M^z(0) \rangle &= \langle n_{Tot}(x)(-1)^{\sum_{j=1}^{x-1}(1-n_{Tot}(j))}n_{Tot}(0) \rangle \langle S^z(\rho_{Tot}x)S^z(0) \rangle_{par.Heis}. \\ &\sim \frac{\cos[(2k_F - \pi)x]}{\sqrt{x}} \frac{1}{x} = \frac{\cos[(2k_F - \pi)x]}{x^{K_c + K_s}}. \end{aligned} \quad (9.1)$$

So in the limit  $U \rightarrow \infty$ , the kinks attached to the holon and spinon give rise to an al-

gebraic decay with a factor  $1/x^{K_c} = 1/\sqrt{x}$  and  $1/x^{K_s} = 1/x$  respectively. The spinons cause kinks in the internal spin system, as is seen by the spins, and destroy the internal spin structure. The kinks connected to the holons have an obscuring effect to these internal spin correlations and cause the spin spin correlator to decay with the extra factor  $1/\sqrt{x}$ , so that  $\langle S^z(x)S^z(0) \rangle \sim \cos(2k_F x)/(x\sqrt{x}) = \cos(2k_F x)/x^{K_s+K_c}$ . Note that the extra decaying term  $1/\sqrt{x}$  is connected to the fact that the spin correlations in the Heisenberg chain are antiferromagnetic. For if the spins were effectively parallel, the spin correlator would yield

$$\begin{aligned} \langle M^z(x)M^z(0) \rangle_{aligned} &= (-1)^x \langle n_{tot}(x)n_{tot}(0) \rangle \langle S^z(\rho_{tot}x)S^z(0) \rangle_{par. Heis.} \\ &\sim (-1)^x \rho_{tot}^2 \frac{1}{\rho_{tot}x} = (-1)^x \frac{\rho_{tot}}{x^{K_s}}, \end{aligned} \quad (9.2)$$

and we would directly see the internal spin structure by measuring  $\langle M^z(x)M^z(0) \rangle$ .

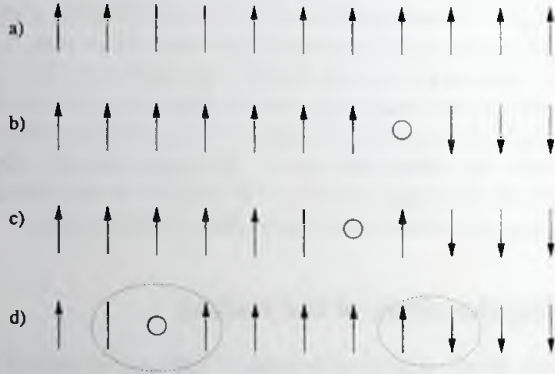


Figure 9.1: The operator  $S^z(x)(-1)^{\pi \sum_{j=-\infty}^{x-1} n_{tot}(j)}$  for the different configurations in figure 1.1. This operator is equal to the staggered magnetization  $M^z(x)$  depicted in the figure 4.4, only now holons do not produce kinks in this function.

We can repair the damage of kinks connected to the holons by considering the string operator  $(M')^z(x)$  defined by

$$(M')^z(x) = M^z(x)(-1)^{\sum_{j=-\infty}^{x-1} (1-n_{tot}(j))} = S^z(x)(-1)^{\sum_{j=-\infty}^{x-1} n_{tot}(j)}, \quad (9.3)$$

instead of the staggered magnetization  $M^z(x)$ . This operator removes the kink caused by the holon. We depicted this operator in figure 9.1, using the configurations selected in figure 1.1. The typical anti-ferromagnetic configuration in figure 1.1a, has turned into a ferromagnetic chain. Introducing a hole will now cause a kink in this ferromagnetic like

chain which is connected to the spinon as the holon moves to the left (Figure 9.1d). This function is very similar to the staggered magnetization  $M^z(x)$ , only it is not sensitive to the holons. So the holons do not produce kinks like they did in  $M^z(x)$ . If we now consider the spin spin correlator  $\langle (M')^z(x)(M')^z(0) \rangle$ , we obtain for  $U \rightarrow \infty$  the topological correlator  $O_{top}(x)$

$$\begin{aligned}
 O_{top}(x) &= \langle (M')^z(x) (M')^z(0) \rangle \\
 &= \langle (M')^z(x) (-1)^{\sum_{j=0}^{x-1} (1-n_{tot}(j))} (M')^z(0) \rangle \\
 &= -\langle S^z(x) (-1)^{\sum_{j=1}^{x-1} n_{tot}(j)} S^z(0) \rangle \\
 &\approx \langle n_{tot}(x) n_{tot}(0) \rangle \langle S^z(\rho_{tot}x) S^z(0) \rangle_{par.Heis.} \\
 &\sim (\rho_{tot})^2 \frac{1}{\rho_{tot}x} = \frac{\rho_{tot}}{x} = \frac{\rho_{tot}}{x K_s}, \tag{9.4}
 \end{aligned}$$

as was shown in equation (5.4) in chapter 5. And thus we obtain the rescaled internal Heisenberg spin spin correlations. This can also be explained by saying that the operator  $(-1)^{\sum_{j=1}^{x-1} n_{tot}(j)}$  in  $O_{top}(x) = -\langle S^z(x) (-1)^{\sum_{j=1}^{x-1} n_{tot}(j)} S^z(0) \rangle$  removes the antiferromagnetic staggering in the internal spin space turning it to ferromagnetic like interactions and yielding a similar expression as in equation (9.2).

The topological correlator  $O_{top}(x)$  for  $U \geq 0$  has also been considered. The analytic expression for  $U = 0$  together with DMRG calculations show that

$$O_{top}(x) = \langle (M')^z(x) (M')^z(0) \rangle \sim \frac{G_s}{x K_s}, \tag{9.5}$$

with  $G_s(\rho_{tot}, U)$  depicted in figure 8.11. These results can also be interpreted in terms of holons and spinons using a formula similar to the one used by Parola and Sorella described in section 4.3.3. Namely, away from the  $U \rightarrow \infty$  limit we can use a similar analysis as in (4.83) for the staggered spin correlator

$$\begin{aligned}
 \langle M^z(x) M^z(0) \rangle &= \sum_{j=2}^{x+1} \langle n_s(x) \delta \left( \sum_{l=0}^x n_s(l) - j \right) n_s(0) \rangle \langle S^z(j-1) S^z(0) \rangle_{internal} \\
 &= \sum_{j=2}^{x+1} \langle n_s(x) \delta \left( \sum_{l=0}^x n_s(l) - j \right) n_s(0) \rangle (-1)^{j-1} \langle S^z(j-1) S^z(0) \rangle_{par.} \\
 &\approx \langle n_s(x) (-1)^{\sum_{j=1}^{x-1} (1-n_s(j))} n_s(0) \rangle \langle S^z(\rho_s x) S^z(0) \rangle_{par.}, \tag{9.6}
 \end{aligned}$$

where the internal spin interactions are described by  $\langle S^z(j) S^z(0) \rangle_{internal} = (-1)^j \langle S^z(j) S^z(0) \rangle_{par.}$ . The DMRG calculations described in the previous chapter show that

$$\langle n_s(x) (-1)^{\sum_{j=1}^{x-1} (1-n_s(j))} n_s(0) \rangle = \frac{F_c \cos[(2k_F - \pi)x]}{x K_c}. \tag{9.7}$$

So also away from the  $U \rightarrow \infty$  limit the contributions to the staggered spin can be subdivided into a part coming from the holons giving rise to a decaying term  $1/x^{K_c}$  and

a part coming from the spinons which yields a term  $\langle S^z(\rho_s x) S^z(0) \rangle_{par.} \sim 1/x^{K_s}$ . This indicates that in calculating  $\langle M^z(x) M^z(0) \rangle$  for  $U \geq 0$ , the wave function can be thought of to first order as constructed in a similar way as in the limit  $U \rightarrow \infty$  used by Parola and Sorella. The difference is that now we only consider the single occupied sites. So for general  $U$  we first place the single occupied electrons with unspecified spins over the lattice such that  $\langle n_s(x) n_s(0) \rangle \sim \rho_s^2$  and  $\langle n_s(x) (-1)^{\sum_{j=1}^{x-1} n_s(j)} n_s(0) \rangle = F_c \cos(2k_F x)/x^{K_s}$  and subsequently we distribute the spins over these electrons like the spins on a chain with a spin correlator  $\langle S^z(x) S^z(0) \rangle_{internal} \sim (-1)^x/x$ . Note that in this construction the doubly occupied sites are equivalent to empty sites. This is natural since for doubly occupied sites  $S^z(x) = 0$  hence like empty sites, they do not contribute to the staggered spin correlator  $\langle M^z(x) M^z(0) \rangle$ .

Using this interpretation, we can eliminate of the decay caused by the kinks connected to the holons by considering the topological correlator  $O_{top}(x)$  which equals

$$\begin{aligned} \langle M^z(x) (-1)^{\sum_{j=1}^{x-1} (1-n_{tot}(j))} M^z(0) \rangle &= \langle n_s(x) n_s(0) \rangle \langle S^z(\rho_s x) S^z(0) \rangle_{par.} \\ &= \rho_s^2 \frac{H_s(\rho_{tot}, U)}{(\rho_s x)^{K_s}} = \rho_s \frac{H_s(\rho_{tot}, U)}{x}, \end{aligned} \quad (9.8)$$

where we have defined  $\langle S^z(x) S^z(0) \rangle_{par.} = H_s(\rho_{tot}, U)/x^{K_s}$ .

So in order to be consistent with the DMRG result (9.5), we find  $H_s(\rho_{tot}, U) = G_s(\rho_{tot}, U)/\rho_s$ . These values are depicted in figure 9.2. In the limit  $U \rightarrow \infty$  the internal spin is ordered like a Heisenberg chain with  $\langle S^z(x) S^z(0) \rangle_{par.} = \langle S^z(x) S^z(0) \rangle_{par. Heis.} \sim 1/x$  and the prefactor  $H_s(\rho_{tot}, U)$  is independent of  $\rho_{tot}$ . The data in figure 9.2 show that for values of  $U$  away of the limit  $U \rightarrow \infty$  the prefactor  $H_s(\rho_{tot}, U)$  start to depend on the density  $\rho_{tot}$  and the internal spin system is a rescaled Heisenberg chain.

## 9.2 Removing the effects of the spinons

In the previous section we found that by considering the topological correlator we remove the effect of the holon in the spin correlator. So in calculating  $O_{top}(x)$ , we are left with the spinons which contribute to the spin correlations in the internal spin space.

One can wonder whether we can construct an operator which does the opposite and only filters out the effect of the spinons, leaving the holons intact. To obtain such an operator we have to multiply the staggered magnetization  $M^z(x)$  with the string operator  $M^z(x) (-1)^{\sum_{j=-\infty}^{x-1} (1-n_{tot}(j))}$  instead of the operator  $(-1)^{\sum_{j=-\infty}^{x-1} (1-n_{tot}(j))}$  which we did previously in (9.3). This yields the operator

$$(M'')^z(x) = (M^z(x))^2 (-1)^{\sum_{j=-\infty}^{x-1} (1-n_{tot}(j))}. \quad (9.9)$$

This is accomplished by multiplying the square of the staggered magnetization  $(M^z(x))^2$  with the string operator  $(-1)^{\sum_{j=-\infty}^{x-1} (1-n_{tot}(j))}$ . This correlator is not sensitive to fluctuations caused by the spinons in the internal spin system. The way the configurations in figure 1.1 are viewed by this operator are shown in figure 9.3, showing that there is only

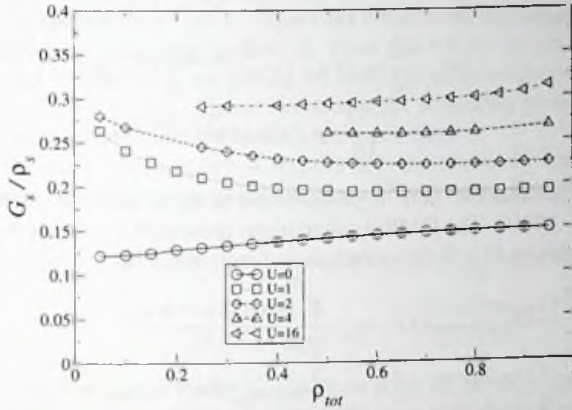


Figure 9.2: The quotient  $H_s(\rho_{tot}, U) = G_s(\rho_{tot}, U)/\rho_s$  as function of the total density  $\rho_{tot}$  for different values of the Coulomb repulsion  $U$ .

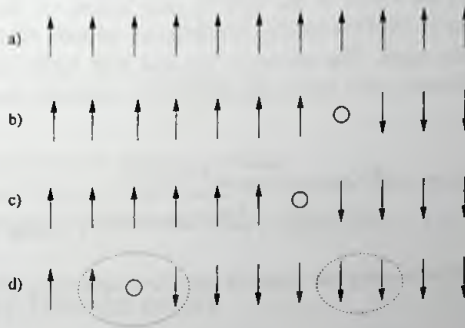


Figure 9.3: The operator  $(M^2(x))^2(-1)^{\pi \sum_{j=-\infty}^{x-1} (1-n_{tot}(j))}$  for the different configurations in figure 1.1. This operator is equal to the staggered magnetization  $M^2(x)$  in the figure 4.4 only spinons do not produce kinks in this function.

one kink which is connected to the holon as it moves to the left. Note that a spinon has no effect on this kink operator. To calculate this effect of removing of the spinons on the correlation function, we have to consider the correlator

$$\begin{aligned}
 O_{top(holon)}(x) &= \langle (M^z(x))^2 (-1)^{\sum_{j=1}^{x-1} (1-n_{tot}(j))} (M^z(0))^2 \rangle \\
 &= \frac{1}{16} \langle n_s(x) (-1)^{\sum_{j=1}^{x-1} (1-n_{tot}(j))} n_s(0) \rangle \\
 &= -\frac{(-1)^x}{16} \langle n_s(x) (-1)^{\sum_{j=1}^{x-1} n_s(j)} n_s(0) \rangle.
 \end{aligned} \tag{9.10}$$

Here, we used the fact that  $(M^z(x))^2$  is proportional to  $n_s(x)$  with  $(M^z(x))^2 = n_s(x)/4$  and  $(-1)^{n_{tot}(j)} = (-1)^{n_s(j)}$ . The DMRG calculations presented in chapter 8 showed that for Coulomb interactions  $U \geq 0$  this correlations function equals

$$O_{top(holon)}(x) = \frac{F_c \cos[(2k_F - \pi)x]}{16 x^{K_c}}. \tag{9.11}$$

The wave vector  $2k_F - \pi$  can be seen as  $\pi/l_{holons}$  where  $l_{holons} = 1/(1 - \rho_{tot})$  is the distance between the holes if they would crystallize in a lattice. Comparing this with the unperturbed spin-spin correlation function  $\langle M^z(x)M^z(0) \rangle \sim \cos[(2k_F - \pi)x]/x^{K_s + K_c}$ , we find that the correlation function decays more slowly than  $\langle M^z(x)M^z(0) \rangle$ . This is the result of removing the fluctuations induced by the spinons and we are left with the decay caused by the holons.

### 9.3 Removing the effects of spinons and holons

After having removed the effect of the spinons and holons on the spin separately, a natural question to ask is whether we can remove the spinons after we have squeezed out the holons and vice versa. The answer is yes and both operations are described by the same operator. Namely, first squeezing the holons and then removing the spinons would yield

$$\begin{aligned}
 M^z(x) &\rightarrow M^z(x) (-1)^{\sum_{j=-\infty}^{x-1} (1-n_{tot}(j))} \\
 &\rightarrow (M^z(x))^2 ((-1)^{\sum_{j=-\infty}^{x-1} (1-n_{tot}(j))})^2 = (M^z(x))^2.
 \end{aligned} \tag{9.12}$$

On the other site, first removing the spinons and then squeezing out the holons would give

$$\begin{aligned}
 M^z(x) &\rightarrow (M^z(x))^2 (-1)^{\sum_{j=-\infty}^{x-1} (1-n_{tot}(j))} \\
 &\rightarrow (M^z(x))^2 ((-1)^{\sum_{j=-\infty}^{x-1} (1-n_{tot}(j))})^2 = (M^z(x))^2.
 \end{aligned} \tag{9.13}$$

So we obtain the function  $(M^z(x))^2$  if we squeeze out the holons and remove the effect of the spinons. This function is 1/4 for singly occupied states and 0 for empty or doubly occupied sites. Therefore  $\langle (M^z(x))^2 (M^z(0))^2 \rangle$  is proportional to the distribution of

singly occupied sites, in a background of empty and doubly occupied sites and can be written as  $\langle n_s(x)n_s(0) \rangle / 16$ . How do we interpret this?

After we squeezed out both the spinons and the holons, the spin texture has totally disappeared and we are left with the fluctuations of the lattice sites on which the spins are defined. So the function  $\langle (M^z(x))^2 (M^z(0))^2 \rangle$  measures the correlations of the lattice sites on which the internal spin is defined. Note that we do not get any information of the doubly sites: In removing the holons we have lost all information about the position on the doubly occupied sites. This is because in the squeezing process we did not only squeeze out the holes, but also the doubly occupied sites.

For the  $U \rightarrow \infty$  limit,  $n_s(x) \rightarrow n_{SF}(x)$  and the correlator can be written as the density density operator for spinless fermions with  $\rho_{SF} = \rho_s = \rho_{tot}$  and equals

$$\begin{aligned} \langle (M^z(x))^2 (M^z(0))^2 \rangle &= \frac{i}{16} \langle n_s(x)n_s(0) \rangle = \frac{i}{16} \langle n_{SF}(x)n_{SF}(0) \rangle \\ &= \frac{1}{16} \left[ \rho_{tot}^2 - \frac{1 - \cos(2\pi \rho_{tot}x)}{4\pi^2 x^4} \right] \\ &= \frac{1}{16} \left[ \rho_{tot}^2 - \frac{1 - \cos(4k_F x)}{4\pi^2 x^2} \right]. \end{aligned} \quad (9.14)$$

This is precisely what one would expect according to the Woynarovich-Ogata-Shiba solution (5.1). For  $U \rightarrow \infty$  all spins are on singly occupied sites which are distributed like spinless fermions with  $\rho_{SF} = \rho_{tot}$ .

For  $U = 0$  this function the up and down electrons behave like independent spinless fermions and the function equals

$$\begin{aligned} \langle n_s(x)n_s(0) \rangle &= 2\rho_{SF}^2 + (2 - 8\rho_{SF})\langle n_{SF}(x)n_{SF}(0) \rangle + 4\langle n_{SF}(x)n_{SF}(0) \rangle^2 \\ &= \rho_{tot}^2 \left( 1 - \frac{\rho_{tot}}{4} \right)^2 + (-\rho_{SF}^2 + 2\rho_{SF} - 1) \left( \frac{1 - \cos(2k_F x)}{\pi^2 x^2} \right) \\ &\quad + \frac{(1 - \cos(2k_F x))^2}{\pi^4 x^4}. \end{aligned} \quad (9.15)$$

as is shown in (8.15). Here we used  $\rho_{tot} = 2\rho_{SF}$ .

For intermediate  $U$  we only calculated the constant term  $\rho_s = \langle n_s(x) \rangle$  of the correlation function  $\langle n_s(x)n_s(0) \rangle$ . This is depicted in figure 8.7.

## 9.4 Summary Hidden order

Let us summarize what we have found. Our quest started with the Woynarovich-Ogata-Shiba solution (5.1) describing the structure of the wave function in the limit  $U \rightarrow \infty$ . In that limit the wave function is built from first placing the electrons with unspecified spin over the lattice like spinless fermions and subsequently distributing the spins over these electrons like the spins on an undoped Heisenberg chain. This construction gives rise to the sublattice parity topological order which indicates that spins are anti-parallel over holes. Because of this hidden order we can use the topological correlator  $O_{top}(x) =$

$-\langle S^z(x)(-1)^{\sum_{j=1}^{x-1} n_{tot}(j)} S^z(0) \rangle$  to measure the spin correlations in the internal spin space. Our calculations show that  $O_{top} \sim 1/x^{K_s}$ , also away from the  $U \rightarrow \infty$  limit. Together with the results discussed in the previous section this suggest that we can extend the Woyнарovich-Ogata-Shiba solution for all positive  $U$  in the following manner.

When calculating the spin-spin correlation function  $\langle S^z(x)S^z(0) \rangle$ , one can effectively think of the wave function being constructed in the following two steps: First distribute the electrons of singly occupied sites over the lattice with density  $\rho_{SF} = \rho_s$  such that to first order  $\langle n_s(x)n_s(0) \rangle \sim \rho_s^2$  and  $\langle n_s(x)(-1)^{\sum_{j=1}^{x-1} n_s(j)} n_s(0) \rangle = F_c \cos(2k_F x)/x^{K_c}$ . Subsequently, distribute the spins of these singly occupied sites over these lattice sites like spins on a spin chain with correlations given by  $\langle S^z(x)S^z(0) \rangle_{internal} = (-1)^x H_s/x^{K_s}$ . Note that  $H_s$  is  $U$  and  $\rho_{tot}$  dependent. In this construction the position of doubly occupied sites is not specified. But since  $S^z(y) = 0$  for a doubly occupied site, they are treated as empty sites and we can neglect them in the calculation of the spin spin correlation function.

Note that it is only correct to think of the wave function being constructed in this way in the calculation of  $\langle S^z(x)S^z(0) \rangle$ . For instance in calculating the density density correlations function  $\langle n_{tot}(x)n_{tot}(0) \rangle$ , the doubly occupied sites do contribute and we have to know how to distribute the doubly occupied sites in between the singly occupied sites.

Due to this construction one can think of the holes as providing an antiferromagnetic interaction exchange between its neighboring spins. And similar to the case  $U \rightarrow \infty$ , this gives rise to quasi sublattice parity order as is demonstrated in (9.8). In the one dimensional Hubbard model this order is only quasi long ranged and not true long ranged with  $O_{top}(x) = C \neq 0$  as for the Haldane spin-1 chain. This is because spins in the internal spin space of the spin-1 chain have discrete Ising symmetry and not a continuous symmetry as they do in the Hubbard model. Due to the Mermin Wagner theory [12], the latter can only have quasi long range order.

We end the thesis with a comparison of the sublattice parity order with a local  $Z_2$  symmetry.

## 9.5 Local Gauge Symmetry

Finally, we want to discuss the possibility that the sublattice parity order described in this thesis turns into a local  $Z_2$  symmetry. To do so, let us define the  $Z_2$  variable  $\sigma(j) = (-1)^{1-n_{tot}(j)}$ . As charge and spin are decoupled, we may shift the charge degrees of freedom to the lattice formed by the midpoints of the bonds between the sites of the original lattice (the bond-, or dual lattice, with coordinates  $(j, j+1)$ ) while concurrently retaining the spin degrees of freedom on the original lattice. That is, we can define

$$\sigma(j, j+1) \equiv \sigma(j). \quad (9.16)$$

Using this notation, the topological correlator  $O_{top}(x)$  can be written as

$$\begin{aligned} O_{top}(x) &= \langle M^z(0) (-1)^{\sum_{j=1}^{x-1} (1-n_{tot}(j))} M^z(x) \rangle \\ &= \langle M^z(0) \left[ \prod_{(ij) \in \Gamma} \sigma(i, j) \right] M^z(x) \rangle. \end{aligned} \quad (9.17)$$

where  $\Gamma$  is the path connecting the point 0 and  $x$ . This is nothing else than the gauge invariant correlation function of a theory containing a  $SU(2)$  'matter' field  $\vec{M}$  coupled to an Ising gauge field. The product  $\prod_{\Gamma} \sigma$  can be identified with a Wilson-line [75] of the  $Z_2$  gauge theory which has to be inserted to keep the matter-field correlator gauge invariant. By the same token, the 'normal' spin correlator  $\langle M^z(x) M^z(0) \rangle$  is not gauge invariant, because the Wilson line is missing, and our observation that  $\langle M^z(x) M^z(0) \rangle$  is more rapidly decaying than  $O_{top}(x)$  which could signal the presence of local  $Z_2$  symmetry.

Let us explain this in some more detail. Imagine that an effective, long wavelength theory is realized with a Hamiltonian invariant under the following  $Z_2$  gauge transformation,

$$\begin{aligned} \sigma(x, x+1) &\rightarrow \eta(x) \sigma(x, x+1) \eta(x+1) \\ \vec{M}(x) &\rightarrow \eta(x) \vec{M}(x), \end{aligned} \quad (9.18)$$

with arbitrary  $\eta(y) = \pm 1$ . Here  $\sigma(x, x+1)$  is the value of the  $Z_2$  variable on bond  $(x, x+1)$ . Given this symmetry, some very general statements follow regarding the behavior of correlation functions. First consider the spin correlator  $\langle M^z(0) M^z(x) \rangle$ . Since  $\langle M^z(x) M^z(0) \rangle \rightarrow -\langle M^z(x) M^z(0) \rangle$  under the transformation equation (9.18) at either 0 or  $x$ , the correlator has to vanish: it is not gauge invariant. Since the gauge symmetry is emergent an energy scale should exist below which it becomes active. An energy scale implies a length scale  $l_{gauge}$  and therefore  $\langle M^z(x) M^z(0) \rangle \sim \exp(-x/l_{gauge})$ . So an unavoidable consequence of a full realization of the  $Z_2$  gauge symmetry is that correlation function violating the gauge invariance should decay exponentially faster than the gauge invariant ones. This induces a complication. In our case  $\langle M^z(x) M^z(0) \rangle$  decays only algebraically faster than the supposedly gauge invariant correlator  $O_{top}(x)$ . And thus the system is not exactly Ising gauge symmetric.

This exact gauge symmetry does occur in the Haldane spin-1 chain described by den Nijs and Rommelse [18]. As mentioned before, in this system  $\langle M^z(x) M^z(0) \rangle$  does decay exponentially faster than the operator  $O_{top}(x)$ . Batista and Ortiz [76] showed that the Haldane spin-1 chain can be mapped onto a  $t - J^z$  model with an additional  $U(1)$  charge breaking superconductor term. So although the local symmetry does not occur in the Hubbard chain, this proves that it can exist in one dimensional fermion systems like it does in two dimensional high  $T_c$  superconductors. But instead of having just one confining phase in one dimension, in two dimensions the phase diagram is richer, and there is also room for a deconfining and Higgs phase.



# Bibliography

- [1] J. M. Luttinger, *J. Math. Phys.* **4**, 1154 (1963).
- [2] J. Voit *Rep. Prog. Phys.* **58**, 977 (1995); H. J. Schulz, G. Cuniberti and P. Pieri in *Field Theories for Low-Dimensional Condensed Matter Systems*, G. Morandi *et al.*, Eds. Springer (2000), cond-mat/9807366.
- [3] L. D. Landau, *Sov. Phys. JETP* **3**, 920 (1956); L. D. Landau, *Sov. Phys. JETP* **5**, 101 (1957); L. D. Landau, *Sov. Phys. JETP* **8**, 70 (1958).
- [4] J. Hubbard, *Proc. Roy. Soc.* **A276**, 238 (1963).
- [5] P. M. Chaikin, T. C. Lubensky, *Principles of Condensed Matter Physics*, Cambridge Univ. Press (1995).
- [6] E. Ising, *Z. Physik* **31**, 253 (1925).
- [7] *Exactly Solved Models in Statistical Mechanics.*, R. J. Baxter, Academic Press (1982).
- [8] For instance see T. D. Schultz, D. C. Mattis, and E. H. Lieb, *Rev. Mod. Phys.* **36**, 856 (1964).
- [9] H. Kamerlingh Onnes, *Leiden Commun.* **120b**, **122b**, **124c** (1911).
- [10] J. Bardeen, L. N. Cooper and J. R. Schrieffer, *Phys. Rev.* **108**, 1175 (1956).
- [11] L. N. Cooper, *Phys. Rev.* **104**, 1189 (1965).
- [12] N. D. Mermin and H. Wagner, *Phys. Rev. Lett.* **17**, 1133(1966); P. C. Hohenberg, *Phys. Rev.* **158**, 383 (1967).
- [13] J. Zaanen and Z. Nussinov, proceedings of the LT23 conference 2002, Hiroshima, Japan.(cond-mat/0209437 and cond-mat/0209441); to be published in *Phys. C*.
- [14] S. Sachdev and T. Morimari, cond-mat/0207167; Y. Zhang, E. Demler and S. Sachdev, *Phys. Rev. B.* **66**, 094501 (2002).
- [15] J. G. Bednorz and K. A. Müller, *Z. Phys. B*, **64**, 189 (1986)

- [16] P. E. Lammert, D. S. Rokhsar and J. Tomer, Phys. Rev. Lett. **70**, 1650 (1993).
- [17] T. Senthil and M. P. A. Fischer, Phys. Rev. B **62**, 7850 (2000); Phys. Rev. B **63**, 134521 (2001).
- [18] M. den Nijs and K. Rommelse, Phys. Rev. B, **40**, 4709 (1989).
- [19] F. Woynarovich, J. Phys. C **15**, 85 (1982); *ibid.* **15**, 96 (1982).
- [20] M. Ogata and H. Shiba, Phys. Rev. B **41**, 2326 (1990).
- [21] E. H. Lieb and F. Y. Wu, Phys. Rev. Lett. **20**, 1445 (1968).
- [22] A. Parola and S. Sorella, Phys. Rev. Lett. **64**, 1831 (1990).
- [23] H. V. Kruis, I. Martin, A. V. Balatsky, Phys. Rev. B **64**, 054501, (2001).
- [24] A. V. Balatsky, M. I. Salkola and A. Rosengren, Phys. Rev. B **51**, 15547 (1995); M. I. Salkola, A. V. Balatsky and J. R. Schrieffer, Phys. Rev. B **55**, 12648 (1997); I. Martin and A. V. Balatsky, cond-mat/0003142.
- [25] J. Byers, M. E. Flatté and D. Scalapino, Phys. Rev. Lett. **71**, 3363 (1993); M. E. Flatté, Phys. Rev. B. **61**, R14920 (2000).
- [26] W. A. Atkinson, P. J. Hirschfeld, A. H. MacDonald and K. Ziegler, cond-mat/0005487.
- [27] H. Tsuchiura, Y. Tanaka, M. Ogata and S. Kashiwaya, Phys. Rev. Lett. **84**, 3165 (2000).
- [28] A. Polkovnikov, S. Sachdev and M. Vojta, cond-mat/0007431.
- [29] S. H. Pan, E. W. Hudson, K. M. Lang, H. Eisaki, S. Uchida and J. C. Davis, Nature **403**, 746 (2000).
- [30] E. W. Hudson, S. H. Pan, A. K. Gupta, K. -W. Ng and J. C. Davis, Science **285**, 88 (1999).
- [31] Ali Yazdani, C. M. Howald, C. P. Lutz, A. Kapitulnik and D. M. Eigler, Phys. Rev. Lett. **83**, 176 (1999).
- [32] Ch. Renner, B. Revaz, J. -Y. Genoud, K. Kadowaki and Ø. Fischer, Phys. Rev. Lett. **80**, 149 (1998); I. Maggio-Aprile, Ch. Renner, A. Erb, E. Walker, and Ø. Fischer, Phys. Rev. Lett. **75**, 2754 (1995); and references therein.
- [33] A. G. Loeser, Z. -X. Shen, D. S. Dessau, D. S. Marshall, C. H. Park, P. Fournier and A. Kapitulnik, Science **273**, 325 (1996); Z. -X. Shen and Dessau, Phys. Rep. **253**, 1 (1995); M. R. Norman, H. Ding, M. Randeria, J. C. Campuzano, T. Yokoya, T. Takeuchi, T. Takahashi, T. Mochiku, K. Kadowaki, P. Guptasarma and D. G. Hinks, Nature **392**, 157 (1998).

- [34] J. W. Loram, J. L. Luo, J. R. Cooper, W. Y. Liang and J. L. Tallon *J. Phys. Chem. Solids* **62** (1-2), 59-64 (2001).
- [35] V. M. Krasnov, A. Yurgens, D. Winkler, P. Delsing and T. Claeson, *Phys. Rev. Lett.* **84**, 5860 (2000).
- [36] V. J. Emery and S. A. Kivelson, *Nature* **374**, 434 (1995).
- [37] S. Chakravarty, R. B. Laughlin, D. K. Morr and C. Nayak, cond-mat/0005443 (unpublished).
- [38] D. Pines, (to be published in *Physica C* as part of the proceedings of M2S-HTSC-VI, Houston, Feb.2000); see also cond-mat/0002281.
- [39] I. Martin, Gerardo Ortiz, A. V. Balatsky and A. R. Bishop, cond-mat/0003316 (unpublished).
- [40] A. Yazdani, B. A. Jones, C. P. Lutz, M. F. Crommie and D. M. Eigler, *Science* **275**, 1767 (1997).
- [41] I. Martin, A. V. Balatsky and J. Zaanen, unpublished.
- [42] See for instance Mahan, Gerald D., in *Many-Particle Physics*, (Plenum Press, New York, 1981), page 469.
- [43] B. Janko, I. Kosztin, K. Levin, M. R. Norman, D. J. Scalapino, *Phys. Rev. Lett.* **82**, 4304 (1999).
- [44] I. Martin and A. V. Balatsky, *Phys. Rev. B* **62** (2000); see also cond-mat/0002043.
- [45] A. Luther and I. Peschel, *Phys. Rev. B*, **9**, 2911 (1974); D. C. Mattis, *J. Math. Phys.* **15**, 609 (1974).
- [46] For an overview of the bosonization method see for example M. Stone, *Bosonization*, World Scientific (1994); S. Rao and D. Sen, cond-mat/0005492; J. von Delft and H. Schoeller, cond-mat/9805275; R. Shankar, *Acta Phys. Pol* **B26**, 1835 (1995).
- [47] D. Senechal, *An introduction to bosonization*, cond-mat/9908262.
- [48] S. Tomonaga, *Prog. Theor. Phys.* **5**, 544 (1950); J. M. Luttinger, *J. Math. Phys.* **4**, 1154 (1963); D. C. Mattis and E. H. Lieb, *J. Math. Phys.* **4**, 1154 (1963).
- [49] J. Kosterlitz and D. Thouless, *J. Phys. C*, **6**, 1181, (1973).
- [50] A. Luther and V. J. Emery, *Phys. Rev. Lett.* **33**, 589 (1974).
- [51] For reviews on the Bethe Ansatz method see V. E. Korepin and F. H. L. Essler, *Exactly solvable Models of strongly correlated electrons*, World Scientific, (1994); Yu. A. Izyumov and Yu. N. Skryabin, *Statistical Mechanics of Magnetically Ordered Systems*, New York, (1988).

- [52] Z. N. C. Ha, *Quantum Many-Body Systems in One Dimension*, World Scientific, (1996).
- [53] H. Bethe, *Z. Phys.* **71**, No. 3-4, 205-226 (1931).
- [54] We used mainly the notation presented in N. Andrei, *Integrable Models in Condensed Matter Physics*, cond-mat/9708087; J. González et al. *Quantum Electron Liquids and High  $T_c$  Superconductivity*, Springer, Heidelberg (1995).
- [55] J. Zinn-Justin and E. Brezin, *C. R. Acad. Sci.* **263** 670 (1966).
- [56] C. N. Yang, *Phys. Rev. Lett.* **19**, 1312, (1967).
- [57] R. R. P. Singh, M. E. Fisher and R. Shankar, *Phys. Rev. B.* **39**, 2562 (1989).
- [58] H. J. Schulz, *Phys. Rev. Lett.* **64**, 2831 (1990).
- [59] H. J. Schulz cond-mat/9412036.
- [60] J. Zaanen, cond-mat/0103255, (2001)
- [61] J. Zaanen, *Phys. Rev. Lett.* **84**, 753 (2000).
- [62] S. R. White, *Phys. Rev. Lett.* **69**, 2863 (1992); S. R. White and R. M. Noack, *Phys. Rev. Lett.* **68**, 3487 (1992)
- [63] K. G. Wilson, *Rev. Mod. Phys.* **47**, 773 (1975)
- [64] C. Lanczos: An iteration method for the solution of the eigenvalue problem of linear differential and integral operators, *J. Res. Nat. Bur. Stand.* **45** 255, (1950); J. K. Cullum and R. A. Willoughby: Lanczos algorithm for large symmetric eigenvalue computations, Birkhauser, Boston (1985)
- [65] I. P. McCulloch and M. Gulácsi, *Europhys. Lett.* **57**, 852 (2002)
- [66] L. C. Biedenharn and J. D. Louck, "Angular Momentum in Quantum Physics", Addison-Wesley, Massachusetts, 1981.
- [67] C. N. Yang and S. C. Zhang, *Mod. Phys. Lett. B* **4**, 759 (1990)
- [68] V. E. Korepin and F. H. L. Essler, *The Hubbard Model*, NATO ASI series, Series V, vol. 343, edited by D. Baeriswyl, D. K. Campbell, J. M. P. Carmelo, F. Guinea and E. Louis, Plenum Press, New York, 1995.
- [69] S. R. White and D. A. Huse, *Phys. Rev. B* **48**, 3844 (1993)
- [70] M. -C. Chung and I. Peschel, *Phys. Rev. B* **62**, 4191 (2000)
- [71] S. R. White, I. Affleck and D. J. Scalapino, cond-mat/0111320
- [72] M. Buchanan, *Nature* **409**, 8-11 (2001).

- [73] S. L. Sondhi, S. M. Girvin, J. P. Carini and D. Shahar, *Rev. of Mod. Phys.* Vol. 69, No. 1 315-333 (1997).
- [74] T. Valla, A. V. Fedorov, P. D. Johnson, B. O. Wells, S. L. Hulbert, Q. Li, G. D. Gu, N. Koshizuka, *Science* **285**, 2110-2113 (1999).
- [75] J. B. Kogut, *Rev. Mod. Phys.* **51**, 659 (1979).
- [76] C. D. Batista and G. Ortiz, *Phys. Rev. Lett.* **86**, 1082 (2001).

*BIBLIOGRAPHY*

[The following text is extremely faint and illegible, appearing to be a list of references or a bibliography.]

## List of publications

- *Impurity-induced resonant state in a pseudogap state of a high- $T_c$  superconductor*, H. V. Kruis, I. Martin, and A. V. Balatsky, Phys. Rev. B **64**, 054501 (2001).
- *The geometric order of stripes and Luttinger liquids*, J. Zaanen, O. Y. Osman, H. V. Kruis, Z. Nussinov and J. Tworzydło, Phil. Mag. B **81**, 1485 (2001)
- *Geometry and topological order in Luttinger liquid state*, H. V. Kruis, I. P. McCulloch, Z. Nussinov and J. Zaanen, submitted to Europhysics Letters.

### Publications of the Author

1. *Journal of the Royal Society of Medicine*, 1954, 47, 100-102.
2. *Journal of the Royal Society of Medicine*, 1955, 48, 100-102.
3. *Journal of the Royal Society of Medicine*, 1956, 49, 100-102.
4. *Journal of the Royal Society of Medicine*, 1957, 50, 100-102.

## Samenvatting

De natuurkunde van de vaste stof beschrijft het gedrag van immense hoeveelheden deeltjes. Zo huisvest een gram metaal al de onvoorstelbare hoeveelheid van  $10^{23} = 100.000.000.000.000.000.000.000$  electronen die allemaal met elkaar wisselwerken, bijvoorbeeld door middel van een afstotende Coulomb kracht. Geconfronteerd met zulke grote aantallen lijkt het haast onmogelijk om theoretische voorspellingen te doen. Toch blijkt dit niet het geval.

In drie dimensies kan een metaal bijvoorbeeld kwalitatief worden beschouwd als een gas van electronen die effectief geen wisselwerking hebben. Dit wordt beschreven door de zogenaamde Fermi vloeistof theorie. Hiermee kunnen vele eigenschappen van vaste stoffen worden verklaard.

Jammer genoeg is deze simpele Fermi vloeistof theorie niet geldig voor een één-dimensionaal systeem. In dit geval moeten we ons wenden tot de Luttinger vloeistof theorie. De elementaire excitaties van dit model zijn de zogenaamde spinonen en holonen, die schematisch zijn afgebeeld in figuur 1.1 van hoofdstuk 1. Deze quasideeltjes hebben lading  $e$  en spin  $1/2$  en beschrijven collectieve lading en spin fluctuaties die bosonisch van karakter zijn. Een voorbeeld van een Luttinger vloeistof is het één-dimensionale Hubbard model. Dit model beschrijft bewegende electronen met spin  $1/2$ , die elkaar beïnvloeden door een afstotende Coulomb kracht wanneer ze op dezelfde roosterplaats zijn. De golf functie voor dit systeem wordt gegeven door de zogenaamde Bethe Ansatz oplossing en beschrijft de ingewikkelde wijze waarop de lading- en de spinvrijheidsgraden met elkaar zijn verweven. De Luttinger vloeistoffen die worden gerepresenteerd door dit Hubbard model zijn het onderwerp van studie in dit proefschrift. Hierbij zullen we aantonen dat voor alle positieve Coulomb interacties  $U$  deze systemen de zogenaamde subrooster pariteits orde herbergen.

Deze orde is het best zichtbaar wanneer we de Coulomb kracht in het Hubbard model erg groot nemen. Woyanovich, Ogata en Shiba hebben laten zien dat voor deze limiet de lading en spin vrijheidsgraden enigszins ontkoppelen en de golf functie op de volgende wijze kan worden opgebouwd. Allereerst, plaats de electronen over de keten op een manier zoals men zou doen bij fermionen die geen spin dragen, de zogenaamde spinloze fermionen. Verdeel vervolgens de spin over deze posities zoals wordt gedaan in een antiferromagnetische Heisenberg spin keten. Deze procedure is weergegeven in figuur 5.1 van hoofdstuk 5.

Deze constructie suggereert dat er achter de gecompliceerde Bethe Ansatz golf functie een simpel spin systeem schuil gaat, dat kan worden verkregen door alle gaten uit het

systeem te persen. Dit inwendige spin systeem is alleen toegankelijk voor de spinnen en kan niet direct worden waargenomen door een experimentator in het laboratorium. Voor deze externe waarnemer is dit spin systeem verborgen achter de beweging van de gaten waardoor hij (alternerende) spin correlaties meet als  $\langle M^z(x)M^z(0) \rangle \sim 1/x^{K_s+K_c}$ , in plaats van  $\langle M^z(x)M^z(0) \rangle \sim 1/x^{K_s}$ , geldig voor een Heisenberg spin keten. Dit interne spin systeem samen met de hierboven beschreven opbouw van de golffunctie zorgen ervoor dat de subrooster pariteit algebraïsch is geordend. Omdat dit interne spin systeem niet direct zichtbaar is voor de waarnemer, wordt deze orde ook wel als een verborgen orde aangeduid.

Maar allereerst, wat stelt de subrooster pariteit voor? Subrooster pariteit is sterk verbonden met de bipartietheid, de tweedeligheid, van het rooster. Een rooster is bipartiet wanneer het kan worden onderverdeeld in twee subroosters  $A$  en  $B$ , zodanig dat alle  $A$  plaatsen worden omringd door  $B$  roosterplaatsen en andersom. We kunnen dit op twee manieren doen, namelijk volgens  $\dots A - B - A - B \dots$  en  $\dots B - A - B - A \dots$ . Voor een antiferromagnetisch spin systeem worden deze twee toestanden weergegeven met een  $Z_2$  variabele  $p = \pm 1$  die we aanduiden als de subrooster pariteit. Dit is weergegeven in figuur 1.3 van hoofdstuk 1. De subrooster pariteit is van groot belang in de hierboven beschreven constructie van de golffunctie.

Stel we beginnen met een intern spin systeem met een subrooster pariteit  $p = +1$ , en plaatsen daarin vervolgens de gaten. Samen met deze gaten voegen we aan het systeem ook roosterplaatsen toe. Deze verstoren de oorspronkelijke subrooster pariteit van het interne spin systeem en zorgen ervoor dat elke keer wanneer we een gat passeren de subrooster pariteit van teken verandert. Anders gezegd, de tekenwisselingen van de subrooster pariteit zijn verbonden aan de positie van de gaten. Dit wordt aangeduid als de ordening van de subrooster pariteit en kan worden vergeleken met een kink in een telefoon snoer zoals afgebeeld op de voorkant van dit proefschrift. Net zoals een gat de subrooster pariteit van de keten verandert, verandert de kink de draairichting van het telefoonsnoer. Aan de ene kant draait het rechtsom en aan de andere kant draait het linksom. Omdat in het Hubbard model de gaten door het rooster bewegen, veroorzaakt dit een extra verval van  $1/x^{K_c}$  in de correlator  $\langle M^z(x)M^z(0) \rangle$  in vergelijking met de spin correlaties in het interne systeem.

Deze subrooster pariteits orde kan worden aangetoond door het berekenen van de niet-lokale string correlator  $O_{top}(x) = \langle M^z(x)(-1)^{\sum_{j=1}^{x-1}(1-n_{tor}(j))}M^z(0) \rangle$ . Omdat de term  $(-1)^{\sum_{j=1}^{x-1}(1-n_{tor}(j))}$  een minteken verbindt aan elk gat in de keten, verwachten we dat wanneer de subrooster pariteit is geordend, deze term de subrooster pariteit van het interne spin systeem herstelt. In dat geval meten we direct de spin correlaties van het interne systeem zonder enige ladings fluctuaties en vinden we dat  $O_{top}(x) \sim 1/x^{K_s}$  gelijk de spin correlator in het interne spin systeem. In dit proefschrift laten we zien dat dit voor het Hubbard model inderdaad het geval is, niet alleen voor grote  $U$ , maar voor alle positieve  $U$ . Dit bewijst dat de subrooster pariteit voor deze waarden is geordend.

Voor deze tussenliggende Coulomb interacties kunnen we de golffunctie op gelijksoortige manier opgebouwd denken als voor de limiet waar  $U$  groot is. Alleen beschrijft deze constructie slechts de electronen van enkel bezette roosterposities. Dit gaat op de volgende manier. Eerst worden deze electronen van de enkel bezette roosterpunten in

het rooster geplaatst en vervolgens wordt de spin over deze posities verdeeld zoals in een antiferromagnetische spin keten. Over de verdeling van dubbelbezette roosterplaatsen wordt hierbij geen uitspraak gedaan. Deze constructie is alleen geldig in de berekening van de spin correlator  $\langle M^z(x)M^z(0) \rangle$ , waaraan dubbel bezette toestanden niet bijdragen.

Het aantonen van de verborgen algebraïsche subrooster pariteits orde in Luttinger vloeistoffen gerepresenteerd door het positieve  $U$  Hubbard model is het belangrijkste resultaat van dit proefschrift. Hoewel Luttinger vloeistoffen al in vele studies zijn onderzocht is deze orde nog niet eerder aangetoond. Het bewijs hiervan is in dit proefschrift op de volgende manier opgebouwd.

Het begint met een inleidend hoofdstuk waarin we de oorsprong van de subrooster pariteit uitleggen. Hierbij maken we een connectie met eerder gedaan onderzoek.

Voordat we ons daarna gaan bezig houden met de verborgen orde in Luttinger vloeistoffen, beschouwen we in hoofdstuk 2 het zogenaamde pseudogap gebied in hoge temperatuur supergeleiders en bestuderen het effect van een enkele verontreiniging, die al dan niet magnetisch van aard is. We voorspellen dat elke depletie van toestanden rond het Fermi nivo aanleiding geeft tot het bestaan van resonante toestanden, ongeacht de microscopische oorsprong van deze pseudogap toestand.

In hoofdstuk 3 vatten we de belangrijkste eigenschappen van een Luttinger vloeistof samen. Gebruikmakend van de bosonizatie methode, leiden we resultaten af voor onder andere de dichtheids en spin correlatie functies. Verder bosonizeren we het één dimensionale Hubbard model, en geven zo het verband weer tussen het Hubbard model en Luttinger vloeistoffen.

In hoofdstuk 4 introduceren we de Bethe Ansatz golf functie voor het Hubbard model en gebruiken deze oplossingen voor het berekenen van de spin correlator  $\langle S^z(x)S^z(0) \rangle$  in de limiet voor grote Coulomb kracht.

In hoofdstuk 5 bestuderen we de subrooster pariteits orde in het Hubbard model zoals deze volgt uit de Bethe Ansatz oplossing voor grote  $U$ . We introduceren de topologische correlator  $O_{1op}(x) = \langle M^z(x)(-1)^{\sum_{j=1}^{x-1}(1-n_{tot}(j))}M^z(0) \rangle$ , die kan worden gebruikt voor het aantonen van de subrooster pariteits orde. Vervolgens laten we zien dat in de grote  $U$  limiet  $O_{1op}(x) \sim 1/x^{K_s}$ , wat aangeeft dat de subrooster pariteit in deze limiet inderdaad is geordend.

In hoofdstuk 6 beschouwen we een andere limiet van het Hubbard model, namelijk het geval van geen interacties ( $U = 0$ ). De electronen kunnen dan worden beschouwd als spinloze fermionen. We berekenen de topologische correlator  $O_{1op}(x)$  en laten zien dat ook hier de subrooster pariteit is geordend.

Na het vaststellen van de subrooster pariteits orde voor de gevallen  $U = 0$  en grote  $U$ , proberen we in hoofdstuk 7 de bosonizatie methode te gebruiken voor het aantonen van de subrooster pariteits orde voor tussenliggende Coulomb afstotingen. Maar het blijkt dat bosonizatie niet uitgerust voor het berekenen van niet-lokale operatoren als  $O_{1op}(x)$ .

Om toch uitsluitsel te krijgen op deze vraag voerde Ian McCulloch zogenaamde DMRG berekeningen uit. De resultaten hiervan worden geanalyseerd in hoofdstuk 8 en laten zien dat de algebraïsche subrooster pariteit orde ook geldt voor alle positieve waarden van de Coulomb kracht.

In het laatste hoofdstuk interpreteren we alle gevonden resultaten en analyseren we

de subrooster pariteits orde in termen van spinonen en holonen. Ook beschrijven we het verband met lokale ijk symmetrie.

## Curriculum Vitæ

Ik ben geboren op maandag 22 januari 1973 om 10 over 8 in de morgen aan de Krui-  
zemuntstraat 887 te Apeldoorn. In deze stad ging ik naar de basisschool *de Gong* en  
was leerling aan het *Myrtus College* dat later overging in de scholengemeenschap *de*  
*Heemgaard*, alwaar ik mijn VWO-diploma behaalde.

In 1991 heb ik mij voor wiskunde en natuurkunde ingeschreven aan de universiteit  
van Utrecht. Tijdens mijn doctoraalstudie heb ik als studentassistent bij de Faculteit  
wiskunde gewerkt. Mijn afstudeeronderzoek in de theoretische natuurkunde verrichtte  
ik onder leiding van prof. dr. H. van Beijeren en betrof het bepalen van een syste-  
matische diagrammatische dichtheidsexpantie van de Lyapunov exponent van een twee  
dimensionaal Lorentz gas. Met een scriptie over dit onderwerp rondde ik in de zomer  
van 1997 zowel de natuurkunde als de wiskunde studie af.

Vlak daarna trad ik in dienst van de universiteit Leiden als assistent in opleiding. On-  
der leiding van prof. dr. J. Zaanen deed ik promotie onderzoek aan sterk wisselwerkende  
electronen. De resultaten hiervan zijn beschreven in dit proefschrift.

Tijdens mijn aanstelling bezocht ik zomerscholen en conferenties in Kollum, Jeruza-  
lem, Cambridge, Leiden en Rome. In het jaar 2000 bracht ik van mei tot september een  
werkbezoek aan het Nationaal Laboratorium in Los Alamos, New Mexico in de VS, al-  
waar ik met dr. A. V. Balatsky en dr. I. Martin heb samengewerkt. Tijdens mijn promotie  
heb ik de werkcolleges van de vakken Thermodynamica, Speciale Relativiteitstheorie,  
Statistische Fysica I en Quantum Theorie I geleid.

*[The text in this section is extremely faint and illegible. It appears to be a biographical narrative or a list of achievements, but the specific details cannot be discerned.]*

## Nawoord

Aan het einde van dit boekje, is het tijd om even terug te kijken. Het was een lange en zware tocht en ik had het niet kunnen klaren zonder een aantal mensen.

First of all, I would like to thank Zohar Nussinov, with whom I worked during half of my research. Zohar, your kindness, expertise and intelligence have helped me tremendously.

Also, I would like to thank Ian McCulloch for help with the figures. It was a pleasure to work with you.

Verder wil ik mijn familie, en in het bijzonder mijn ouders, bedanken voor de constante liefdevolle steun in deze lange, niet altijd even gemakkelijke tijd. Het is fijn dat ik altijd op jullie kan rekenen.

Barbara, dankjewel voor je luisterend oor. Jacco, het was een plezier een kamer op het instituut met je te delen. Onno, tof dat je me hebt willen helpen met de voorkant van dit boekje. Michiel, bedankt voor je vriendschap.

En tenslotte Marlies, ik vind je lief.

# Stellingen

behorende bij het proefschrift

*"On Hidden Order in Luttinger Liquids"*

1. Het is opmerkelijk dat de verborgen orde beschreven in dit proefschrift zich zo lang aan het zicht heeft weten te onttrekken.

*Dit proefschrift.*

2. In een spinloos fermion systeem op een rooster met periodieke randvoorwaarden geldt voor grote afstanden  $x$  en dichtheden  $\rho_{SF} = N/V \neq 1$ , met  $N$  het aantal fermionen in de totale keten van lengte  $V$ ,

$$\langle (-1)^{\sum_{j=1}^x n_{SF}(j)} \rangle = \frac{A^2 \sqrt{2}}{\sqrt{\sin(\frac{\pi N}{V})}} \frac{\cos(\frac{\pi x N}{V})}{\sqrt{\frac{V}{\pi} \sin(\frac{\pi x}{V})}}.$$

Hierbij is  $n_{SF}(j)$  de dichtheidsoperator op roosterpunt  $j$  en  $A = 0.645002448$ .

*Dit proefschrift, hoofdstuk 6.*

3. Bij de berekening van de niet lokale operatoren beschreven in dit proefschrift is bosonizatie niet te vertrouwen.

*Dit proefschrift, hoofdstuk 7.*

4. De verborgen orde in de Haldane spin-1 keten beschreven door den Nijs en Rommelse duidt op een lokale  $Z_2$  ijsymmetrie.

*Dit proefschrift, hoofdstuk 9.*

5. Het feit dat één dimensionale stripes half gevuld zijn leidt tot verscheidene interne configuraties, zoals de zogenaamde  $2k_F$  en de  $4k_F$ -ordering. Een mogelijke representatie van de  $2k_F$  configuratie zijn Cooper paren in de reële ruimte.

*M. Bosch, W. van Saarloos en J. Zaanen, Phys. Rev. B 63, 092501 (2001).*

6. Met behulp van een zelf consistente benadering van een zogenaamde entanglement-disentanglement overgang, die zowel de actie van de polymeervloeistof op aan de wand vastgeketende moleculen, alsook de reactie van deze ketens op de vloeistof meeneemt, kan worden aangetoond dat de stress aan de wand een lokaal maximum heeft als functie van de stroomsnelheid. Dit leidt tot een oscillerende volume flux, de zogenaamde spurtinstabiliteit.

*J.L.A. Dubbeldam en J. Molenaar, Phys. Rev. E 67, 011803 (2003).*

7. Het niet isotroop zijn van de mobiliteit van de vortices in een type II supergeleider kan leiden tot een instabiliteit in het front tussen de vortices en anti-vortices.

*C. Baggio, M. Howard en W. van Saarloos, nog te publiceren.*

8. Frequentie ontappingsen maken het mogelijk om eenvoudig de lengte van een optische resonator te kalibreren.

*J. Dingjan, proefschrift "Multi-mode optical resonators and wave chaos" (2003).*

9. In veel wereldsteden ontsieren uitgespuwde stukjes kauwgom de straat. Pogingen om de kauwgom in straatputten te deponeren leveren nauwelijks een bijdrage aan de oplossing van dit probleem.

*<http://michiel.mmbase.net/kauwgom/report/>*

H.V. Kruis  
19 juni 2003